THESIS FOR THE DEGREE OF LICENTIATE OF ENGINEERING

Climate Simulation of an Attic Using Future Weather Data Sets

- Statistical Methods for Data Processing and Analysis

VAHID MOUSSAVI NIK

Department of Civil and Environmental Engineering
CHALMERS UNIVERSITY OF TECHNOLOGY
Göteborg, Sweden 2010

Climate Simulation of an Attic Using Future Weather Data Sets

- Statistical Methods for Data Processing and Analysis

VAHID MOUSSAVI NIK

Lic 2010:1
ISSN: 1652-9146

Department of Civil and Environmental Engineering
Division of Building Technology
Chalmers University of Technology
SE-412 96 Göteborg
Sweden
Telephone + 46 (0)31-772 1000
http://www.chalmers.se

Chalmers Reproservice
Göteborg, Sweden 2010

Climate Simulation of an Attic Using Future Weather Data Sets
- Statistical Methods for Data Processing and Analysis

VAHID MOUSSAVI NIK
Department of Civil and Environmental Engineering
Division of Building Technology
Chalmers University of Technology

Abstract

The effects of possible climate changes on a cold attic performance are considered in this work. The hygro-thermal responses of the attic to different climate data sets are simulated using a numerical model, which has been made using the International Building Physics Toolbox (IBPT).

Cold attic, which is the most exposed part of the building to the environment, is classified as a risky construction in Sweden. Mould growth on internal side of the attic roof, due to condensation of water vapor from the surrounding environment has been increasing over the last decade, and thereby the risk for degrading the performance of construction.

The attic studied in this work is a naturally ventilated space under a pitched roof on top of a 2 storey building. Climate inside the attic has been simulated using different weather data sets for the period of 1961-2100 in four cities of Sweden: Gothenburg, Lund, Stockholm and Östersund. The weather data sets, which are the results of climate simulations, enclose different uncertainties. The uncertainties related to differences in spatial resolutions, global climate models (GCMs), CO_2 emission scenarios and initial conditions are considered here. At the end enormous climate data sets are used in this study.

Analysis of the long term climate data demands suitable statistical methods. Two methods have been applied from meteorology: a nonparametric method for assessing the data without tracking of time, and a parametric method for decomposition of the parameter variabilities into three constructive parts. Looking into the decomposed components of the parameter and its variabilities enables to analyze the data with different time resolutions.

Applying the selected statistical methods helps in understanding of the importance of different uncertainties of the weather data and their effects on the attic simulation.

Keywords: HAM simulation, attic, climate change, variability decomposition, climate uncertainty

List of publications

This thesis consists of papers presented, accepted, or submitted in international peer reviewed conferences.

I. M. Nik, V. , Sasic Kalagasidis, A., Long term simulation of the hygro-thermal response of buildings Results and questions, *Proceedings of Building Physics Symposium*, Leuven, October 29-31 2008.

II. Sasic Kalagasidis A., Nik V., Kjellström E., Nielsen A. (2009), " Hygro-thermal response of a ventilated attic to the future climate load in Sweden", *Proceedings of the fourth International Building Physics Conference*, Istanbul, Turkey, pp. 519-526.

III. Nik, V., Sasic Kalagasidis, A., STATISTICAL METHODS FOR ASSESSMENT OF LONG-TERM HYGRO-THERMAL PERFORMANCE OF BUILDINGS, submitted to the *International Conference on Building Envelope Systems and Technologies, ICBEST 2010*, Vancouver, Canada, June 27-30, 2010.

IV. Nik, V., Sasic Kalagasidis, A., INFLUENCE OF THE UNCERTAINTIES IN FUTURE CLIMATE SCENARIOS ON THE HYGRO-THERMAL SIMULATION OF AN ATTIC, submitted to the *International Conference on Building Envelope Systems and Technologies,* ICBEST 2010, Vancouver, Canada, June 27-30, 2010.

V. Nik, V., The uncertainties in simulating the future hygro-thermal performance of an attic related to global climate models, accepted in the 10th REHVA World Congress, Clima 2010, Antalya, Turkey, May 9-12, 2010.

Contents

Paper III: STATISTICAL METHODS FOR ASSESSMENT OF LONG-TERM HYGRO-THERMAL PERFORMANCE OF BUILDINGS

Paper IV: INFLUENCE OF THE UNCERTAINTIES IN FUTURE CLIMATE SCENARIOS ON THE HYGRO-THERMAL SIMULATION OF AN ATTIC

Paper V: The uncertainties in simulating the future hygro-thermal performance of an attic related to global climate models

Acknowledgments

This work has been carried out at the Division of Building Technology of the Department of Civil and Environmental Engineering at Chalmers University of Technology, under the supervision of Professor Anker Nielsen and Associate Professor Angela Sasic Kalagasidis. I express my deepest gratitude to my supervisors. Their knowledge and experience helped me enormously during the research.

Dr. Angela Sasic Kalagasidis has supported me with her deep knowledge in HAM modeling and building physics. I am greatly indebted to her for the insightful comments and illuminating guidelines.

This research has been conducted in collaboration with the Rossby centre at Swedish Meteorological and Hydrological Institute (SMHI). I would like to appreciate Dr. Erik Kjellästrom. He has helped me with the weather data and supported me with his knowledge in meteorology. His comments have always been a source of motivation for extending the research.

I would like to thank all my colleagues at the Division of Building Technology. It is a very pleasant experience to work in the friendly environment of this division.

This project has been financed by FORMAS, the Swedish Research Council for Environment, Agricultural Sciences and Spatial Planning. This is most gratefully acknowledged.

Last but not least, my sincere thanks are extended to my family, specially my parents for their continuous support.

Nomenclature

Symbol	Unit	Description
a_x		Yule-Kendall skewness
e	mbar	Partial pressure at the surface
F	-	Absorption of radiation by water vapor
I_{DH}	W/m^2	Direct Solar radiation on Horizontal surface or solar beam
I_{dH}	W/m^2	Diffusive Solar radiation on Horizontal surface
I_{DN}	W/m^2	Direct normal radiation
I_H	W/m^2	Global radiation
I'_{DN}	W/m^2	Intensity of direct radiation in the direction of normal
$i(\lambda)$	W/m^2 µm	intensity of radiation of wavelength λ
$i_0(\lambda)$	W/m^2 nm	Mean value of spectral radiation in an interval centered on λ
k_e	-	Correction factor
m	-	Optical air mass
m_a	kg	Mass of air
m_v	kg	Mass of vapor
m_x		median
N_c	-	Cloud coverage
N_d	-	Number of day
P	Pa	Pressure
$\overline{R}$	J/K.mol	Gas constant (8.314 J/K.mol)
S_x		Interquartile range
SH	kg/kg	Specific humidity
T	°C or K	Temperature
$T_{y,d}$	°C	Daily mean temperature on day d and in year y
T'_y	°C	mean temperature anomaly of the season (or period) in year y
$T''_{y,d}$	°C	Residual daily anomaly temperature
$\overline{T}$	°C	30-year mean temperature of a season (or period)
$\hat{T}_d$	°C	mean seasonal cycle
W	kg/kg	Humidity ratio
z_t	degree	Zenith angle
α_d	-	Coefficient of absorption for particular scatter

α_r	-	Coefficient of absorption for molecular scatter
β	-	Coefficient of turbidity
γ	kg/kg	Specific humidity
θ_h	degree	Solar height
λ	µm	Wavelength
σ_{tot}		Total variability
σ'		Interannual variability
σ_y''		Intraseasonal variability
$\hat{\sigma}$		Variability induced by the seasonal cycle of the season
σ_{tot}^2		Total daily variance
σ'^2		Interannual variance
$\sigma_y''^2$		Intraseasonal variance in year y
$\hat{\sigma}^2$		Variance induced by the seasonal cycle
$\emptyset$	-	Relative humidity
ω	kg/ kg	Humidity ratio

Abbreviations

AOGCM	coupled Atmosphere-Ocean General Circulation Model
CCSM3	Community Climate System Model
ECMWF	European Centre for Medium range Weather Forecasts
GCM	General Circulation Models – Global Climate Model
GHG	Green House Gas
HadCM3	Hadley Centre Coupled Model
IPCC	Intergovernmental Panel on Climate Change
MSLP	Mean Sea Level Pressure
PROBE	Prototype Biomass and Evapotranspiration model
RCA	Rossby Centre regional Atmospheric climate model
RCM	Regional Climate Model
SRES	Special Report on Emissions Scenarios
SST	sea surface temperature

1. Introduction

Durability and performance of buildings is strongly affected by the environmental conditions. The outdoor climate is one condition which plays a big role in the functioning of buildings. The building performance should be adjusted to the variable outdoor climate conditions; both in short term and long term. Designing of the building services and construction should be optimized to fulfill the expected indoor conditions and durability of the building during its lifetime. The sustainable design, construction and retrofitting of buildings demands a long term view of their performance. It is possible to make such a projection by knowing the future climate conditions.

Studying the sustainability of the Swedish built environment can be done by hygro-thermal analysis of buildings towards climate change. In this work the analysis has been provided for a cold attic. The ventilated attic with pitched roofs, or cold attic, is a common construction part of the Swedish buildings. Attic is the most exposed part of the building to the environment. Daily, seasonal and diurnal weather impacts and variations are directly manifested on the roof surfaces. Depending on how well the attic is separated from the surroundings thermally and also in terms of moisture and air-tightness, these climatic loads may have consequences like melting and freezing of snow, condensation and freezing of water vapor from air and, as a result, mossy covering or mould growth. Problems with high humidity levels in cold attics have been remarkably increasing in Sweden over the last decade. Beside of negative effects on the construction durability, the significant mould growth on the wooden parts of cold attics can degrade the indoor air quality by inducing the mould odor. Nowadays cold attics are classified as the most problematic part of the existing buildings in Sweden.

The analysis of the future hygro-thermal performance of the cold attic is possible by using the future weather data, which have been provided by the Rossby centre, a climate modeling research group at the Swedish Meteorological and Hydrological Institute (SMHI). Climate models can never be certain. There are different uncertainty factors in simulation of the climate. These uncertainties appear in the building simulations. On the other hand, working with the future climate extends the analysis tens of decades. For example in this report simulations have been done for 140 years on hourly basis. Handling the huge data sets and considering the uncertainty factors demand suitable statistical methods.

In this work the indoor climate of a cold attic have been studied numerically. The heat and moisture (HAM) simulation of the attic has been done in the Simulink toolbox of Matlab using the

International Building Physics Toolbox (IBPT). Simulations are done on hourly basis. The total time of simulation is 140 years in most of the cases, from 1961 to 2100. Different weather data sets are applied to the attic model as the outdoor climate. The weather data sets are simulation results of different climate models. There are different sources of uncertainty in climate models which affect the weather data and consequently the attic simulation results. These uncertainty factors are considered in this work: spatial resolution, global climate model, CO_2 emission scenario and initial conditions. For each uncertainty factor the indoor climate of the attic is simulated and results are presented in separate chapters. The attic has been simulated for four cities in Sweden: Gothenburg, Lund, Stockholm and Östersund. Each chapter discusses the outdoor and indoor climate conditions of one or more cities in different seasons.

In meteorology different weather data sets are usually compared for long periods, i.e. 30 years. Some of the statistical methods, which have been used in meteorology to study the long term data sets, are applied in this work. The methods can be divided into two groups: nonparametric and parametric. In the nonparametric methods there is no track of time. One of the nonparametric methods, which is introduced in this work, is a hypothesis developed by Ferro (Ferro et al. 2005). The parametric methods are able to track the time. Here, a decomposition method of Fischer and Schär (Fischer & Schär 2009) is used. In this method the variabilities of parameters are decomposed into three constructive components. Looking into the decomposed components of the parameter and its variabilities enables to analyze the data with different time resolutions.

This report contains the following chapters:

In chapter 2 the weather data, which has been received from the Rossby centre, and the process of preparation of the data for HAM simulations are described.

Chapter 3 contains a short description of the attic model. It is more described in paper II.

Chapter 4 is about the statistical methods that are used in this work. The climate data in the next chapters are analyzed using the methods. Paper III is also about the statistical methods.

In chapter 5 the effects of having different spatial resolutions, 25km and 50km, on the distribution of the outdoor and indoor climate data is studied using the nonparametric statistical methods.

Chapter 6 concentrates on the effects of having different global climate models (GCMs) on the results. Different GCMs generate different climate conditions. The nonparametric and parametric comparison of the outdoor and indoor climate data reveals the uncertainties caused by the GCMs. Paper V also considers the same problem. Paper V considers a similar subject.

In chapter 7 the climate conditions for three cities of Gothenburg, Stockholm and Östrersund are presented. The effects of having different CO_2 emission scenarios in each city are considered. More description is available in paper IV.

Chapter 8 compares three different initial conditions for the climate data of Stockholm during winter. Again the nonparametric and parametric comparison of the indoor and outdoor is presented.

In chapter 9 some conclusion are presented.

2. Weather data

The weather data is received from the Rossby centre in Swedish Meteorological and Hydrological Institute (SMHI). There are different sets of data which are the simulation results of several climate models. Different parameters in the climate models cause variations in the climate data sets. The weather data is mostly provided for the period of 1961-2100 (140 years). In some cases it is less than 140 years. In most of them the number of days in each year is the same as the calendar, for example there is one leap year after 3 years. But some of the models generate data for years with equal days, 365 days or even 306 days. So in some cases when there is a comparison between models, the number of days is not the same. But it can be neglected for long term comparisons.

In this chapter different features of the weather data that have been used in this project is described: global climate model (GCM), regional climate model (RCM), emission scenarios, etc. For ease of use in the future a short description of the naming method for the weather files and its meanings is presented. The weather data need to be processed and prepared for the building simulations. The process is described in the section of "Preparing the parameters of the weather data for simulations".

2.1. About the climate model from the Rossby centre

As the concerns on climate change impacts keep on increasing, the use of climate change projections is becoming increasingly essential on all sectors that deal with weather, water and climate (Persson et al. 2007).

It was appointed by the Swedish Government in June 2005, to assess the vulnerability of the Swedish society to climate change, by means of mapping regional and local consequences of climate change, related costs and damages. In addition, the Commission was to suggest measures to reduce the vulnerability and consider some other aspects on taking action.

Several sets of climate data have been used as input data for the numerical simulations. The climate data has been provided by the Rossby Centre which is a part Swedish Meteorological and Hydrological Institute (SMHI). The Rossby Centre pursues advanced climate modeling: development, evaluation and application of regional climate modeling in climate and climate change research.

The climate data that has been used in this project is a version of the Rossby Centre regional atmospheric model, RCA3. This model includes a description of the atmosphere and its interaction with the land surface. It includes a land surface model and a lake model, PROBE. The performance of

RCA3 has been evaluated with “perfect” boundary condition experiments in which the model is run using boundary conditions from ECMWF Reanalysis experiment ERA40. ERA40 has been recognized as the most comprehensive account of the state and behavior of the atmosphere during the last four decades. RCA3 has converged to both ERA40 and concurrent observations of different kinds (Persson et al. 2007).

The use of regional climate models is not in predicting weather. Instead they provide a consistent and comprehensive tool for understanding the physics and sensitivity of the regional climate system.

2.1.1. Climate modeling and experimental setup

Climate modeling is pursued by means of models of varying complexity ranging from simple energy-balance models to complex three-dimensional coupled global models. On a global scale GCMs (global climate models, also known as general circulation models) are used. These consist of individual model components describing the atmosphere and the ocean. They also describe the atmosphere-ocean interactions as well as with the land surface, snow and sea ice and some aspects of the biosphere. Regional climate models (RCMs) are used to downscale results from the GCMs, to achieve a higher spatial resolution over a specific region. The main advantage of the finer resolution that is feasible in RCMs, is a better description of local topography, land-sea distribution and other land surface properties. These have an influence on surface and near-surface climate conditions (Persson et al. 2007).

The uncertainties of projected regional climate change arise from a number of factors. One is the external forcing scenarios like emission scenario which changes the greenhouse gas and aerosol concentrations. Another factor concerns the changes in the large-scale circulation determined by the GCM. It depends both on the model formulation and internal variability. Different RCMs can respond differently to the forcing conditions. A handle on these uncertainties can be gained when several models, forcing scenarios and simulations are considered. Whenever the results do not vary much across models and scenarios, it can be taken as an indication of robustness and perhaps of a useful degree of certainty (Persson et al. 2007).

Future climate change depends on changes in the external forcing of the climate system and, depending on which time-scale considered, to some degree on unforced internal variability in the climate system. Future changes in the atmospheric content of greenhouse gases and aerosols are not known, but the changes are assumed to be within the range of a set of scenarios developed for the IPCC (Intergovernmental Panel on Climate Change). These scenarios build on consistent

assumptions of the underlying socioeconomic driving forces of emissions, such as future population growth, economic and technical development. The global mean net warming response is rather uniform across these emissions scenarios during the next few decades but diverges more and more after that. The three emissions scenarios which have been used sample quite a lot of the spread of the scenarios developed for the IPCC, as well as the ensuing global mean warming (Persson et al. 2007).

The regional climate change signal is to a large extent determined by the large-scale climate response to emissions that is solved with a GCM. This enters in regional climate modeling as boundary conditions. Changes in seasonal mean temperature and precipitation over Europe are examples of variables for which there is uncertainty associated with the boundary conditions.

Uncertainties due to boundary conditions and radiative forcing dominates for changes in seasonal mean conditions (Persson et al. 2007). RCM uncertainty can also be large, especially for extreme conditions (E. Kjellström et al. 2007). The sampling uncertainty is generally less significant for larger projected changes than smaller ones.

2.1.2. Naming of the weather files

At the Rossby centre a pattern is used for naming the weather files. Here is an example of the file name:

RCA3_ECHAM5_A1B_1_50km_p1_q2m.dat

1) *RCA3* shows the regional climate model
2) *ECHAM5* shows the forcing global climate model
3) *A1B* shows the emission scenario
4) (A1B)*_1* shows the initial condition
5) *50km* shows the spatial resolution in extracting the data
6) *p1* shows the location of the data or the city
7) *q2m* shows the parameter

The Rossby acronyms are as the following:

1) Regional climate model

   RCA3

   HIRHAM: not available

   RACMO: not available

   REMO: not available

2) Forcing global climate model

CCSM

CNRM

ECHAM5

HADCM3

IPSL

3) Emission scenario

A2

B2

A1B

4) Initial condition

In the data that we have there are three initial conditions for A1B emission scenario

A1B_1

A1B_2

A1B_3

5) Spatial resolution in extracting the data

50 km: all the data sets are with this spatial resolution

25 km: has been provided for the following data sets up to the time of writing this report

RCA3_ECHAM5_A1B_3

RCA3_ERA40

12.5 km: No data has been received with this spatial resolution up to the time of writing this report.

6) Location

The data have been provided for four cities in Sweden. The data have been extracted from the closest gridboxes to the centre of the city.

p1: Gothenburg

p2: Lund

p3: Stockholm

p4: Östersund

7) Parameters

lwdwnsrf: downward longwave radiation at the surface [W/m2] (time resolution: 30 minutes)

swdwnsrf: corresponding shortwave radiation [W/m2] (time resolution: 30 minutes)

t2m: air temperature at the 2-metre level [K] (time resolution: 3 hours)

q2m: specific humidity at the 2m level [kg water/kg air] (time resolution: 3 hours)

u10m: WE wind speed components at the 10-metre level [m/s] (time resolution: 3 hours)

v10m: SN wind speed components at the 10-metre level [m/s] (time resolution: 3 hours)

totprec: total precipitation [mm] (time resolution: 30 minutes)

snowprc: snow precipitation [mm] (time resolution: 30 minutes)

totcov: total cloud coverage [0-1] (time resolution: 3 hours)

ps: total air pressure [N/m^2](time resolution: 30 minutes)

lowcc: cloudiness of low-level clouds [0-1]

midcc: cloudiness of mid-level clouds [0-1]

highcc: cloudiness of high-level clouds [0-1]

precwtr: rain precipitation [mm] (time resolution: 6 hours)

2.2. Regional climate model

The regional climate model system developed at the Rossby Centre has been used for downscaling the climate simulations. The climate scenarios used here are produced by RCA3, a version of the Rossby Centre regional atmospheric model (E. Kjellström et al. 2005). RCA cover Europe with a rotated longitude-latitude grid with a horizontal resolution of 0.44^o (approximately 50 km) and 24 vertical levels in the atmosphere. The time step is 30 minutes in RCA3. The weather data of four different GCMs have been used for doing the simulations. The transient experiments with RCA3 are continuous for the whole time period including also the recent decades.

There are some other regional climate models like HIRHAM, RACMO and REMO. The only RCM which has been used in this work is RCA3.

RCA3 has been evaluated against present-day climate. Given appropriate boundary conditions these studies show that RCA is capable of reproducing many aspects of the observed climate, both in terms of means and variability. For RCA3 Kjellström et al. (2005) show that seasonal mean temperature errors were generally within $\pm 1^oC$ except during winter when two major biases were identified; a positive bias in the north-eastern parts of the model domain, and a negative bias in the Mediterranean region. The reasons for these biases were traced back to the cloud water content, the downward longwave radiation, and the clear-sky downward shortwave radiation. They all contribute to underestimations in the diurnal temperature range and the annual temperature range in many areas in the model. These underestimations are most pronounced in the extremes. Compared to the observational climatologies RCA3 tends to overestimate precipitation in northern Europe during summer and underestimate it in the southeast (Persson et al. 2007).

2.3. Global climate model

A global climate model (GCM) is a mathematical model of the general circulation of a planetary atmosphere or ocean which is based on the Navier-Stokes equations on a rotating sphere with thermodynamic terms for various energy sources like radiation and latent heat. Climate model experiments can be carried out using coupled atmosphere-ocean general circulation models (AOGCMs). These models are applied with different external forcing factors as changing greenhouse gas concentrations, changes in solar intensity, etc. AOGCMs generally have a rather coarse spatial resolution (often 100-300 km). A commonly used approach to improve the resolution is to use a regional climate model (RCM) for downscaling the results from the AOGCM.

Differences between different GCMs depend both on differences in the formulation of the GCMs and on differences in initial conditions used in the GCMs in the different climate change experiments.

The Rossby centre has used the driving data from three global climate models, HadAM3H, ECHAM4/OPYC3 and ECHAM5/MPI-OM. In addition to initial conditions, the driving data consists of lateral boundaries and sea ice/sea surface temperatures. These fields are taken from the global model every six hours in the simulations.

The following are short descriptions of the different global climate models:

HadAM3H is the atmospheric component of the Hadley Centre coupled atmosphere ocean GCM HadCM3 that can be run with higher resolution (1.875° longitude × 1.25° latitude). Because HadAM3H excludes the ocean, the simulations with this model used sea surface temperature (SST) and sea ice distributions derived from observations in the control period (1961-1990). For the future time period it used the same observed data plus the climate change signal from earlier, lower resolution HadCM3 experiments.

HadCM3 (abbreviation for *Hadley Centre Coupled Model, version 3*) is a coupled atmosphere-ocean general circulation model (AOGCM) developed at the Hadley Centre in the United Kingdom. It was one of the major models used in the IPCC Third Assessment Report in 2001.

Unlike earlier AOGCMs at the Hadley Centre and elsewhere (including its predecessor HadCM2), HadCM3 does not need flux adjustment (additional "artificial" heat and freshwater fluxes at the ocean surface) to produce a good simulation. The higher ocean resolution of HadCM3 is a major factor in this; other factors include a good match between the atmospheric and oceanic components; and an improved ocean mixing scheme. HadCM3 has been run for over a thousand years, showing little drift in its surface climate (Gordon et al. 2000).

HadCM3 is composed of two components: the atmospheric model HadAM3 and the ocean model (which includes a sea ice model). Simulations often use a 360-day calendar, where each month is 30 days.

ECHAM5 is a coupled atmosphere-ocean GCM developed at DKRZ, the Deutsches Klimarechenzentrum GmbH, and the Max-Planck Institute for Meteorology in Hamburg. It was run at T42 spectral resolution corresponding to a horizontal grid spacing of 2.8^{o} in the atmospheric part. ECHAM5/MPI-OM is the successor of ECHAM4/OPYC3. One of the improvements of the model compared to ECHAM4/OPYC3 is that it does not require a flux adjustment between the atmosphere and the ocean. The current simulation is one of the contributions to the IPCC AR4 work from the DKRZ and the Max-Planck Institute for Meteorology. In a comparison with observations ECHAM5/MPI-OM has been shown to perform well in terms of surface pressure patterns in west-central Europe indicating that the large-scale circulation over Europe is realistic. The simulation was performed at T63 resolution (1.875° × 1.875°).

CCSM3: The Community Climate System Model (CCSM3) is a state-of-the-art coupled global circulation model that has been developed under the auspices of the National Center of Atmospheric Research (NCAR) Boulder, USA. The modules for the atmosphere, land surface, sea ice, and ocean components are linked through a coupler that controls the exchange of energy and water between the components. The current version 3 of CCSM has been released in June 2004 and since then it has been widely used for climate studies (Wyser et al. 2006).

CNRM: The CNRM-CM3 global coupled system is the third version of the ocean-atmosphere model initially developed at CERFACS (Toulouse, France), then regularly updated at Center National Weather Research (CNRM, METEO-FRANCE, Toulouse). CNRM-CM3 also now includes a parameterization of the homogeneous and heterogeneous chemistry of ozone, a sea ice model, GELATO2, and TRIP river routing from Tokyo University (Salas-Mélia et al. 2006).

IPSL: The *IPSL* "Earth system model" builds on all model developments achieved in four of the *IPSL* laboratories, *LMD*,*LODYC*, *LSCE*, *SA*, and from collaborations with *LGGE* for the high latitudes climate, *LOA* for the modeling of direct and indirect effects of the aerosols, *UCL/ASTR* for the new version of the sea-ice model, and *CERFACS* for the coupler. Successive versions of the global coupled model have been developed since 1995. They benefit from interactions within the GASTON group, created

at that time to favor technical exchanges between French groups in Toulouse and Paris working on ocean-atmosphere coupled simulation (Marti et al. 2006).

In this report there is no result with the IPSL global climate model.

2.4. ERA40 data

ERA40 is a re-analysis driven experiments which have been performed with the RCA in the Rossby centre to provide a realistic baseline regional climate. The climate projections based on global scenarios can be compared to ERA40. The boundary conditions for the experiments are taken from the European Centre for Medium range Weather Forecasts (ECMWF) ERA40 data set, extended with operational analyses to cover the whole period from 1961 to 2005. These data were downloaded on a 2^{o} horizontal resolution and 60 vertical levels, and interpolated for use with the RCA grid (Persson et al. 2007).

2.5. Future emissions scenarios

Three emission scenarios are available in this work: B2, A1B and A2 emissions scenarios from the IPCC Special Report on Emissions Scenarios (SRES). HadAM3H and ECHAM4/OPYC3 were run with observed forcing conditions for the time period until 1990 and with these emissions scenarios after that. ECHAM5/MPI-OM was run with observed forcing conditions until the year 2000 before switching to the A1B emissions scenario (Persson et al. 2007).

The IPCC SRES scenarios include emissions of anthropogenic greenhouse gases and aerosol precursors and/or types. Corresponding atmospheric concentration projections are also made available, after running the emissions through carbon cycle models. Because of the simplicity of the RCA radiation code, the net effect of these changes was approximated by an equivalent increase in the CO_2 concentration. In the RCAO experiments the equivalent CO_2 concentrations were held constant for the whole 30-year periods. The control run value of 353 ppm_v (1961-1990) was raised in the B2 simulations to 822 ppm_v and in the A2 simulations to 1143 ppm_v representing the period 2071-2100. In the RCA3 simulations the equivalent CO_2 concentrations were allowed to change with time and the numbers for each year are interpolated linearly from the decadal values shown in Table 2 (Persson et al. 2007).

Table 2.1 shows the radiative forcing and the CO_2 concentration. The anthropogenic radiative forcing includes the effect of greenhouse gases plus the indirect and direct effects of aerosols under the SRES B2, A1B and A2 emissions scenarios. The equivalent CO_2 concentration for a certain time is calculated using the radiative forcing ($F=5.35\ln(CO_2/CO_{2ref})$ where CO_{2ref} is the concentration in 1990.

The RCA radiation code enables the use of a variable CO_2 concentration (as well as water vapor), whereas other anthropogenic greenhouse gases are accounted at their present levels. It means the historical equivalent CO_2 concentrations need to be lower than the ones inferred from the greenhouse gas concentrations in the atmosphere, to compensate for the constant methane etc. concentrations. The equivalent CO_2 concentration profiles in this case also include a net negative forcing contribution of atmospheric aerosols (Persson et al. 2007).

Table 2.1 Radiative forcing and the CO_2 concentration for different CO_2 emission scenarios (NA= Not Applicable). [Table is from(Persson et al. 2007)]

Year	Radiative forcing [W/m^2]			Equivalent CO_2 concentration [ppm_v]		
	B2	A1B	A2	B2	A1B	A2
1950	NA	NA	NA	NA	313	NA
1960	0.39	0.39	0.39	313	313	313
1970	0.41	0.41	0.41	314	314	314
1980	0.68	0.68	0.68	331	331	331
1990	1.03	1.03	1.03	353	353	353
2000	1.33	1.33	1.32	373	373	373
2010	1.82	1.65	1.74	409	396	403
2020	2.36	2.16	2.04	453	436	426
2030	2.81	2.84	2.56	492	495	470
2040	3.26	3.61	3.22	536	572	532
2050	3.7	4.16	3.89	581	634	602
2060	4.11	4.79	4.71	628	713	702
2070	4.52	5.28	5.56	678	781	823
2080	4.92	5.62	6.4	730	832	963
2090	5.32	5.86	7.22	787	871	1123
2100	5.71	6.05	8.07	847	902	1316

2.6. The spatial resolution of the weather data

The Rossby centre provides the weather data using the RCA3 for different spatial resolutions: 50km×50km, 25km×25km and 12.5km×12.5km. All of the data sets have been provided for the 50km-grid (we call it coarse grid). For some cases the 25km-grid resolution is available (we call it fine grid). The city area is covered by nine 50km grids. The 5th grid is the closest to the centre. For the 25km resolution, the number of grids is multiplied by four. Four 25km grids should be selected as the corresponding grids for the central grid in the coarse resolution. The information for selecting the grids is described here. The comparison of the spatial resolutions has been made which is described in chapter 5.

Extracting the weather data for cities for finer scales

Starting with the 50km grid, there are 9 grid boxes where number 5 is the central one (the one with latitude and longitude closest to the grid box). This can be illustrated by the numbers 1-9.

7 8 9

4 5 6

1 2 3

The data are written from southwest to northeast where 5 is the gridbox closest to the city locations. Downscaling from 50km-grid to 25km-grid changes the plot as the following. Each number has been written four times corresponding to the finer 25km-grid.

7 7 8 8 9 9

7 7 8 8 9 9

4 4 5 5 6 6

4 4 5 5 6 6

1 1 2 2 3 3

1 1 2 2 3 3

As long as we are only interested in the 50km-grid simply grid number 5 is extracted for the city, grid 7 for the northwest etc. When data for the 25km-grid is extracted any of the four grid boxes labeled 5 above may be the central grid box closest to the city in question. As an example if it is the one in to the southwest (lower left) it means that the 9 points of 25km-grid data (columns 1-9)

7 8 9

4 5 6

1 2 3

will correspond to

4 5 5

4 5 5

1 2 2

in the above downscaled plot. So, if we want to compare with the 50km-grid we have to take the four labeled 5 in the lowermost figure that corresponds to 5,6,8,9 in the 25km-grid.

For getting the weather data for different cities the data of the closest grid point to the latitude/longitude of the city is extracted. Also the data from the 8 surrounding grid boxes is extracted.

Below are the indices that have been used in the Rossby centre for extracting the data (numbers are indices in the regional model domain covering all the Europe). The central values in the respective pairs indicate longitudinal and latitudinal indices to be extracted. For example for Gothenburg at 50km would be grid box (43, 64) where 43 is the west-east index and 64 the north-south.

p(1) = 42,44,63,65	Gothenburg at 50km
p(2) = 43,45,58,60	Lund at 50km
p(3) = 46,48,75,77	Östersund at 50km
p(4) = 49,51,66,68	Stockholm at 50km
p(1) = 84,86,126,128	Gothenburg at 25km
p(2) = 86,88,117,119	Lund at 25km
p(3) = 92,94,151,153	Östersund at 25km
p(4) = 99,101,133,135	Stockholm at 25km

Comparing the two sets of data (50 km vs. 25 km) shows that the central numbers differ by either 2n or 2n-1. So, for aggregating 4 grid boxes in the 25km-grid to compare with the corresponding one of the central grid box at the 50km grid slightly different grid boxes should be used for the different cities. This means that we should use;

Grid boxes 5,6,8,9 for Gothenburg

Grid boxes 1,2,4,5 for Stockholm

Grid boxes 2,3,5,6 for Lund

Grid boxes 2,3,5,6 for Östersund

Where 1-9 are according to the data which are written from southwest to northwest

7 8 9

4 5 6

1 2 3

2.7. Initial conditions

Climate simulations with global climate models for the 20th and 21st centuries generally start with preindustrial conditions. This is often taken as the year 1860 which is well before any large changes in atmospheric composition due to human activities. In this way the climate models can simulate the evolution of climate change taking into consideration the effect of changes in forcing (like greenhouse gas (GHG) concentrations, aerosol content, etc). The problem is that the initial conditions back in 1860 are not known. There are no surface based observations of climate variables like temperature and precipitation, but only at a few points and mostly so in Europe and North America, the southern hemisphere is virtually free of observations.

There should be a start point to set up and perform climate simulations. Initial conditions are needed for the full three-dimensional fields in the atmosphere and oceans. Also starting conditions

for the soil models and sea-ice models are needed. In addition to this it is needed to prescribe the physiography (orography, type of soils, vegetation cover, etc).

Climate models are set up and run for pre-industrial conditions as part of their testing. These runs start from some (more or less) arbitrary initial conditions representative of preindustrial conditions (prescribed GHG concentrations, aerosol content, solar constant, vegetation cover, etc.). These simulations should not show any long-term drift in long simulations (of the order of 1000 years or so) as forcing conditions are kept constant. These simulations are referred to as (preindustrial) control runs. Such a long simulation does not show long-term trends but it shows variability from year to year and from decade to decade (as does the climate system).

By taking some arbitrary conditions from the 1000 year control run it is possible to get initial conditions representative of preindustrial conditions. This is what was done at the Max-Planck Institute when they set up the ECHAM_A1B_1/2/3 simulations. So, they simply took a state from the long control run, for example 1st of January in model year 230, as initial conditions for one experiment, 1st of January from model year 562 for the second and 1st of January from model year 980 for the third. The evolution with time in these three simulations differs as the initial conditions are not the same. These differences are present throughout the simulations, i.e. both in the 20th and the 21st century.

2.8. Preparing the weather data for simulations

The weather data that is received from the Rossby centre should be prepared for the simulations in order to fit the proper format of the weather data in IBPT. Conversion of the raw data to the proper input data for the simulation is done by coding in Matlab. The conversion is done in three phases: 1) changing the format of the data, 2) changing the time step to one hour, 3) calculating the proper parameter from the raw data. The first two are applied to all the data sets and the last one to data sets like relative humidity and direct normal radiation or solar beam.

The weather data that are used in the simulations are matrices containing 12 parameters:

1. Time [sec]
2. Air temperature [^{o}C]: It is multiplied by 10 to avoid decimals.
3. Relative humidity [%]
4. Global radiation [W/m^2]
5. Diffusive horizontal radiation [W/m^2]
6. Direct normal radiation or Beam [W/m^2]
7. Long wave sky radiation [W/m^2]

8. Global illuminance: It is not used in the simulations, set as zero.
9. Diffuse horizontal illuminance: It is not used in the simulations, set as zero.
10. Direct normal illuminance: It is not used in the simulations, set as zero.
11. Wind direction [degree]
12. Wind speed [m/s]: It is not used in the simulations, set as zero.

2.8.1. Time

Its unit is second. Different parts of the weather data that we have from the Rossby centre at SMHI have been collected in each 3 hours or each 30 minutes. Calculation of the hourly data is done by coding in Matlab. The Simulink simulations are done on hourly time resolution (3600 seconds).

2.8.2. Air temperature

Its unit is degree Celsius. In the weather data that we use in IBPT it is multiplied by 10 to avoid decimal places. But during calculations it is multiplies by 0.1 to get the real temperature.

2.8.3. Relative humidity

The relative humidity in the weather file should be in percent. For example it is 90(%) not 0.9.
In the calculated data from the Rossby centre there is no 'relative humidity'. There we have 'specific humidity'. The following procedure is done in Matlab to find the *relative humidity* from the *specific humidity* and *total air pressure* from the Rossby centre data.

Definitions

Humidity ratio, W (alternatively, the moisture content or mixing ratio, also in some references its symbol is **ω**) is ratio of the mass of water vapor to the mass of dry air (Moran & Shapiro 2003).

$$\omega = m_v/m_a \qquad (2.1)$$

The humidity ratio can be expressed in terms of partial pressures and molecular weights (Moran & Shapiro 2003):

$$\omega = \frac{m_v}{m_a} = \frac{M_v p_v V/\bar{R}T}{M_a p_a V/\bar{R}T} = \frac{M_v p_v}{M_a p_a}$$

$$\omega = 0.622 \frac{p_v}{p - p_v} \qquad (2.2)$$

Specific Humidity is the ratio of the mass of water vapor to the total mass of the moist air.

$$SH = \gamma = M_w/(M_w + M_{da})$$

In terms of humidity ratio:

$$\gamma = W/(1 + W) \qquad (2.3)$$

Relative humidity, Ø is the ratio of the mole fraction of water vapor, y_v , in a given moist air sample to the mole fraction in a saturated moist air sample, $y_{v,sat}$, at the same mixture temperature and pressure (Moran & Shapiro 2003):

$$\emptyset = \frac{y_v}{y_{v,sat}})_{T,p}$$

Since $p_v=y_v\ p$ and $p_g=y_{v,\ sat}\ p$;

$$\emptyset = \frac{p_v}{p_g})_{T,p} \qquad (2.4)$$

What we have from the Rossby centre

p: total air pressure ($p_{dry\ air}+p_{vapor}$ or p_a+p_v) [Pa]

γ: Specific Humidity [kg water/kg air]

The applied procedure

Here the procedure of reaching to the *relative humidity* from the *specific humidity* is described.

a) Using *γ* and (2.3) results in finding the humidity ratio, *W* or *ω*.
b) Using *ω*, total air pressure (*p*) and (2.2) results in finding the vapor pressure, p_v. If the total air pressure, *p*, is not available we can use *p=101325 Pa* as a standard value for air pressure.
c) Finding the saturation pressure of water vapor in Pascal according to the following relations (ASHRAE 2001):

When water temperature $\leq 0°C$;

$$\ln p_{vs} = \frac{C_1}{T} + C_2 + C_3T + C_4T^2 + C_5T^3 + C_6T^4 + C_7 \ln T$$

where

C_1=-5.674 535 9 E+03

C_2= 6.392 524 7 E+00

C_3=-9.677 843 0 E-03

C_4= 6.221 570 1 E-07

C_5= 2.074 782 5 E-09

C_6=-9.484 024 0 E-13

C_7= 4.163 501 9 E+00

When water temperature $> 0°C$;

$$\ln p_{vs} = \frac{C_8}{T} + C_9 + C_{10}T + C_{11}T^2 + C_{12}T^3 + C_{13} \ln T$$

(6 of chap. 6 of ref. [1])

where

C_8=-5.800 220 6 E+03

C_9= 1.391 499 3 E+00

C_{10}=-4.864 023 9 E-02

C_{11}= 4.176 476 8 E-05

C_{12}=-1.445 209 3 E-08

C_{13}= 6.545 967 3 E+00

ln=natural logarithm

p_{vs}=saturation pressure, Pa

d) Finding the relative humidity, Ø, using relation (2.4).

e) RH should be between 0 and 1. In some instances, the calculated RH is more than 1. They are replaced with one in the code.

2.8.4. Global radiation

It is global shortwave radiation. The global radiation is in W/m^2 and it is provided in the weather data from the Rossby centre. Sometimes the global radiation is mixed with the total solar radiation; the sum of direct, diffuse, and ground-reflected radiation; however, because the ground reflected radiation is usually insignificant compared to direct and diffuse, for all practical purposes global radiation is said to be the sum of direct and diffuse radiation only.

Global radiation = direct solar radiation + diffuse radiation from the sky

Total radiation = global radiation + reflected radiation from ground and other parts of the environment (Kunzel 1996)

2.8.5. Diffuse horizontal radiation

The diffuse horizontal radiation is not available in the Rossby centre data. It has been calculated according to Taesler and Andersson (Taesler & Andersson 1984). For finding the diffuse horizontal radiation we need to know about the cloudiness and direct radiation (normal and then horizontal). Calculating the beam is described later. Here relations which have been used to calculate the diffuse horizontal radiation are described:

When the sky is clear:

$$I_{dH} = \eta\, I_H \qquad (2.5)$$

$$\eta = \frac{1}{1+8\,(\sin\theta_h)^{0.7}} \qquad (2.6)$$

When the sky is clear:

$$I_H = I_{dH} + I_{DH} \quad (2.7)$$

$$I_{DH} = I_{DN} \sin \theta_h \quad (2.8)$$

I_H: global radiation (W/m^2)

I_{dH}: diffusive horizontal radiation (W/m^2)

I_{DH}: direct horizontal radiation or BEAM (W/m^2)

η: A coefficient that has been determined by fitting a curve to the measurements of solar radiation carried out by Lunelund over the period 1927-33.

θ_h: solar height (degree)

2.8.6. Direct normal radiation or Beam

The direct irradiance on an area perpendicular to the sun.

The direct normal solar radiation, beam, is not provided by the Rossby centre. It has been calculated based on the work by Taesler and Andersson. Their method is called ENLOSS model (Taesler & Andersson 1984). In some other references it is called SOLTIMSYN model (IEA 1996).

a) What we have from the Rossby centre

I_H: Global radiation

N_c: Cloud coverage. Hourly cloud coverage.

A number between 0 (0/8) and 1 (8/8)

b) The applied procedure

1) We need the *solar height* in the calculations. If we name the hourly angle that is found from the HAM-Tools simulation ¥ then the solar height is:

$$\theta_h = 90 - ¥$$

2) Finding the *air mass*

"In astronomy, airmass is the optical path length through Earth's atmosphere for light from a celestial source. As it passes through the atmosphere, light is attenuated by scattering and absorption; the more atmosphere through which it passes, the greater the attenuation. " (cited from Wikipedia)

Airmass normally indicates relative airmass, the path length relative to that at the zenith at sea level, so by definition, the sea-level airmass at the zenith is 1. Airmass increases as the angle between the source and the zenith increases, reaching a value of approximately 38 at the horizon. Airmass can be less than one at an elevation greater than sea level.

There are different relations and estimations for finding the air mass. Taesler has used a relation in his work (Taesler & Andersson 1984) , but there are other relations with better results. The one that has been used here is the Young formula.

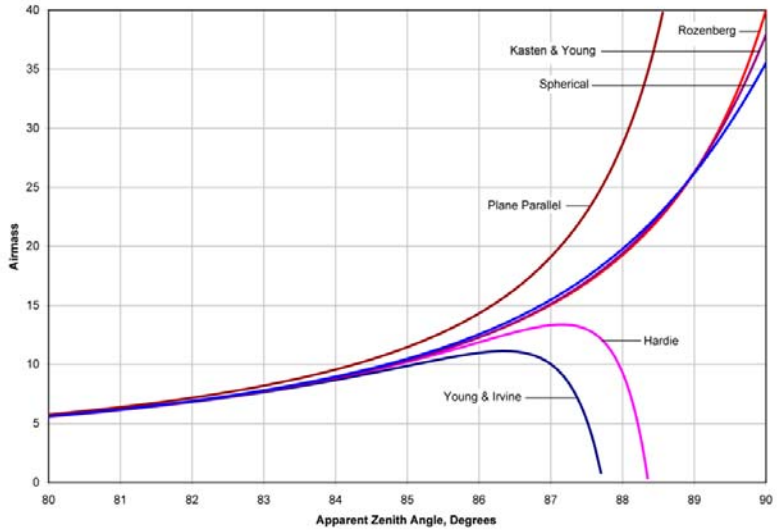

Figure 2.1 Different airmass formula plots (picture is from Wikipedia)

Here is the Young relation:

$$m = \frac{1.002432\ cos^2 z_t + 0.148386 \cos z_t + 0.0096467}{cos^3 z_t + 0.149864\ cos^2 z_t + 0.0.0102963 \cos z_t + 0.000303978} \qquad (2.9)$$

m: air mass (optical air mass) [-]

z_t: zenith angle [degree] $z_t = 90 - \theta_h$

Note that in the Matlab code, angles have been multiplied by $\frac{\pi}{180}$ to be in Radian.

3) Finding partial vapor pressure at the surface in mbar (e)

$$e = \frac{p_v}{100} \qquad (2.10)$$

p_v: vapor partial pressure. Has been described in section 2.8.3.

4) Finding absorption of radiation by water vapor (F)

$$F = 70 + 2.8\ e\ m \qquad (2.11)$$

F: absorption of radiation by water vapor

e: vapor pressure at the surface [mbar]

m: air mass

In the Matlab code *F* matrix is checked. Whenever the global radiation, I_H, is equal to zero the *F* value is set to be zero.

5) Introducing the coefficient of turbidity (β)

Turbidity is the cloudiness or haziness of a fluid caused by individual particles (suspended solids) that are generally invisible to the naked eye, similar to smoke in air. The measurement of turbidity is a key test of water quality. [7]

The coefficient of turbidity, β, is from table 6.1 of ref. [4]. Also you can find it in ref. [5].

Table 2.2 Coefficient of turbidity

Month	β
January	0.04
February	0.04
March	0.05
April	0.06
May	0.07
June	0.07
July	0.065
August	0.06
September	0.055
October	0.05
November	0.04
December	0.04

6) Introducing the Spectral distribution

Table 2.3 shows the spectral distribution of solar radiation outside the atmosphere according to Houghton and Thekaekara (Taesler & Andersson 1984). The intensity of radiation in the wavelength region 0.115-50 nm is divided into 78 band width.

Table 2.3 Spectral distribution of solar radiation outside the atmosphere

λ	$i_0(\lambda)$	λ	$i_0(\lambda)$	λ	$i_0(\lambda)$
0.115	0.000007	0.43	1.66	0.9	0.902
0.14	0.00003	0.44	1.833	1	0.757
0.16	0.00023	0.45	2.031	1.2	0.491
0.18	0.00127	0.46	2.092	1.4	0.341
0.2	0.0108	0.47	2.059	1.6	0.248
0.22	0.0582	0.48	2.1	1.8	0.161
0.23	0.0675	0.49	1.975	2	0.104
0.24	0.0638	0.5	1.966	2.2	0.08
0.25	0.0718	0.51	1.906	2.4	0.063
0.26	0.132	0.52	1.856	2.6	0.049
0.27	0.235	0.53	1.865	2.8	0.039
0.28	0.225	0.54	1.805	3	0.031
0.29	0.488	0.55	1.747	3.2	0.0229
0.3	0.52	0.56	1.716	3.4	0.0168
0.31	0.698	0.57	1.734	3.6	0.0137
0.32	0.84	0.58	1.737	3.8	0.0112
0.33	1.072	0.59	1.721	4	0.0096
0.34	1.087	0.6	1.687	4.5	0.006
0.35	1.107	0.62	1.622	5	0.0038
0.36	1.081	0.64	1.563	6	0.0018
0.37	1.19	0.66	1.505	7	0.001
0.38	1.134	0.68	1.445	8	0.006
0.39	1.112	0.7	1.386	10	0.00025
0.4	1.447	0.72	1.331	15	0.000049
0.41	1.773	0.75	1.251	20	0.000015
0.42	1.77	0.8	1.123	50	4E-07

λ: wavelength (μm)

$i_0(\lambda)$: mean value of spectral radiation in an interval centered on λ (W/m^2 nm)

7) Calculating the intensity of direct radiation in the direction of normal (I'_{DN})

In the SOLTIMSYN model developed by the SHMI, the calculations are based on the spectral distribution of solar radiation outside the atmosphere.

On its passage through the atmosphere, the intensity of radiation in the different wavelength regions diminishes owing to molecular scatter and absorption in accordance with;

$$i(\lambda) = i_0(\lambda)\, e^{-(\alpha_r+\alpha_d)m} \qquad (2.12)$$

$i(\lambda)$: intensity of radiation of wavelength λ (W/m^2 μm)

λ: wavelength (μm)

m: optical air mass see relation (2.9)

α_r: coefficient of absorption for molecular scatter see relation (2.13)

α_d: coefficient of absorption for particular scatter see relation (2.14)

The coefficient α_r describes Rayleigh scatter and is a function of wavelength in accordance with;

$$\alpha_r = 0.00816\ \lambda^{-4} \tag{2.13}$$

The coefficient α_d is a function of wavelength and is subject to high degree of variation depending on the turbidity of the atmosphere;

$$\alpha_d = \beta\ \lambda^{-1.3} \tag{2.14}$$

β: coefficient of turbidity according to Table 2.2

Using the coefficient of absorption in accordance with equations (2.13) and (2.14), coefficient of turbidity in accordance with Table 2.2 and the optical air mass as determined by equation (2.9), the intensity of radiation at the surface of the earth is calculated in accordance with equation (2.12) for an arbitrary wavelength. By integrating (2.12) over the wavelength region of interest, 0.115-50 nm, we obtain the *intensity of direct radiation in the direction of the normal* as;

$$I'_{DN} = \int_{\lambda=0.115}^{\lambda=50} i(\lambda)d\lambda \tag{2.15}$$

I'_{DN} is calculated inside two loops:

*For time=1:24*365*

I'_{DN}*(time)=0*

For i=2:end i is counter for the wavelength, Table 2.3

$$I'_{DN_{time}} = I'_{DN_{time}} +$$

$$abs\left(\frac{i_0(\lambda_i)\exp\left[-\left(0.00816\ {\lambda_i}^{-4} + \beta_{time}{\lambda_i}^{-1.3}\right)m_{time}\right]}{2}\right) +$$

$$abs\left(\frac{i_0(\lambda_{i-1})\exp\left[-\left(0.00816\ {\lambda_{i-1}}^{-4} + \beta_{time}\,{\lambda_{i-1}}^{-1.3}\right)m_{time}\right]}{2}\right)$$

$$\times(\lambda_i - \lambda_{i-1})$$

End of i

$I'_{DN\,time} = I'_{DN\,time} \times (1 - N_c)$ *Effects of cloudiness is calculated at this step*

End of time

Note: In the case of using the values the same as table 2.2, the result of the calculation should be multiplied by 1000.

8) Calculating a *correction factor (k_e)*

The correction factor, k_e, takes account of the eccentricity of the earth's orbit around the sun.

$$k_e = \frac{1}{1353}(1353 + 45.326\cos\omega_N N_d + 0.88018\cos 2\omega_N N_d - 0.00461\cos 3\omega_N N_d + 1.8037\sin\omega_N N_d + 0.09746\sin 2\omega_N N_d + 0.18412\sin 3\omega_N N_d) \quad (2.16)$$

$\omega_N = 2\pi/366$

N_d: $day\ number\ \ 1, 2, \ldots, 365\ (366)$

9) Calculating the *Direct Normal Radiation*

The direct radiation in the normal direction, corrected for the appropriate distance between the earth and the sun, and with respect to the absorption in water is obtained from;

$$I_{DN} = k_e(I'_{DN} - F) \quad (2.17)$$

F: absorption of radiation by water vapor from (2.11)

10) Checking and correcting the I_{DN}

At the instances without any total radiation, I_H=0, the normal direct radiation is replaced with zero.

At the instances with the negative I_{DN}, which means $I'_{DN} < F$, normal direct radiation is replaced with zero.

11) Finding *Direct Solar radiation on Horizontal surface (I_{DH})*

$$I_{DH} = I_{DN}\sin\theta_h \quad (2.18)$$

12) Finding *Diffusive Solar radiation on Horizontal surface (I_{dH})*

When there is no cloud in the sky and N_c=0;

$$I_{dH} = \eta\, I_H \quad (2.19)$$

$$\eta = \frac{1}{1+8\,(\sin\theta_h)^{0.7}} \qquad (2.20)$$

$$I_{DH} = I_H - I_{dH}$$

When the sky is cloudy and N_c>0;

I_{DH} is calculated from (2.18)

$$I_{dH} = I_H - I_{DH} \qquad (2.21)$$

The coefficient η has been determined by fitting a curve to the measurements of solar radiation carried out by Lunelund over the period 1927-33, the results of which are set out in table II:1 in Brown and Isfält (IEA 1996).

13) Checking and correcting the I_{dH} and I_{DH}

In some instances $I_{DH} > I_H$ which causes negative I_{dH} in (2.21). In this case the I_{dH} is replaced with zero.

At the instances with no total radiation, I_H=0, the direct horizontal radiation, I_{DH}, and diffusive horizontal radiation, I_{dH}, is replaced with zero.

2.8.7. Long wave sky radiation

The long wave radiation is available from the Rossby data in W/m^2 for each 30 minutes.

2.8.8. Global illuminance

It is not used in the simulations, set as zero.

2.8.9. Diffuse horizontal illuminance

It is not used in the simulations, set as zero.

2.8.10. Direct normal illuminance

It is not used in the simulations, set as zero.

2.8.11. Wind direction

Wind direction is in degree, between 0^o and 360^o.

The speed data that we have from the Rossby centre contains two elements of the speed vector;

1. Speed vector in the horizontal direction. The positive direction is from West to East.
2. Speed vector in the vertical direction. The positive direction is from South to North.

It is important to note that the arrow tip of the speed vector is located on the coordinate origin.

To find the wind direction, the arctangent of the angle between two velocity elements is found, then we add 180^o to the result to set the angle in the proper way for weather data.

The Matlab command is: Direction=atan2(u, v)*180/π + 180

u is the wind speed in the W-E direction and v is the S-N element.

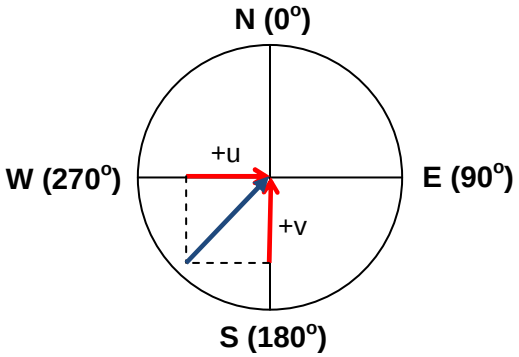

2.8.12. Wind speed

Wind speed is in m/s. It is found in this way:

$$wind\ speed = \sqrt{u^2 + v^2}$$

In the weather data wind speed is multiplied by 10 to avoid decimals.

3. The attic model

In this chapter a brief description about the attic model is presented. Most of the information about the attic model is available in paper iii and some other references. The outdoor climate data which has been introduced as the weather data in chapter one is applied to the numerical model of the attic to simulate the indoor climate. For each outdoor climate data the HAM (Heat, Air and Moisture) simulation is done for the whole period. The length of the periods is mostly 140 years. Simulations are made on hourly steps. The environment is the Simulink toolbox of the Matlab software. The International Building Physics Toolbox (IBPT) is used to define the building components in the Simulink. IBPT is defined as a library in the Simulink environment.

3.1. The attic

Figure 4.1 shows the attic over the residential 2-storey house. The characteristics of the building are described in paper II. The results in this paper are related to the exhaust-only ventilation of the model (Angela Sasic Kalagasidis et al. 2009).

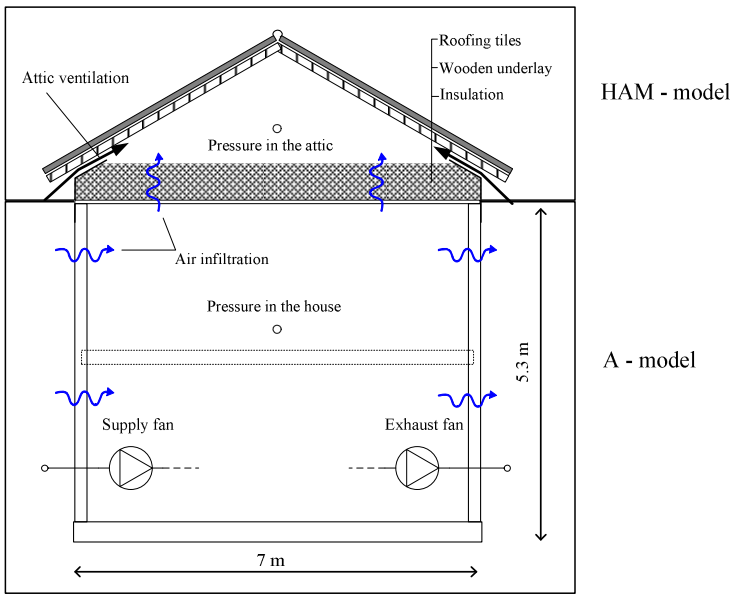

Figure 3.1. The sketch of the cold attic and the house.

3.2. Simulation environment

The HAM simulations have been made in the Simulink toolbox of Matlab (www.mathworks.com) using the IBPT library (www.ibpt.org). More information is available in “HAM-Tools - An Integrated Simulation Tool for Heat, Air and Moisture Transfer Analyses in Building Physics” (A. Sasic Kalagasidis 2004).

4. Statistical methods

Working with future climate scenarios in hygro-thermal simulation of buildings extends the simulation time to tens of decades. In many cases the results are based on hourly or daily calculations. Though it is possible to do the simulations on an hourly basis for a long period, assessing and presenting the results demands suitable statistical methods. For example there are hourly weather data sets from 1961 to 2100. Imagine simulation of a building and analyzing the results for 140 years, on hourly basis, for three different emission scenarios, different resolutions and different global climate models. It is not possible to analyze the results using the ordinary methods that are used in building physics. Handling huge amounts of data demands suitable methods.

None of the future weather data sets is certain. All are the simulation results and nobody is sure if one is going to happen or not. The meteorologists usually do not base their conclusions on short time periods when they are working with the future climate. For example they study or compare the behavior of a parameter in long time periods like 30 years. The trends and the variances are considered for different time periods and different data sets.

Different statistical methods for analyzing and presenting the weather data and simulation results have been used. Some of them are very well known and do not need extra description like probability distribution function (PDF), cumulative distribution function (CDF), histogram etc. Some of the methods need more description which is provided in this chapter.

The statistical methods which are considered here are divided to parametric and nonparametric methods. Nonparametric statistical methods, unlike parametric statistics, make no assumptions about the probability distributions of the variables being assessed. We use the nonparametric methods for comparing the data sets as groups of numbers. The robust nonparametric methods are useful for quick comparison of different sets. It is easy to handle huge data sets using these methods when there is no need for tracking the time (or any other relevant parameter). The nonparametric model and method which are introduced here are boxplot and a hypothesis which has been developed by Ferro (Ferro et al. 2005).

In the parametric methods we have the track of time (or any other relevant parameter). In the case of analyzing the data using more statistical power we use the parametric methods. Parametric methods make more assumptions than non-parametric methods. They can produce more accurate and precise estimates but the robustness of the method can be questioned. The method that is

introduced in this chapter is a robust method which has been developed by Fischer and Schär (Fischer & Schär 2009).

Both the Ferro and Fischer methods have been developed and used in meteorology and are capable for analyzing the long term simulation results. The nonparametric method is used to compare different data sets and different resolutions. The parametric method, which is based on decomposition of the parameter variabilities, is useful in comparing different scenarios, boundary or initial conditions. The method provides a suitable view of the data which enables to measure the effects of influential parameters on the data variations.

4.1. Boxplot

The box plot is based on *robust statistics*. Robust statistics is more resistant (robust) to the presence of outliers comparing to the classical statistics which is based on the normal distribution. Boxplot gives a general view of the data. Before describing the boxplot it is necessary to know about some statistical concepts:

Quantiles

Quantiles are the points that are taken at regular intervals from the cumulative distribution function (CDF) of a variable. If we divide an ordered data into n equal-sized subsets then we will get n-quantiles; the quantiles are the data values marking the boundaries between consecutive subsets. In other words the k^{th} n-quantile for a variable is the value *x* such that the probability that the variable will be less than *x* is at most k / n and the probability that the random variable will be more than *x* is at most (n − k) / n. There are n – 1 quantiles, with k an integer satisfying 0 < k < n (see the Wikipedia or any statistical textbook).

Quartiles

The 4-quantiles are called quartiles. In descriptive statistics, a quartile is any of the three values which divide the sorted data set into four equal parts, so that each part represents one fourth of the sampled population. The lower quartile or first quartile, Q1, cuts off the lowest 25% of the data. The second quartile or median, Q2, cuts data set in half. The upper or third quartile, Q3, cuts off highest 25% of data. The difference between the upper and lower quartiles is called *interquartile range*.

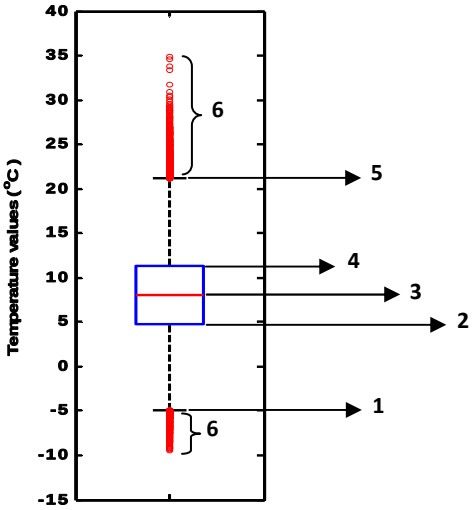

Figure 4.1. Components of a boxplot

The diagram shows the following information about the data:

1. The lower whishker
2. The lower quartile (Q1)
3. The median (Q2)
4. The upper quartile (Q3)
5. The upper whishker
6. The outliers

An outlying observation, or *outlier*, is one that appears to deviate significantly from other members of the sample in which it occurs.

Whishker is the line extends to at most 1.5 times the box width (the interquartile range) from either or both ends of the box. They must end at an observed value, thus connecting all the values outside the box that are not more than 1.5 times the box width away from the box. Accepting this definition results in having some values as outliers which are physically possible to happen.

Figure 4.2. compares a boxplot and probability distribution function (pdf) of a normal N $(0,1\sigma^2)$ distribution.

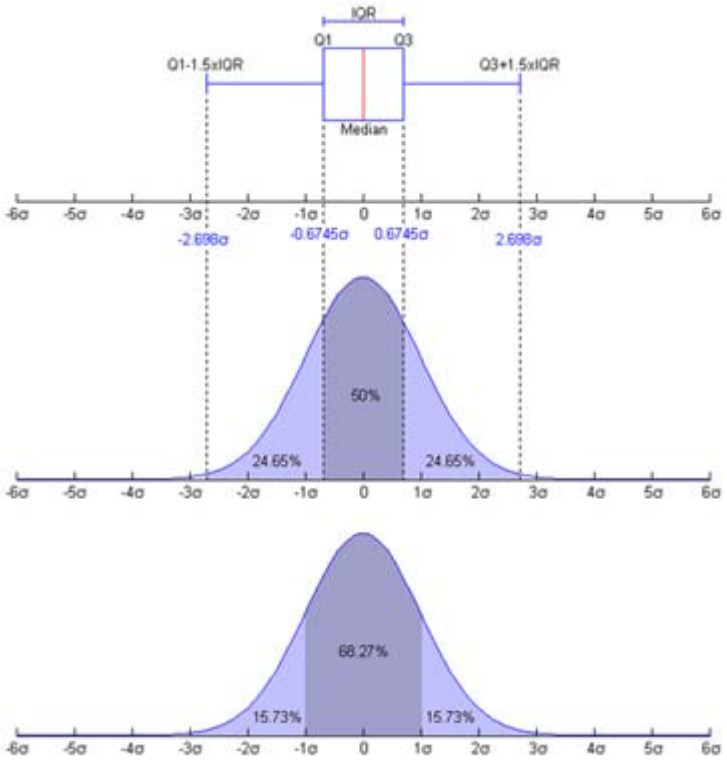

Figure 4.2. Boxplot and a probability density function (pdf) of a Normal N (0,1σ^2) population (figure is from Wikipedia)

4.2. The Ferro hypothesis

Ferro et al. present a simple nonparametric technique based on quantiles for exploring and comparing differences in pairs of probability distribution functions (Ferro et al. 2005). The method uses quantiles to investigate the reason of changes in the probability distribution. The method checks if the changes are due to the shifts in location, scale or both. Changes in location and scale are often measured by sample means and variances, respectively.

The aim is to understand any differences between the probability distributions of two variables. X and Y denote two variables. Their distribution functions are $F(x) = P(X \le x)$ and $G(y) = P(Y \le y)$ where P(A) denotes the probability of an event. Ferro proposes the following hypothesis to understand the changing distributions:

$$\begin{aligned} H_o &: \quad F(z) = G(z) \\ H_S &: \quad F(\sigma_X z) = G(\sigma_Y z) \\ H_L &: \quad F(\mu_X + z) = G(\mu_Y + z) \\ H_{LS} &: \quad F(\mu_X + \sigma_X z) = G(\mu_Y + \sigma_Y z) \end{aligned} \tag{4.1}$$

for all $-\infty < z < \infty$ and unknown constants μ_X, μ_X, $\sigma_X > 0$ and $\sigma_Y > 0$.

Hypothesis H_o claims no difference between F and G. For H_S the difference is only in scale. In H_L the difference is only in location. Finally in H_{LS} the difference is only in location and scale.

There are three useful statistics for summarizing a distribution which are defined based on quantiles;

1- Median:

$$m_X = \hat{x}_{0.5} \tag{4.2}$$

2- Interquartile range:

$$s_X = \hat{x}_{0.75} - \hat{x}_{0.25} \tag{4.3}$$

3- Yule-Kendall skewness measure:

$$a_X = (\hat{x}_{0.75} - 2\hat{x}_{0.5} + \hat{x}_{0.25}) / s_X \tag{4.4}$$

These statistics are resistant measures of the location, scale and shape (asymmetry) of F and can be compared with corresponding measures of G.

Ferro has also used the quantile-quantile plot for the comparison. The cited hypothesis corresponds to different linear relationships between the two sets of quantile:

$$\begin{aligned} H_o: &\quad y_p = x_p \\ H_S: &\quad y_p = \sigma_Y (x_p / \sigma_X) \\ H_L: &\quad y_p = \mu_Y + (x_p - \mu_X) \\ H_{LS}: &\quad y_p = \mu_Y + \sigma_Y (x_p - \mu_X) / \sigma_X \end{aligned} \tag{4.5}$$

for all 0<p<1. The last three equalities (H_s, H_L *and* H_{LS}) are the quantiles for the distribution obtained by adjusting F to have, respectively, the same scale, location, and location and scale as G.

The location parameters, μ_X and μ_Y, are estimated by the medians, m_X and m_Y. The scale parameters, σ_X and σ_Y, are estimated by the interquartile ranges, s_X and s_Y.

4.3. The decomposition method

Different changes in the weather data may affect building performance: long term changes like annual temperature increment or short term changes like increase in intraseasonal day-to-day variability. Besides of comparing the values of the large data sets there is also a need to find and compare the variations of the data sets and studying the influence of different changes of the climate on the building performance. We need to have the track of time in different scales.

In this section a parametric method which has been developed by Fischer and Schär is described (Fischer & Schär 2009). In meteorology weather data sets are usually compared in long time scales,

i.e. 30 years. The method is based on decomposition of the variabilities of a parameter to three components: interannual, intraseasonal and seasonal cycle. At the first step a parameter is decomposed to four components according to relation 3.6. After calculation of the variances, the corresponding variabilities are calculated.

Here the method is described for the daily temperature.

$$T_{y,d} = \bar{T} + \hat{T}_d + T'_y + T''_{y,d} \tag{4.6}$$

$T_{y,d}$: Daily mean temperature on day d (of a total D) and in year y (of a total Y)

$\bar{T}$: The 30-year mean temperature of the season (or period)

$\hat{T}_d$: The mean seasonal cycle relative to $\bar{T}$

T'_y : The mean temperature anomaly of the season (or period) in year y

$T''_{y,d}$: The residual daily anomaly with respect to other components.

The method can be used for different time periods. For example the daily mean temperature can be decomposed in each 30-year period which implies Y=30 in the formulation. If we consider the spring season (March-April-May) then the total number of days in each year will be equal to 92 days (D=92).

The mean seasonal cycle and mean temperature anomaly in (4.6) are defined as:

$$\hat{T}_d = \frac{1}{Y}\sum_{y=1}^{Y}(T_{y,d} - \bar{T}) \tag{4.7}$$

$$T'_y = \frac{1}{D}\sum_{d=1}^{D}(T_{y,d} - \bar{T}) \tag{4.8}$$

This implies: $\sum_{d=1}^{D}\hat{T}_d = 0$, $\sum_{y=1}^{Y}T'_y = 0$ and $\sum_{d=1}^{D}T''_{y,d} = 0$.

The total daily variance can be defined as:

$$\sigma^2_{tot} = \frac{1}{YD}\sum_{y=1}^{Y}\sum_{d=1}^{D}(T_{y,d} - \bar{T})^2 = \frac{1}{YD}\sum_{y=1}^{Y}\sum_{d=1}^{D}(\hat{T}_d + T'_y + T''_{y,d}) \tag{4.9}$$

The variances of each time component are defined as the following;

The interannual variance: $\sigma'^2 = \frac{1}{Y}\sum_{y=1}^{Y} T'^2_y$

The variance induced by the seasonal cycle: $\hat{\sigma}^2 = \frac{1}{D}\sum_{d=1}^{D} \hat{T}^2_d$

The intraseasonal variance in year y: $\sigma''^2_y = \frac{1}{D}\sum_{d=1}^{D} T''^2_{y,d}$.

Having these definitions, relation (9) can be written as:

$$\sigma^2_{tot} = \sigma'^2 + \hat{\sigma}^2 + \frac{1}{Y}\sum_{y=1}^{Y} \sigma''^2_y \qquad (4.10)$$

With the variances, the variability of each component may be found. The total summer temperature variability σ_{tot} is defined as the standard deviation of all summer daily mean temperatures in a 30-year period. The variability components are: interannual variability (σ'), intraseasonal variability (σ_y''), and the variability induced by the seasonal cycle of the season ($\hat{\sigma}$).

5. Spatial resolution

Most of the weather data have been extracted with the resolution of 50km. For these two sets of weather data the spatial resolution of 25km is also available; RCA3_ECHAM5_A1B_3 and RCA3_ERA40. It is important to know how much the spatial resolution will affect the results. Extracting data from different grids for each spatial resolution has been described in section 2.7. In this section we investigate how much the two resolutions of weather data are different and how big is the effect of that difference on the simulation results. Three statistical methods have been selected: histogram, boxplot and the Ferro method where have been described in chapter 4. These robust nonparametric methods are applicable for handling the huge data sets. It is important to remember that there is no time lag between data sets. In other words the data behaves the same during time for the both resolutions. For example if the warmest day occurs in day *n* in the finer resolution, then the coarser one also has the highest temperature in day *n*.

The hourly indoor and outdoor climate data is available for long periods; 140 and 45 years. Checking the compatibility of the two spatial resolutions can be done by comparing the resolutions for the whole period of 140 years or for some specific time periods. The latter provides a more precise comparison especially for the nonparametric methods which the time is not specified.

Different parameters in different seasons for two periods of 1961-1990 and 2071-2100 have been compared together. Because of having four 25km grids corresponding to one 50km grid, the average value of the four 25km grids has been taken in each time step. So the comparison is between the 50km grid and the average value of 25km grids. Simulation of the attic has been made using the central 50km grid weather data and the four corresponding 25km grids.

The nonparametric methods are used for checking the uncertainties related to the spatial resolution of a climate model when the only difference is the grid size in extracting the data from the climate model.

5.1. Histogram

Histogram is a useful tool to plot the density of a data. Histogram displays the tabulated frequency graphically as bars. In the following figures the distribution of parameters for the spatial resolutions of 25km and 50km are shown. Figures do not illustrate the time. They show the frequency of the data for being in a specific interval in the selected period.

Temperature and relative humidity of the outer and inner climate and also the global radiation in Gothenburg are illustrated in the following figures. Figures 5.1 and 5.2 compare the outdoor temperature in four seasons for the periods of 1961-1990 (CTL) and 2071-2100 (SCN). Figures 5.3 and 5.4 compare the relative humidity for that periods and figures 5.5 and 5.6 make the same comparison for global radiation, all for outdoor conditions. Histograms show that the data distributions in two resolutions are very alike. There are some differences for each time period which is reasonable; the two data sets do not have exactly the same location as a result of different resolutions.

Looking at figures 5.7 and 5.8 illustrates the difference between indoor temperatures which happens because of the difference in the input data. The correlation between the 25km and 50km data sets for the indoor climate is not the same as the correlation of the outdoor parameters. The hygro-thermal simulation of the attic is not a linear process. There are several parameters which are influencing the indoor conditions, for example the indoor relative humidity is the result of outdoor temperature and relative humidity, solar radiation, wind speed etc. So the simulation results have been affected by the spatial resolution differences of all the involved parameters. But as it is visible the magnitudes of the correlations have the same order indoor and outdoor. Figures 5.9 and 5.10 show the difference of the indoor relative humidity distribution for two resolutions.

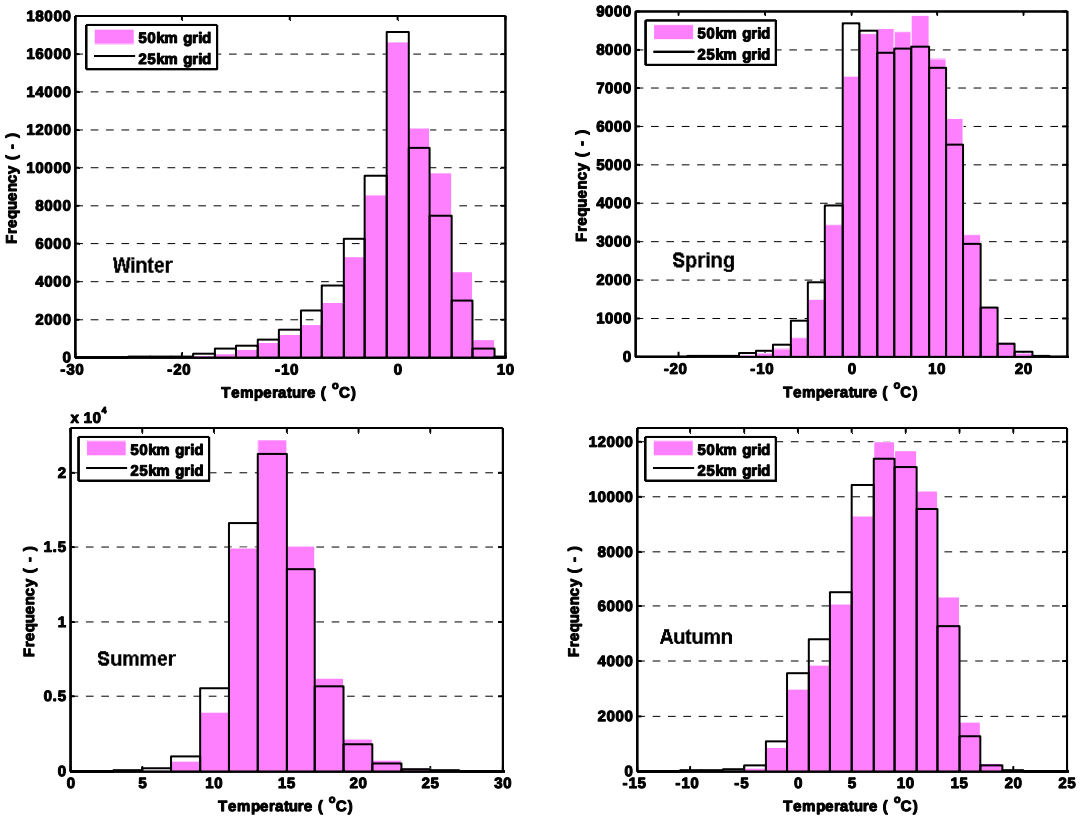

Figure 5.1. Outdoor temperature distribution during CTL for two spatial resolutions in RCA3-ECHAM5-A1B-3

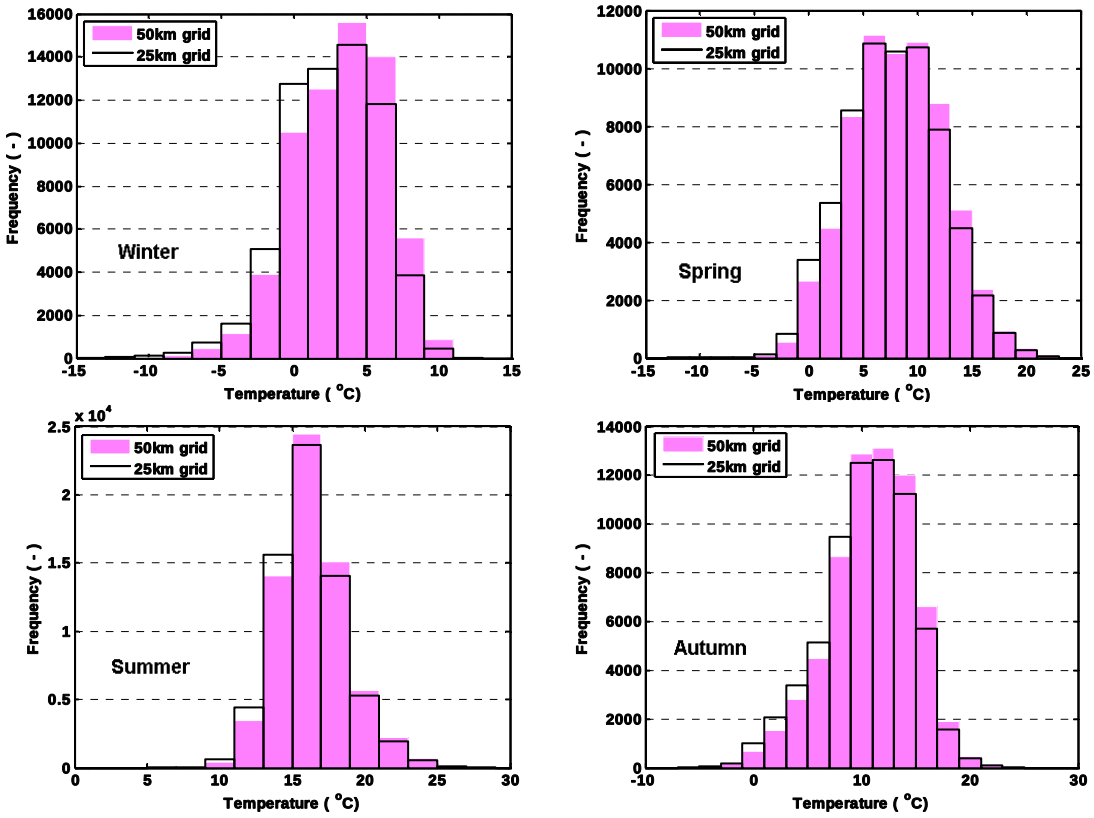

Figure 5.2. Outdoor temperature distribution during SCN for two spatial resolutions in RCA3-ECHAM5-A1B-3

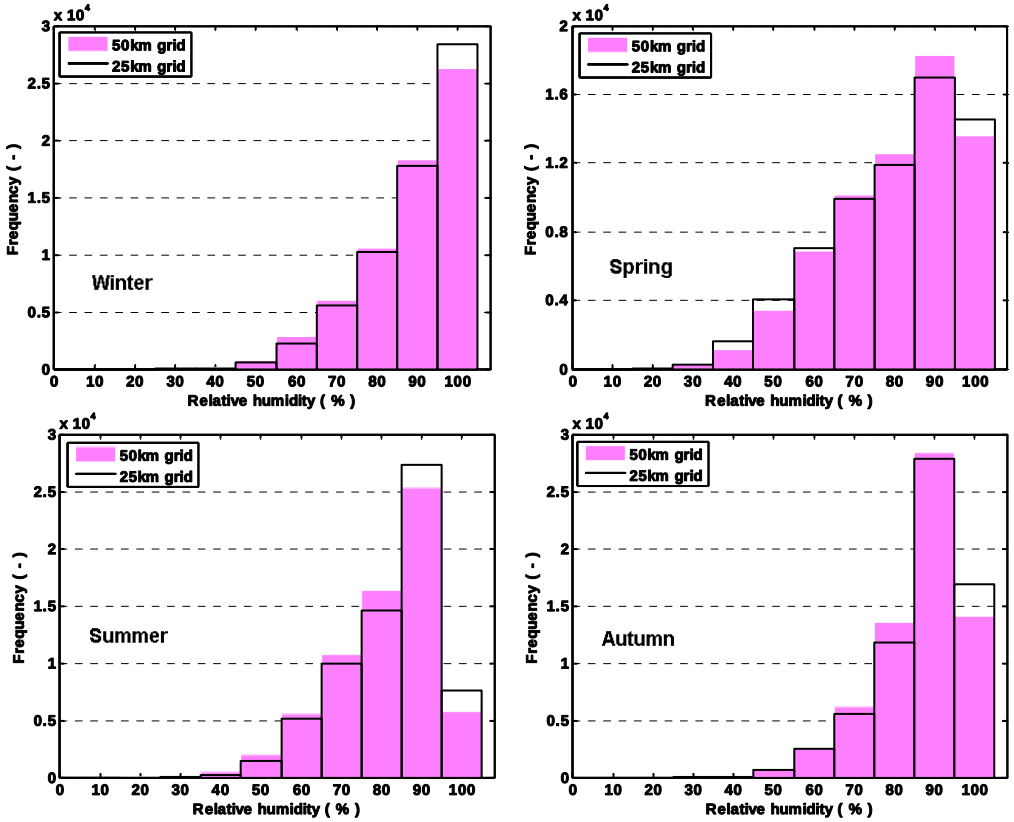

Figure 5.3. Outdoor relative humidity distribution during CTL for two spatial resolutions in RCA3-ECHAM5-A1B-3

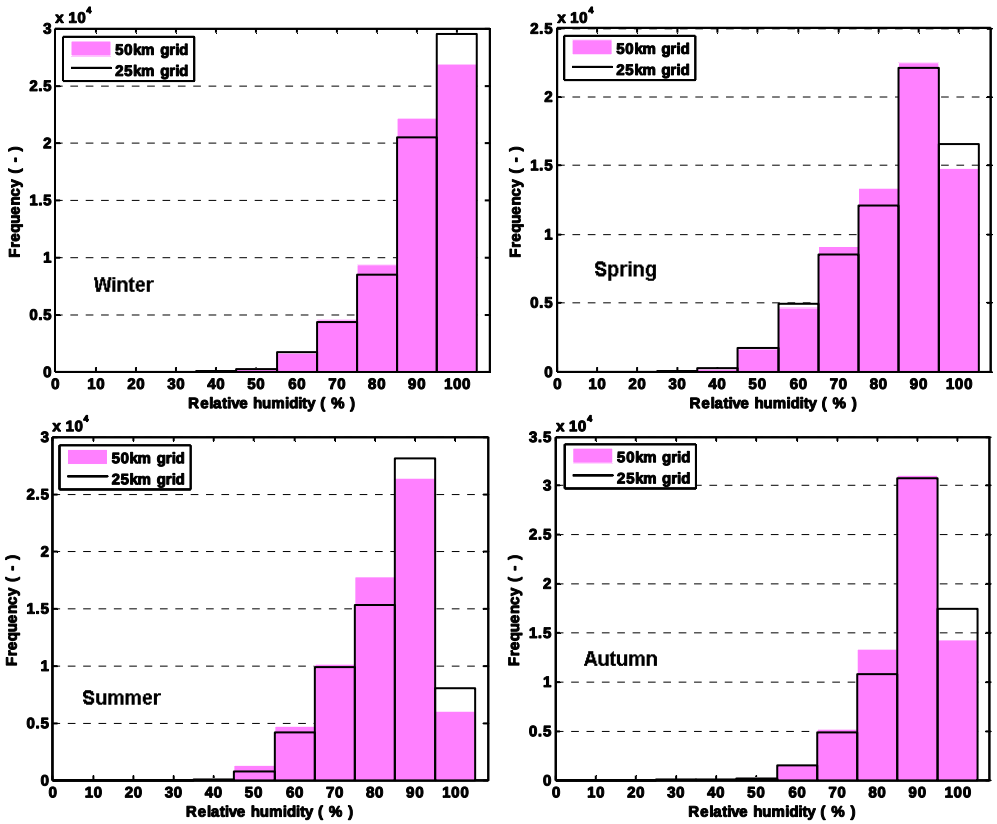

Figure 5.4. Outdoor relative humidity distribution during SCN for two spatial resolutions in RCA3-ECHAM5-A1B-3

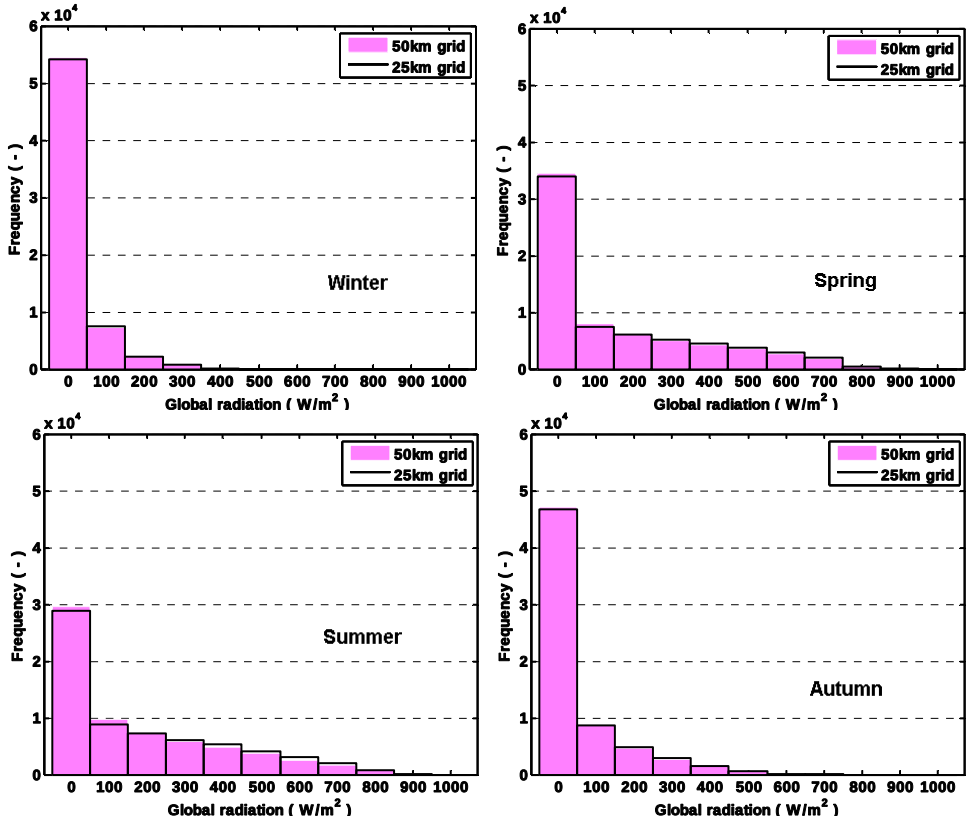

Figure 5.5. Global radiation distribution in CTL for two spatial resolutions in RCA3-ECHAM5-A1B-3

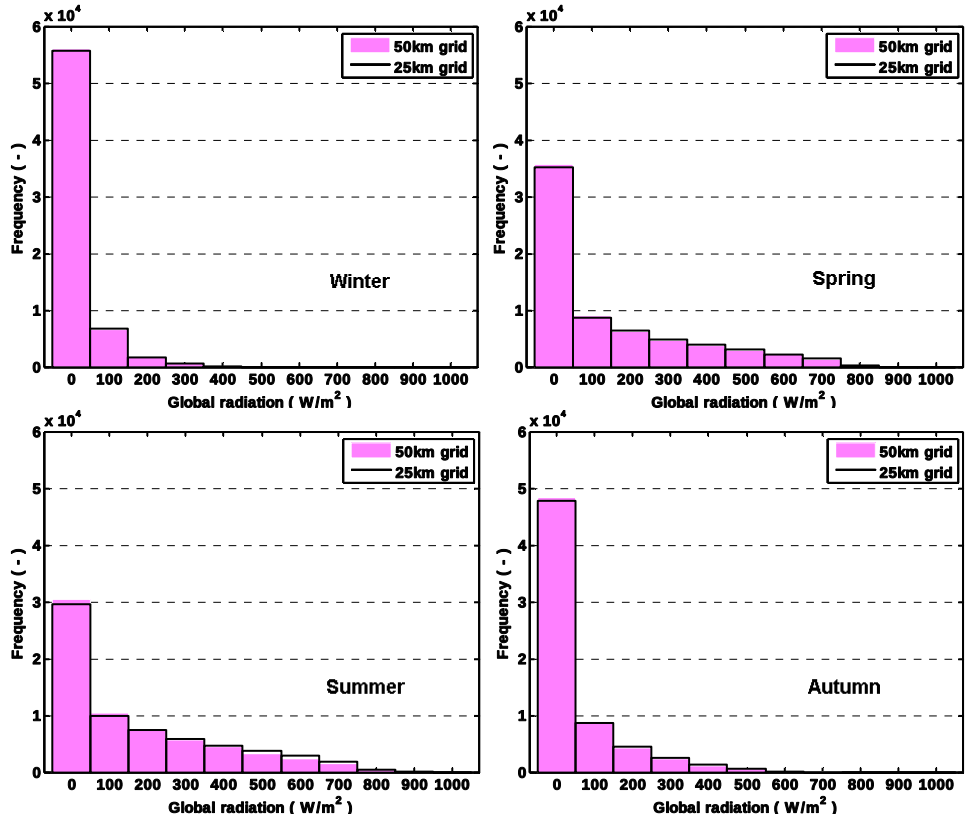

Figure 5.6. Global radiation distribution in SCN for two spatial resolutions in RCA3-ECHAM5-A1B-3

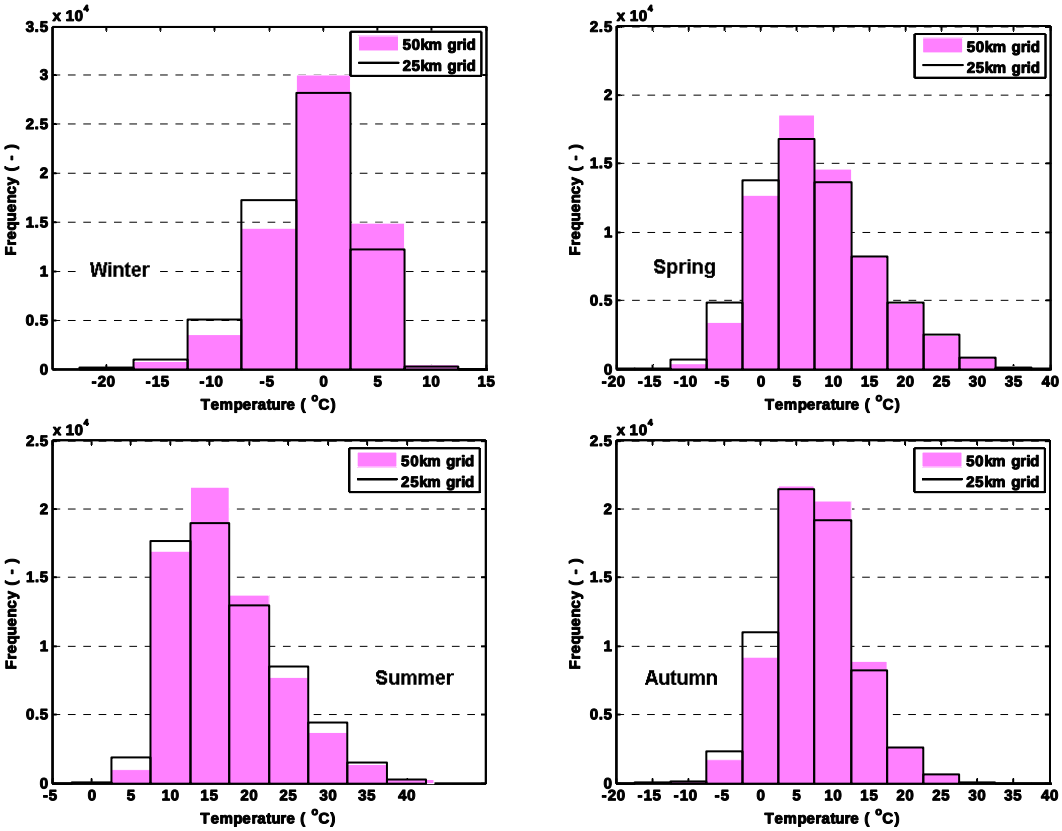

Figure 5.7. Indoor temperature in CTL for two spatial resolutions in RCA3-ECHAM5-A1B-3

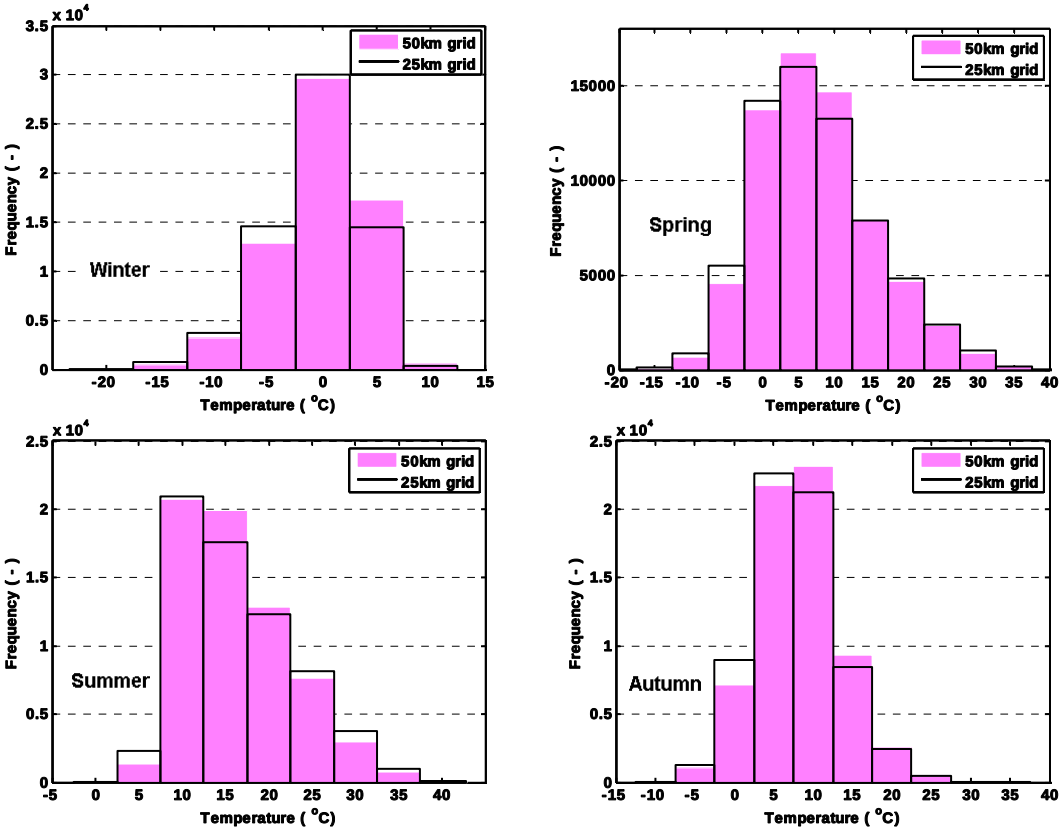

Figure 5.8. Indoor temperature in SCN for two spatial resolutions in RCA3-ECHAM5-A1B-3

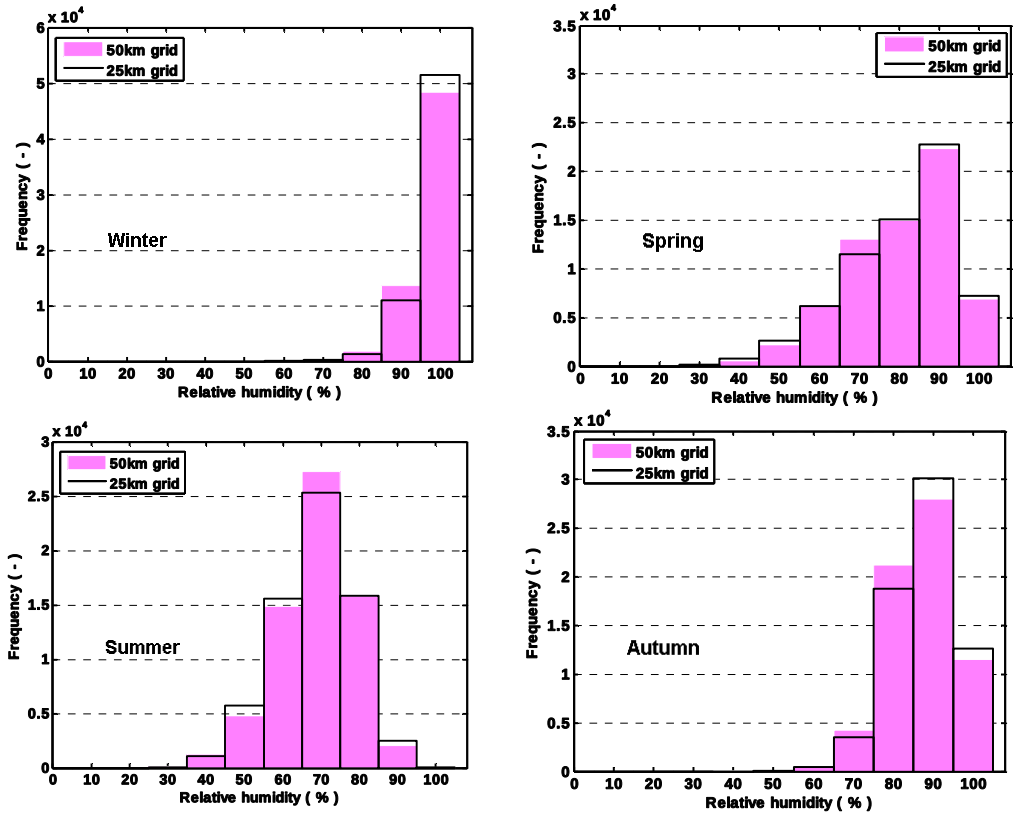

Figure 5.9. Indoor relative humidity in CTL for two spatial resolutions in RCA3-ECHAM5-A1B-3

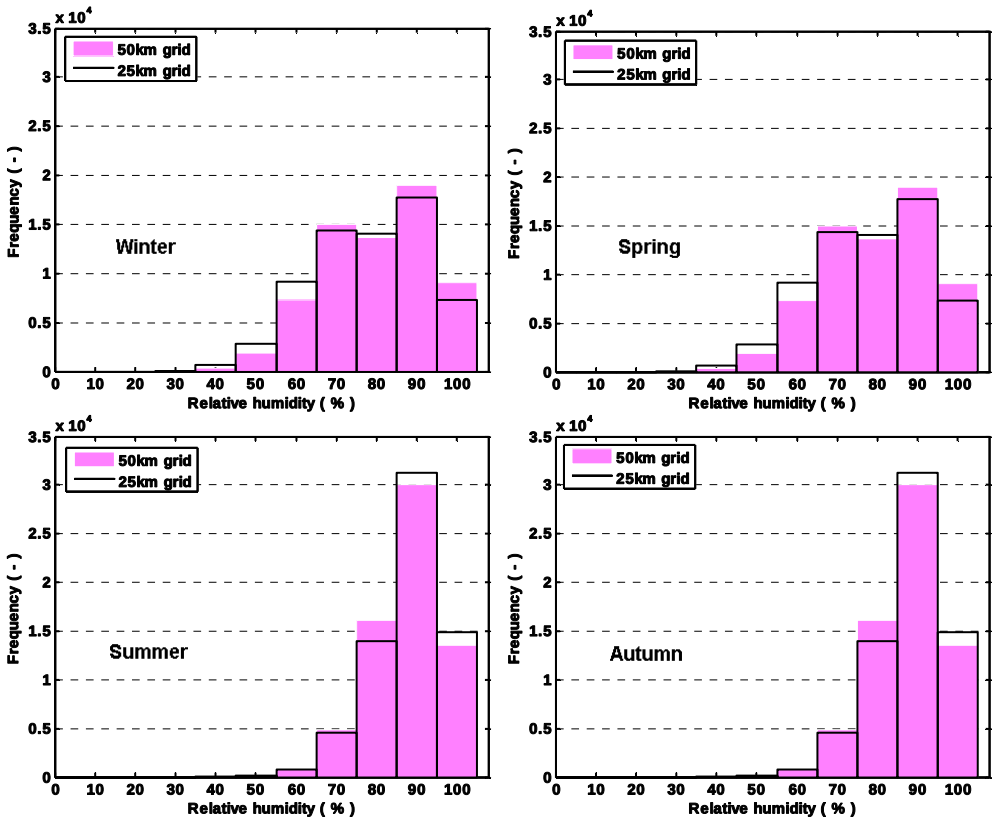

Figure 5.10. Indoor relative humidity in SCN for two spatial resolutions in RCA3-ECHAM5-A1B-3

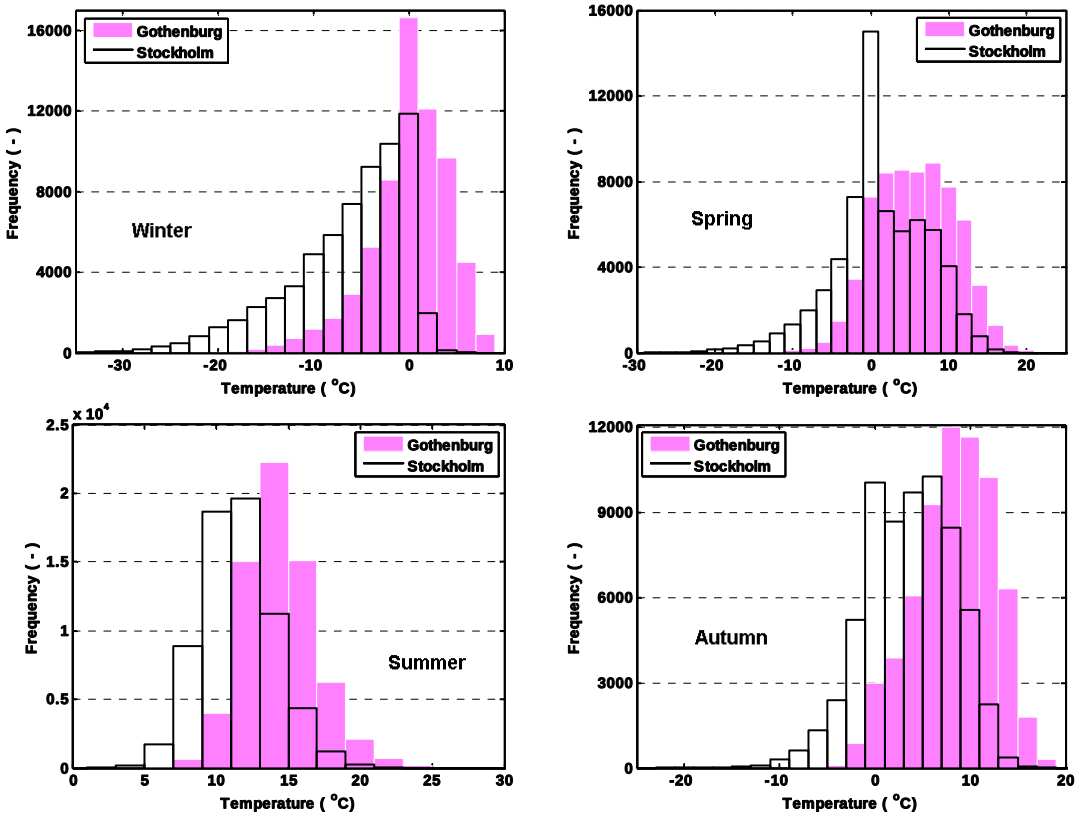

Figure 5.11. Outdoor temperature distribution during 1961-1990 (CTL) in Gothenburg and Stockholm for the spatial resolutions of 50km in RCA3-ECHAM5-A1B-3

Figure 5.11 shows how the histogram looks when the two data sets are really different. Here the outdoor temperature during 1961-1990 has been illustrated for two cities of Gothenburg and Stockholm. These cities have different climate conditions which is completely visible in the figures.

5.2. Boxplot

Boxplot, which is a robust nonparametric statistical model, has been described in section 4.1. Temperature and relative humidity of the outdoor and indoor climate for different time periods are compared using boxplot to investigate the differences between different resolutions (scales) and locations. The investigation is done using two resolutions of RCA3-ECHAM5-A1B-3.

We can get a general view of the data in the whole period of 140 years. This a very rough comparison of the data sets. According to the definition whishker extend to at most 1.5 times the box width. Accepting this definition results in having some values as outliers which are physically possible to happen.

In the first step it is necessary to know how much is the difference between four 25km-grids. Figures 5.12 and 5.13 show temperature and relative humidity of the outdoor and indoor climate in four different grids related to RCA3-ECHAM5-A1B-3. There is not a big difference between the four

neighbor-girds. There are some slight differences in medians, quartiles, whiskers and outliers. It is reasonable to have these differences in grids with different locations.

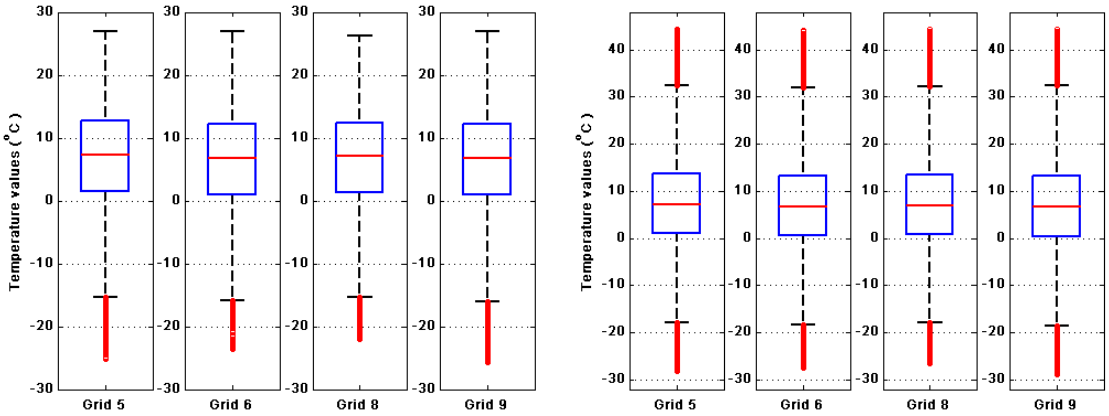

Figure 5.12. Temperature distribution in the four 25km grids of Gothenburg during 1961-2100, left: outdoor, right: indoor

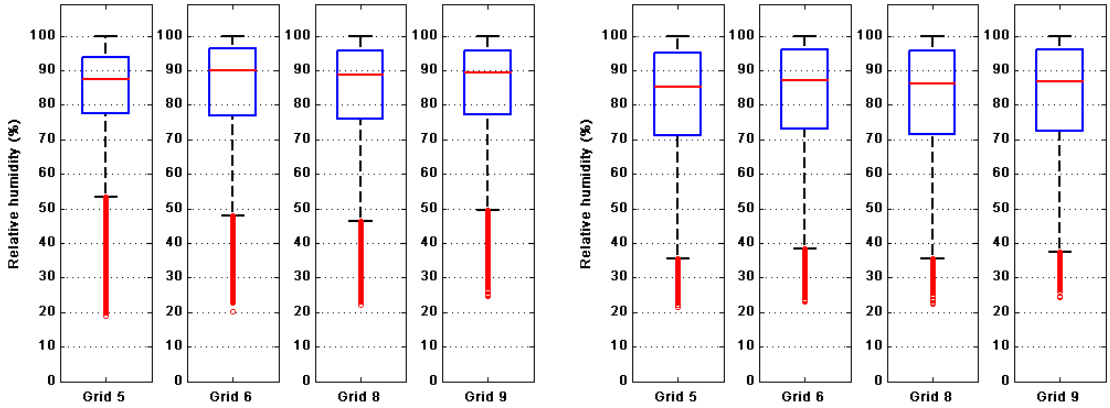

Figure 5.13. Relative humidity distribution in the four 25km grids of Gothenburg during 1961-2100, left: outdoor, right: indoor

Figures 5.14 and 5.15 compare 25km spatial resolution with the 50km resolution. Figures show that the total distributions of the temperature and relative humidity in the period of 140 years inside and outside the attic are very alike for both the resolutions. It is necessary to remember that the four 25km grids are the closest grids to the 50km grid but they are not exactly covering the 50km grid. We should expect some small differences. The differences might be generated by location shift or resolution alteration. The boxplots tell us roughly about the range of data sets. At this level the figures show that the different resolutions are adjusted together.

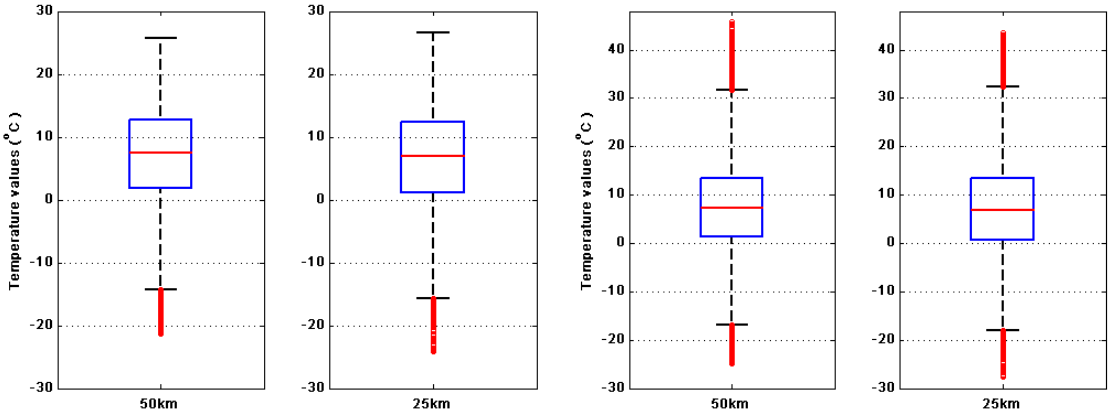

Figure 5.14. Temperature distribution of the average of four 25km grids and the 50km grid in Gothenburg during 1961-2100, left: outdoor, right: indoor

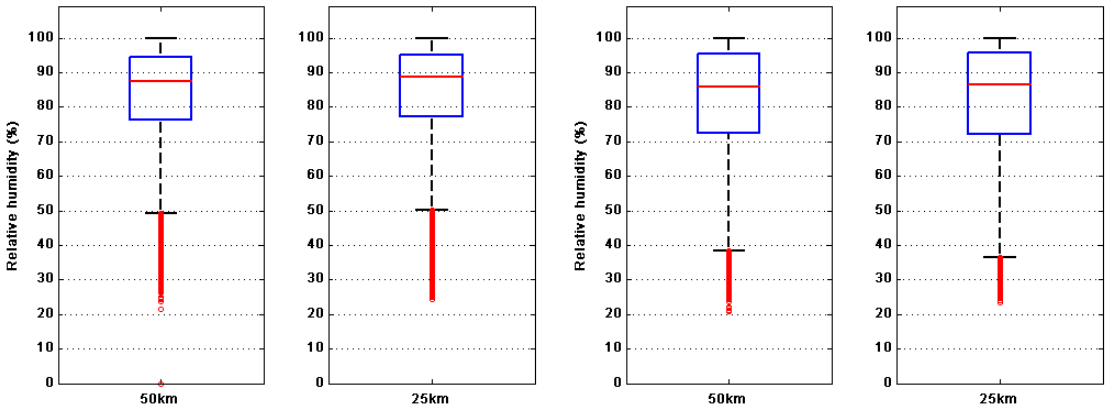

Figure 5.15. Relative humidity distribution of the average of four 25km grids and the 50km grid in Gothenburg during 1961-2100, left: outdoor, right: indoor

Using boxplot helps to compare the climate conditions in different cities rapidly. For example by looking at figures 5.16 and 5.17 we can see the difference between Stockholm and Lund. Lund has a warmer and drier weather. These figures also confirm the idea of using boxplots for illustrating the differences between large sets of data. There is obvious location difference between four cities. The effect of location difference is visible in the following figures. Having these differences also assures us about different resolutions and having small alterations there.

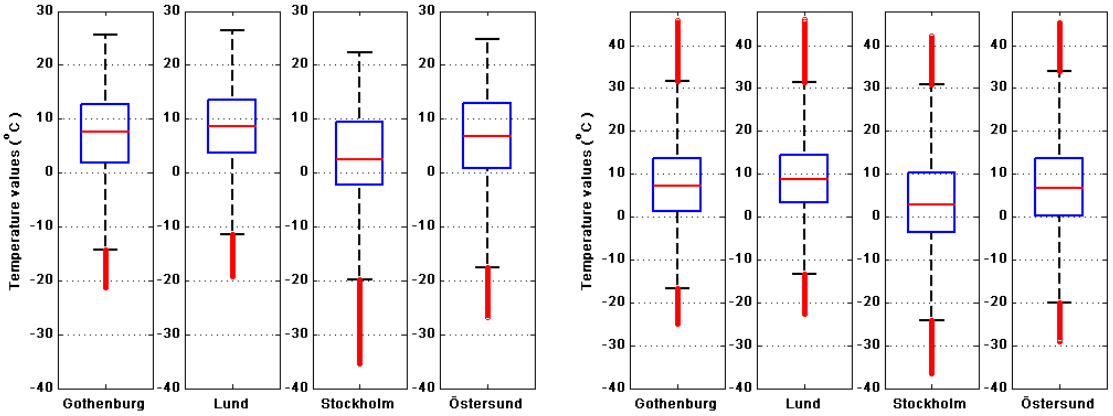

Figure 5.16. Temperature distribution in four cities for the 50km grid during 1961-2100, left: outdoor, right: indoor

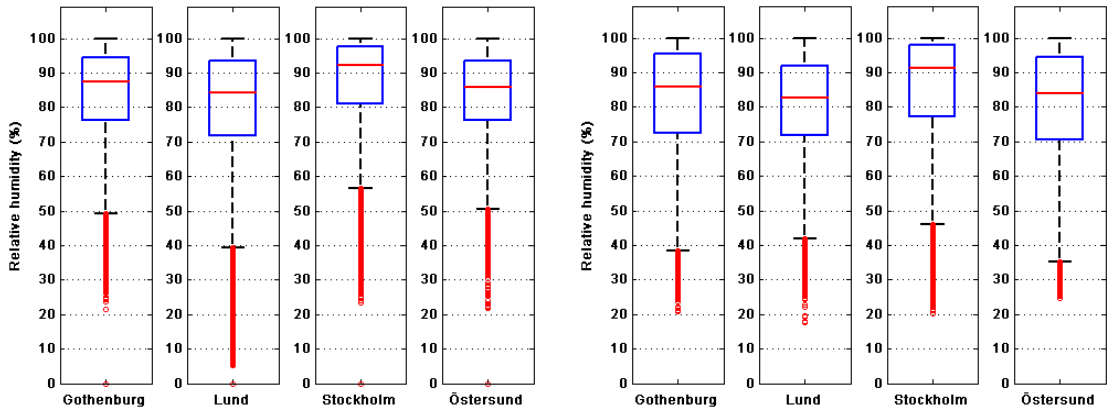

Figure 5.17. Relative humidity distribution in four cities for the 50km grid during 1961-2100, left: outdoor, right: indoor

It is possible to increase the accuracy of this kind of nonparametric comparison by decreasing the time period. For example the following figures compare the two resolutions for different seasons in two time periods, 1961-1990 (CTL) and 2071-2100 (SCN).

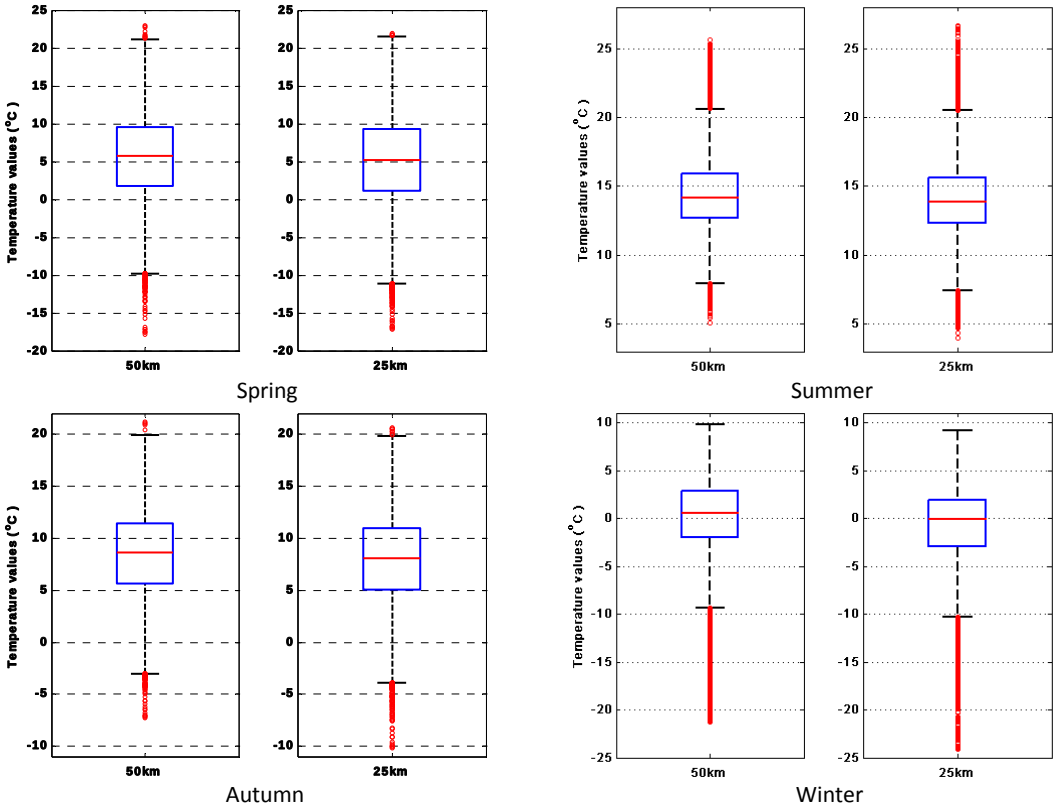

Figure 5.18. Outdoor temperature distribution of the average of four 25km grids and the 50km grid in Gothenburg in four seasons during 1961-1990.

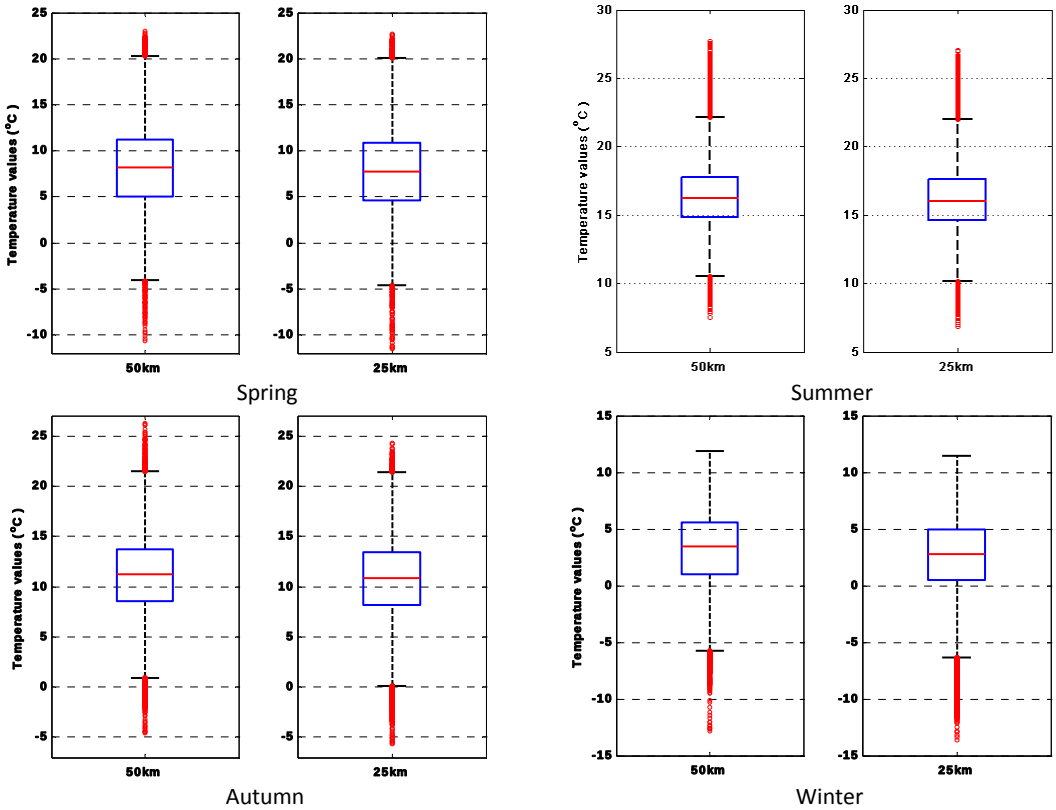

Figure 5.19. Outdoor temperature distribution of the average of four 25km grids and the 50km grid in Gothenburg in four seasons during 2071-2100.

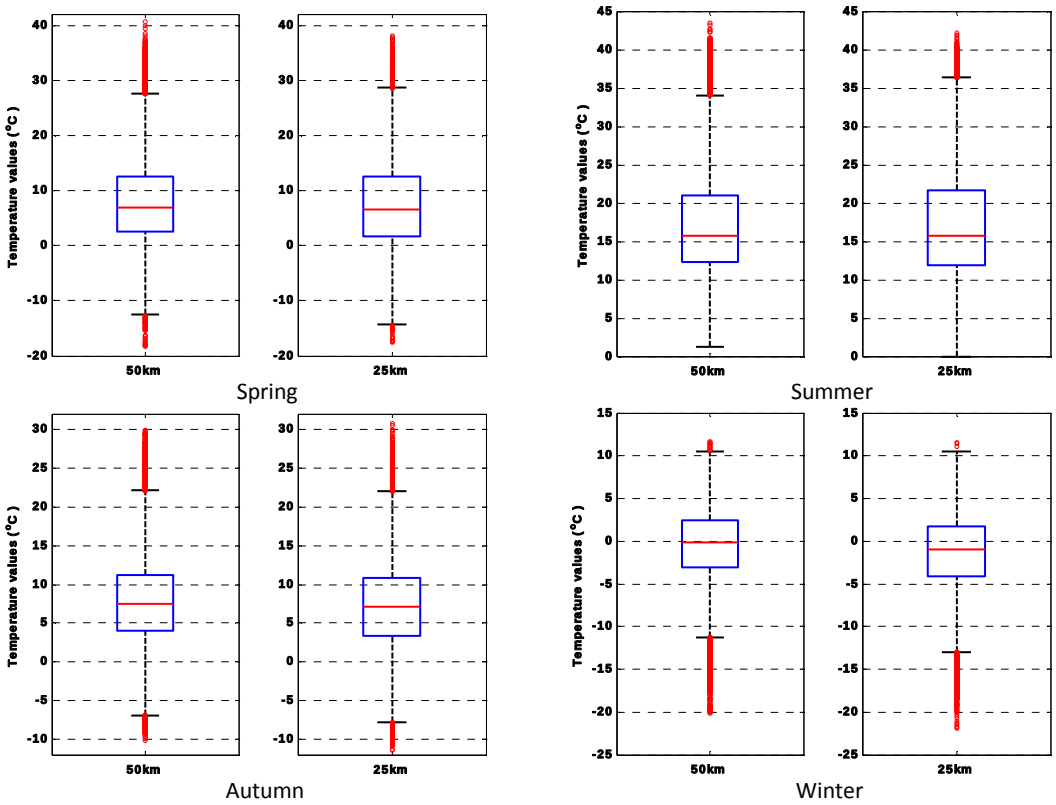

Figure 5.20. Indoor temperature distribution of the average of four 25km grids and the 50km grid in Gothenburg in four seasons during 1961-1990.

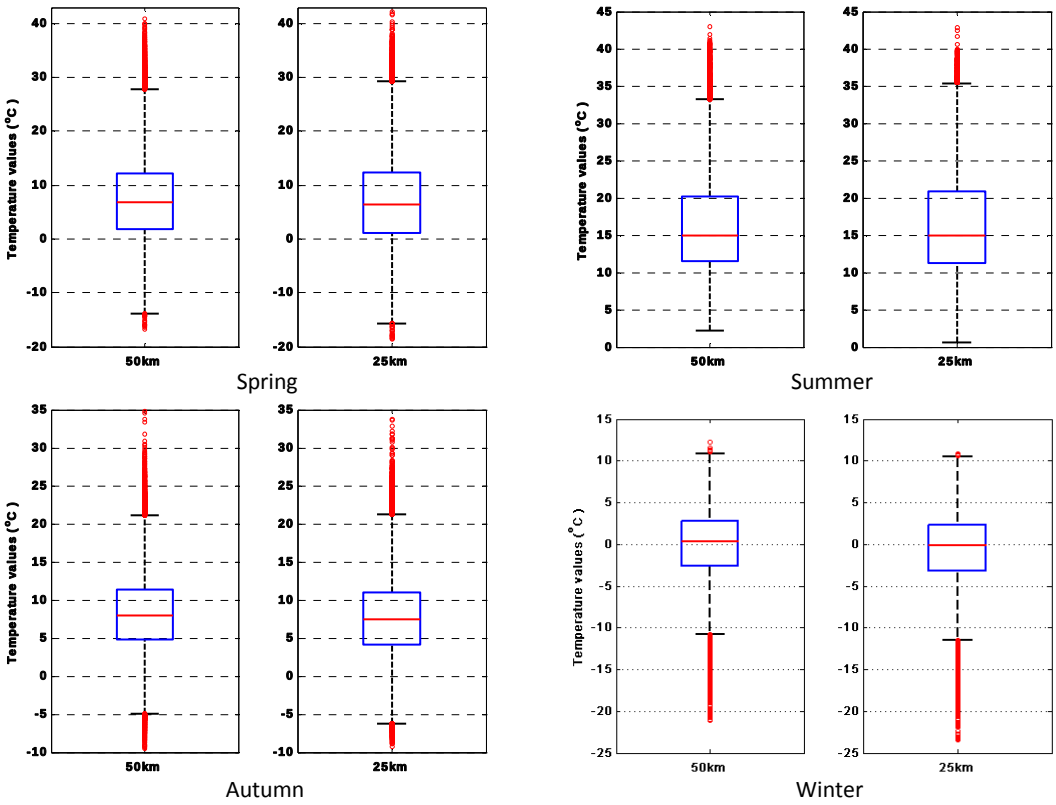

Figure 5.21. Indoor temperature distribution of the average of four 25km grids and the 50km grid in Gothenburg in four seasons during 2071-2100.

5.3. The Ferro hypothesis

Ferro et al. presented a simple nonparametric method based on quantiles for exploring and comparing differences in pairs of probability distribution functions (Ferro et al. 2005). The method has been described in section 4.2. The method checks if the changes are due to the shifts in location, scale or both. Changes in location and scale are often measured by sample means and variances, respectively.

There are some parametric statistical tests for checking the similarity of distribution of weather variables like; T test for equality of means which is unable to detect changes in scale and the F test for equality of variances which is unable to detect changes in location (Von Storch & Zwiers 2001).

In this section the Ferro hypothesis has been applied for comparing two different spatial resolutions of data. At the first step we need to calculate the quantiles of the data distribution. In this work 100 quantiles, from 0.01 to 1 with the step of 0.01, have been calculated by coding in the Matlab software. The cumulative distribution function (CDF) of the data, e.g. temperature, is divided into 100 equal parts and the 100 corresponding quantiles are calculated. The median, Interquartile range and Yule-Kendall skewness are calculated using relations (4.2) to (4.4). These values are used to apply the Ferro hypothesis according to relation (4.5). H_0, H_s, H_L and H_{LS} are calculated. Plotting these results and comparing them with the quantile-quantile graph of the 25km and 50km resolutions helps to investigate the differences and similarities of the two resolutions. Results are described in the following. The data with the 25km spatial resolution are the mean values of four 25km grids corresponding to the analyzed 50km gird.

5.3.1. The quantile-quantile plots

In the following figures the data with the 50km resolution have been assumed as the first parameter (related to the values on the X-axis).

In Figure 5.22 the temperature distribution for the spatial resolutions of 25km and 50km are compared together using the Ferro hypothesis. Temperature values are for Gothenburg during spring in the period of 1961-1990.

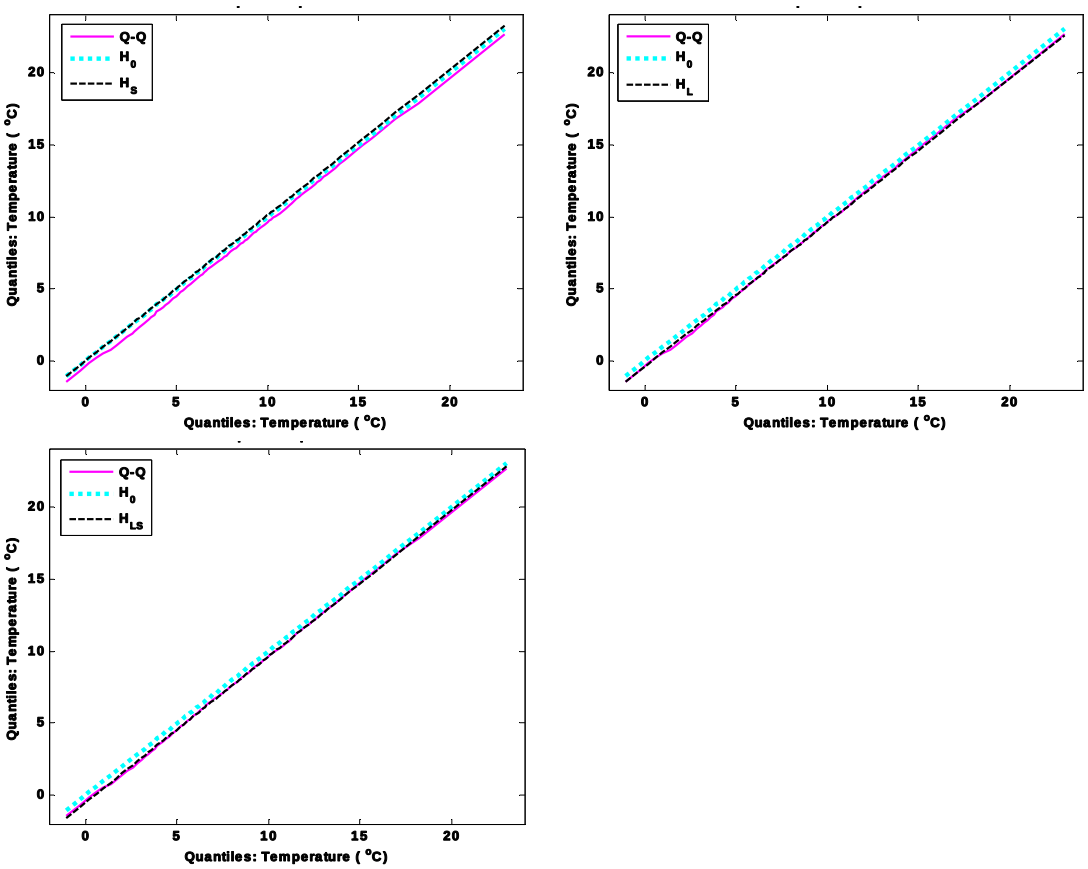

Figure 5.22. Comparison of outdoor temperature distribution in spring for two spatial resolutions of 25km and 50km during 1961-1990 for RCA3-ECHAM5-A1B-3.

The X-axis values of the all the figures are the 100 quantiles of the first parameter. The Q-Q line is the calculated 100 quantiles of the first parameter, e.g. temperature of the 50km resolution, versus 100 quantiles of the other parameter, e.g. temperature of the 25km resolution. The H_o line is the 100 quantiles of the first parameter versus itself. So it is a straight line with the slope of 45 degrees. In the ideal case when the two sets of data are the same the Q-Q and H_o lines are coincident which means the distribution of the data sets are exactly the same.

In the upper left box in the Figure 5.22 the H_S line is the 100 quantiles of the first parameter, 50km resolution, versus the rescaled values of the same parameter. The scale factor is the ratio of interquartile ranges of the two sets of data (S_{25km}/S_{50km}). The interquartile range is a measure for the size of the box in the boxplot. For example when there are two sets of data, in the one with the bigger interquartile range the 50% of the data has been distributed in a wider range. So it will have a bigger box in the boxplot comparing to the data set with smaller interquartile range. The H_S line tells how much the distribution of the 50km data would be different if the interquartile range was equal to the 25km inter quartile range.

In the figure showing the H_L line, upper right in Figure 5.22, the Y-axis values are calculated by subtracting the median of the 50km grid from the X-axis values and adding the median of the 25km resolution as described by the corresponding y_p in relations (4.5). Comparison of this line H_o line shows how having the median of 25km will affect the 50km distribution. In other words the dislocation of the H_L line comparing with H_o line emphasizes the difference in medians between the two sets of data. For example it tells how much the location of the box will be shifted in the boxplot by changing the median of the 50km data set with the 25km.

The distribution of the 50km data set has been affected by both the scale and location factors in the H_{LS} line. It is shown in Figure 5.22, bottom. It shows that by rescaling the interquartile range and shifting the median of the 50km data set, using the factors corresponding to the 25km data set, the quantile-quantile plot of the new distribution of the 50km data set (H_{LS}) almost matches the quantile-quantile plot of the 50km and 25km girds (the Q-Q line). It means that if the values of two data sets were exactly the same but one of them (50km) had the scale and location factors of the other one (25km), then the quantile-quantile plot (Q-Q line) would be H_{LS}. We know that the 50km and 25km data sets are equal in size and they are distributed almost in the same span. Matching of the H_{LS} and Q-Q assures us about having very similar distribution in the 25km and 50km sets of the data. The differences between two sets of data are mostly on the tails which correspond to the extreme values of the data which also have the lower probability. Usually the tail values are corresponding to the outliers in the boxplot.

Comparing the H_{LS} plot in Figure 5.21 with the boxplots reveals some information about the differences between two resolutions and differences between the methods of comparing data sets. In Figure 5.22 the difference between the H_{LS} line and H_o starts to increase from temperature around 18 degrees. According to the other graphs in Figure 5.22 the difference is more caused by the scale difference. Boxplot does not show such information about the data sets.

Applying the Ferro hypothesis for comparing different resolutions of the data is very useful. Beside of having a good view of the data distribution by using quantile and increasing the accuracy of the comparison, the method tells about the source of the difference; scale or location.

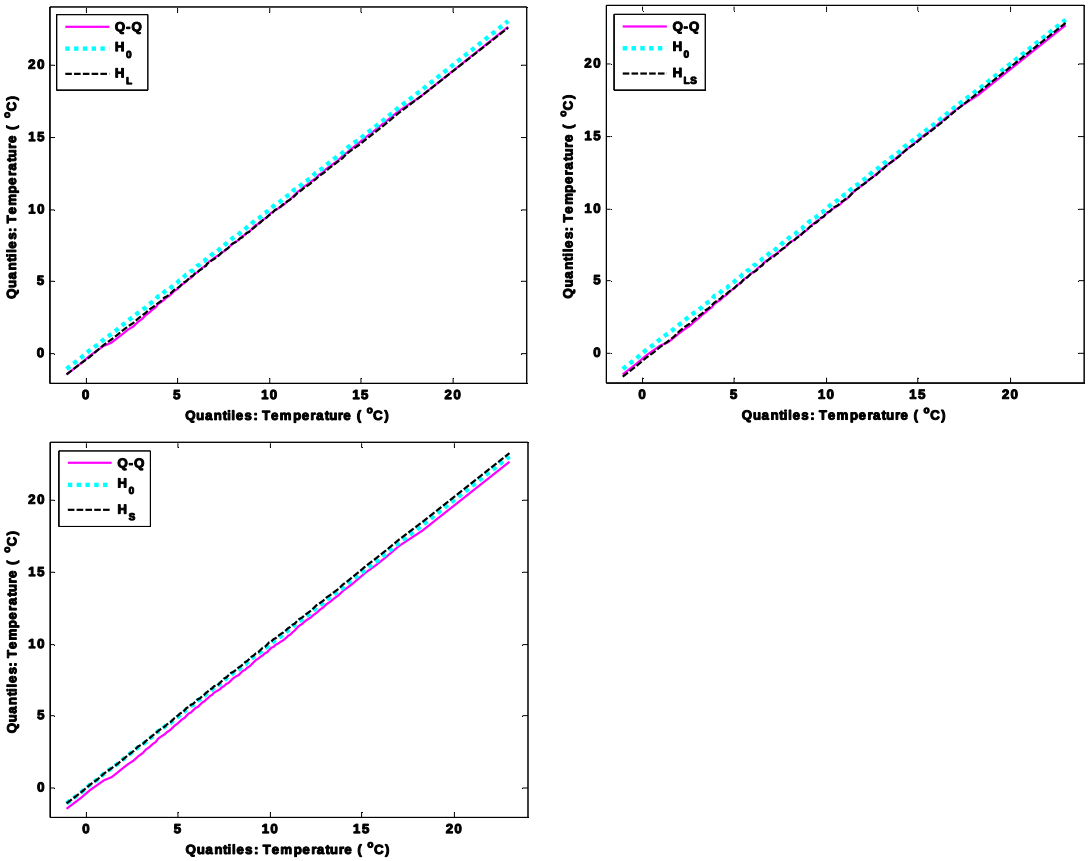

Figure 5.23. Comparison of outdoor temperature distribution in spring for two spatial resolutions of 25km and 50km during 2071-2100 for RCA3-ECHAM5-A1B-3.

Figure 5.23 makes the same comparison using Ferro hypothesis for the spring temperature distribution in Gothenburg during 2017-2100. The coincidence of the H_{LS} and Q-Q lines confirms the similarity of the data sets. The small offset of the Q-Q line between 0°C and 5°C is caused by the location differences according to the H_L and Q-Q lines.

In the following some other data sets are compared for different resolutions using the Ferro hypothesis. Here we compare the location and scale shifts together by showing H_{LS} and Q-Q lines. The largest difference between the 50km and 25km data happens in Stockholm.

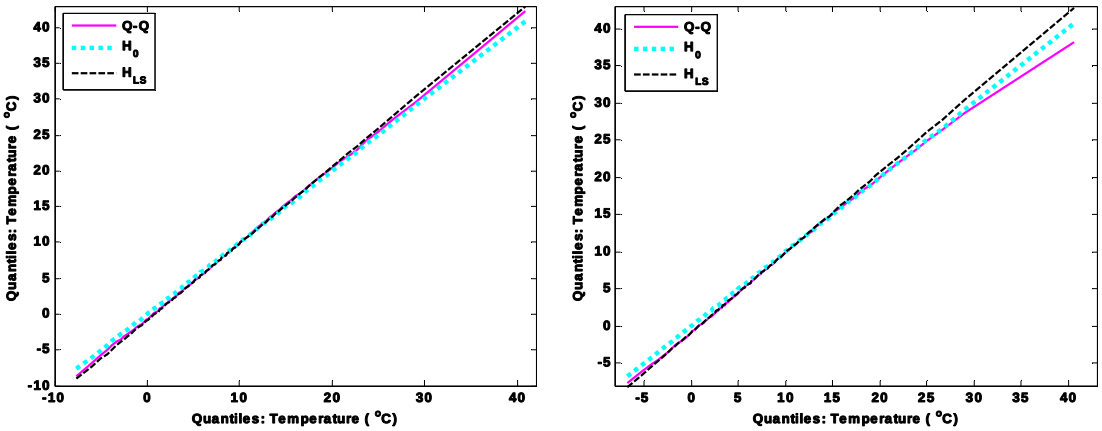

Figure 5.24. Comparison of indoor temperature distribution in spring for two spatial resolutions of 25km and 50km during CTL (left) and SCN (right) periods for RCA3-ECHAM5-A1B-3.

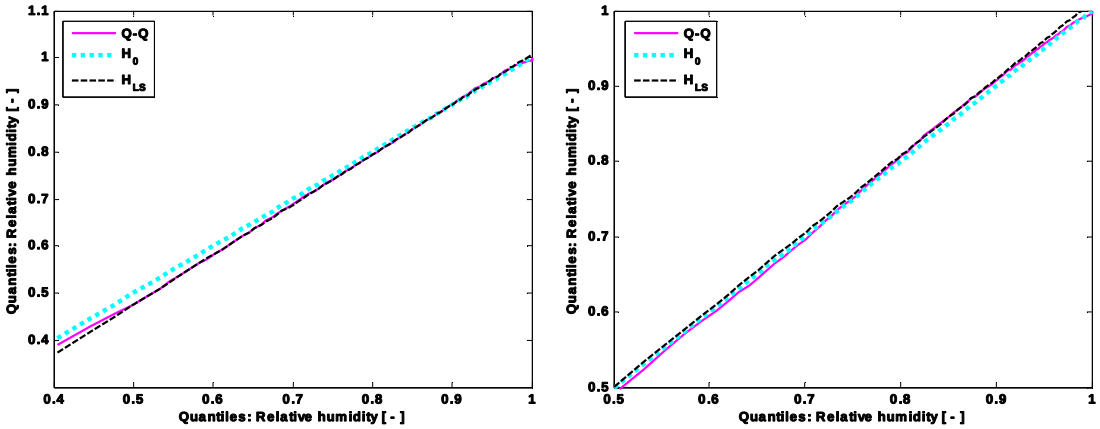

Figure 5.25. Comparison of outdoor relative humidity distribution in spring for two spatial resolutions of 25km and 50km during CTL (left) and SCN (right) periods for RCA3-ECHAM5-A1B-3.

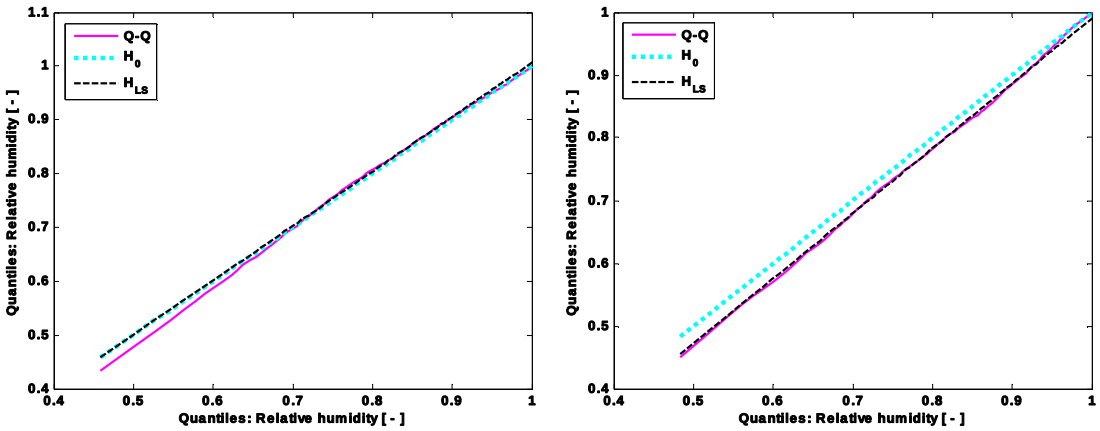

Figure 5.26. Comparison of indoor relative humidity distribution in spring for two spatial resolutions of 25km and 50km during CTL (left) and SCN (right) periods for RCA3-ECHAM5-A1B-3.

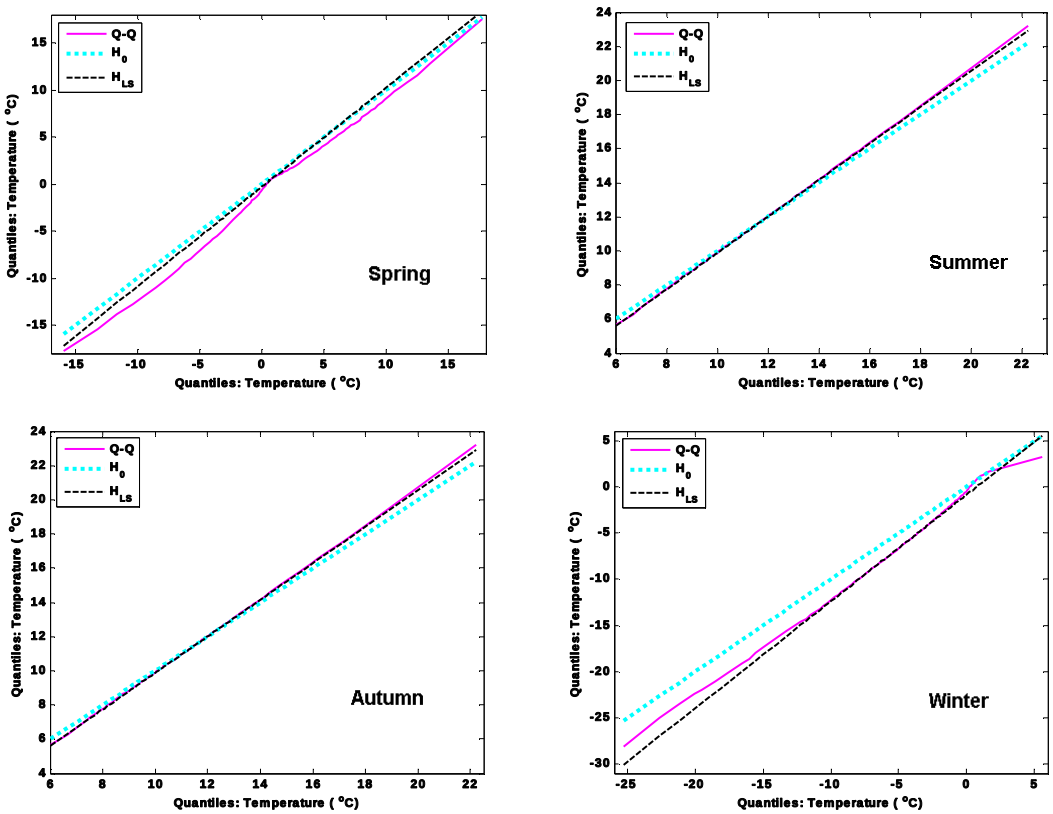

Figure 5.27. Comparison of outdoor temperature distribution in Stockholm for two spatial resolutions of 25km and 50km during CTL period for RCA3-ECHAM5-A1B-3.

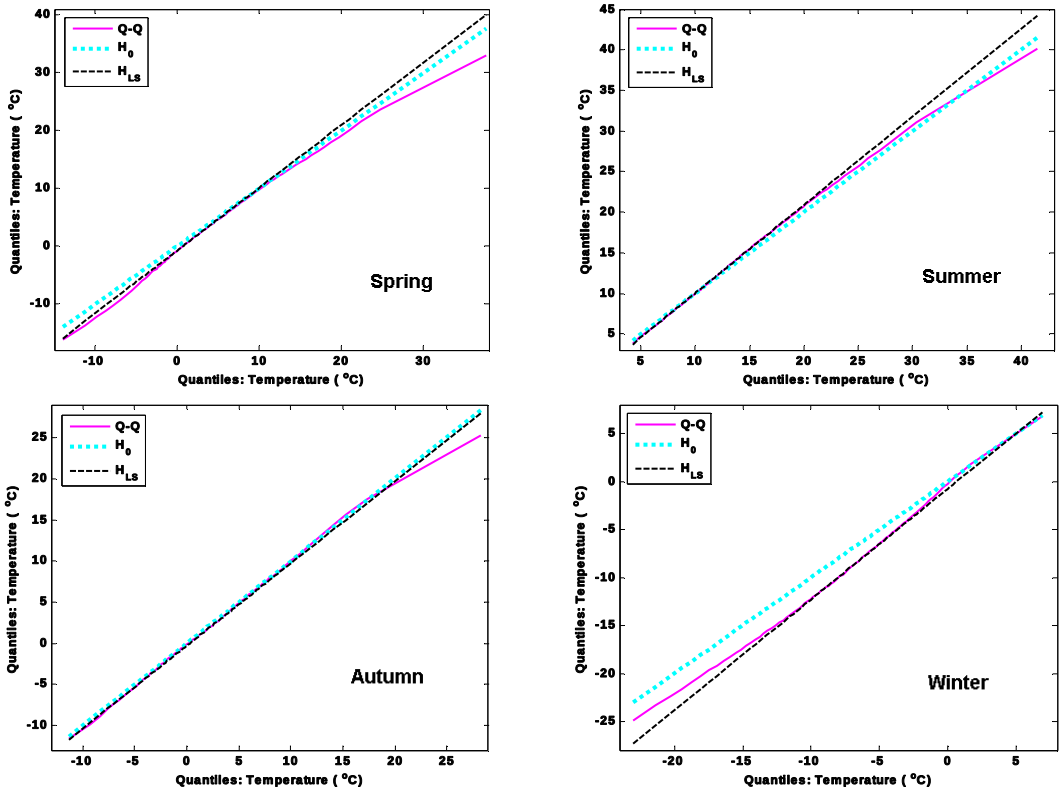

Figure 5.28. Comparison of indoor temperature distribution in Stockholm for two spatial resolutions of 25km and 50km during CTL period for RCA3-ECHAM5-A1B-3.

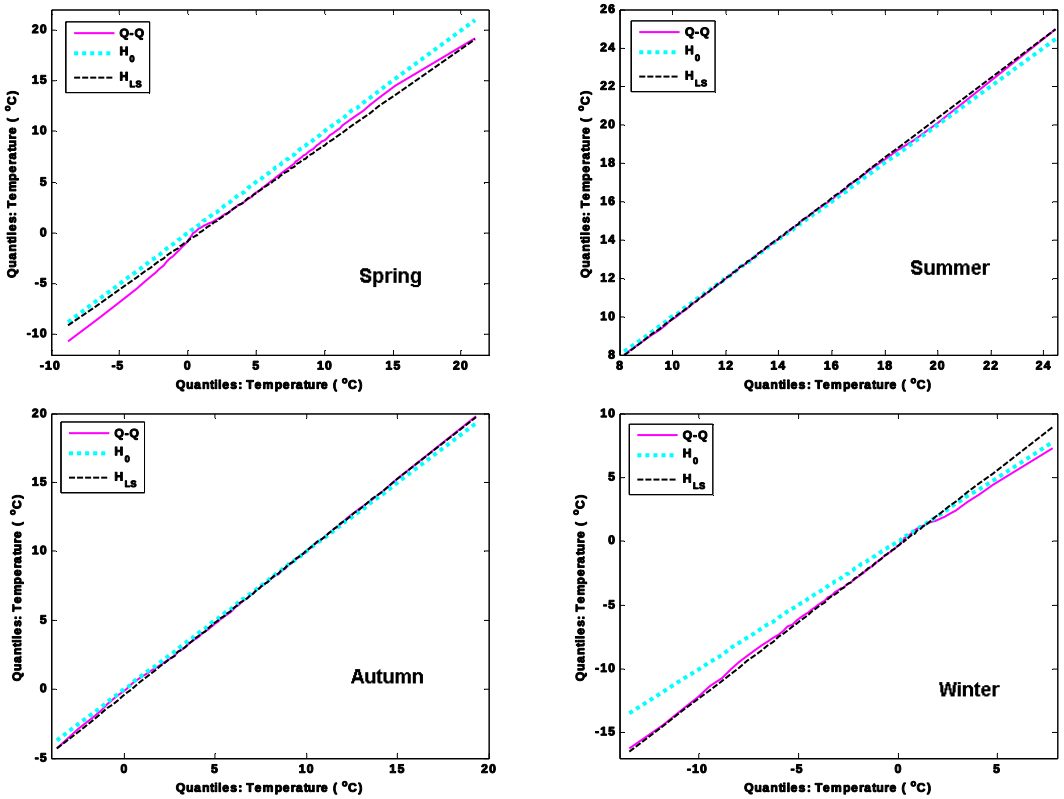

Figure 5.29. Comparison of outdoor temperature distribution in Stockholm for two spatial resolutions of 25km and 50km during SCN period for RCA3-ECHAM5-A1B-3.

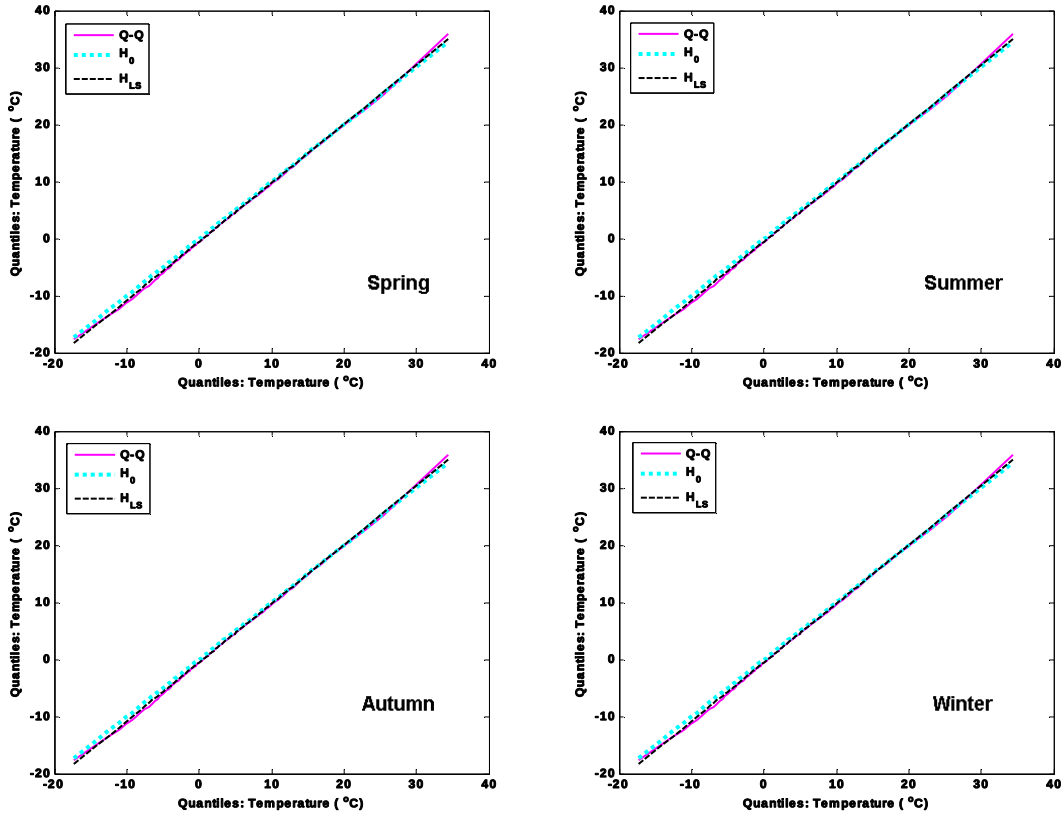

Figure 5.30. Comparison of indoor temperature distribution in Stockholm for two spatial resolutions of 25km and 50km during SCN period for RCA3-ECHAM5-A1B-3.

6. Global Climate Models

One of the future climate uncertainties is uncertainties related to the global climate model (GCM). Most of the weather data that have been used in this project are from the ECHAM5 global climate model, but there are some other weather data which have been used for checking the effects of having different GCMs. In this chapter simulation results of these GCMs are considered: CCSM3, CNRM, ECHAM5 and HadCM3. These global climate models have been described in section 2.3.

All the weather data from different GCMs have been extracted with the spatial resolution of 50km using RCA3. The emission scenario and initial conditions are the same for all the GCMs; A1B_3. Hygro-thermal responses of the attic have been analyzed in the city of Stockholm in different seasons. The period of the simulations is 1961-2100. Results are mainly considered for the periods of 1961-1990 (CTL) and 2071-2100 (SCN).

The outdoor and indoor climates have been compared for different GCMs using the nonparametric and parametric methods. The parametric method is decomposition of parameters and their variabilities which has been described in chapter 3. For the CTL period the GCMs have been also compared with the ERA40 which can be used as a reference.

Looking into differences of the GCMs and comparing the indoor and outdoor climate helps in understanding the sensitivity of the simulation results to different GCMs. It helps to make more general conclusions for the future performance of buildings.

In section 6.1 the indoor and outdoor climate are compared using boxplots and quantile plots. Section 6.2 compares decomposition components of the temperature, relative humidity and global radiation. It is followed by comparing the indoor and outdoor variabilities for different GCMs in the CTL and SCN periods.

Paper V concerns about the same subject during autumn in Stockholm.

6.1. Nonparametric comparison of GCMs

It is interesting to see how much having different global climate models affects the weather data. In this section the outdoor and indoor climate for different global climate models are compared together using the nonparametric methods. To have a better illustration of the climate data different parameters are compared in four seasons during two periods of 1961-1990 (CTL) and 2071-2100 (SCN).

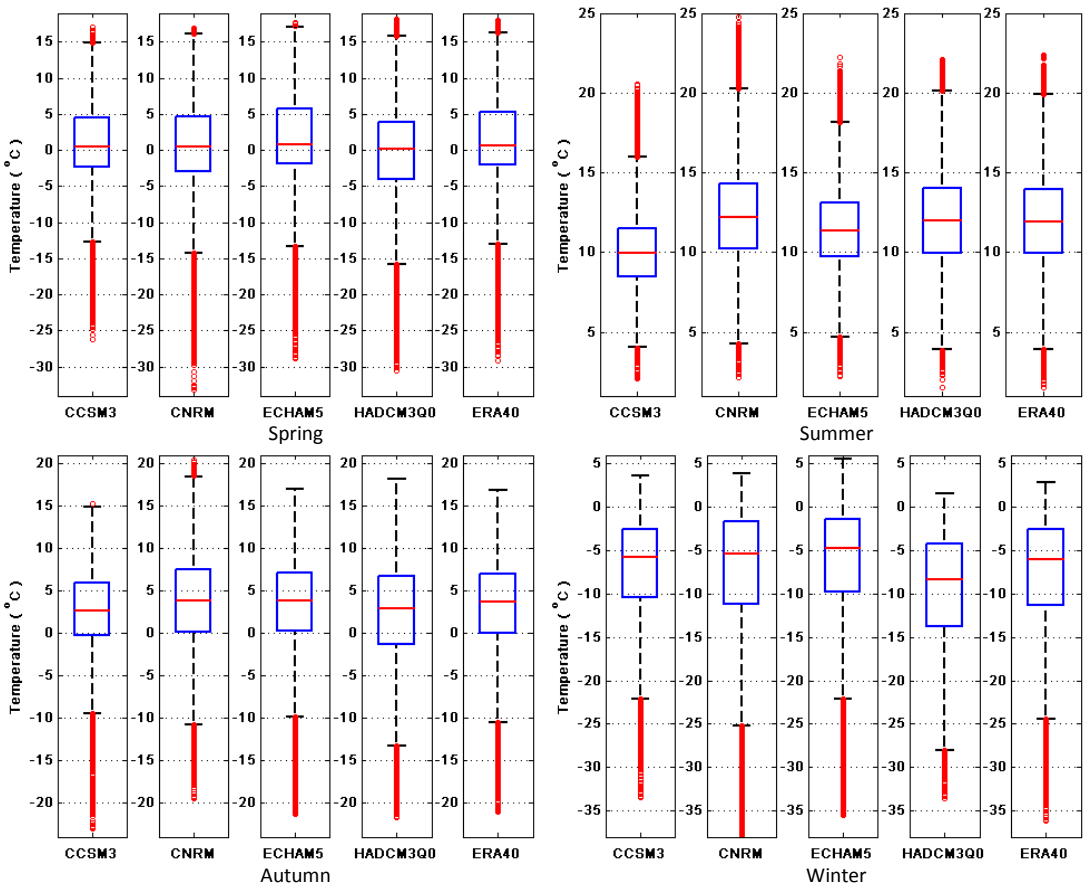

Figure 6.1. Outdoor temperature distribution in Stockholm for different GCMs during CTL period.

Figure 6.1 shows the temperature distribution of the outdoor climate in Stockholm during CTL period for different GCMs. Figure 6.2 shows the same values for inside the attic. The indoor temperature shows almost the same pattern as the outside for the differences between the GCMs. The appearance of the boxplots is almost following the same order indoor and outdoor. It tells again about the linear correlation between the indoor and outdoor temperature. Figures 6.3 and 6.4 show the outdoor and indoor temperature distribution during the SCN (2071-2100) period. The same as the CTL period there is linear correlation between the indoor and outdoor temperatures.

During the CTL period ERA40 is used as a reference.

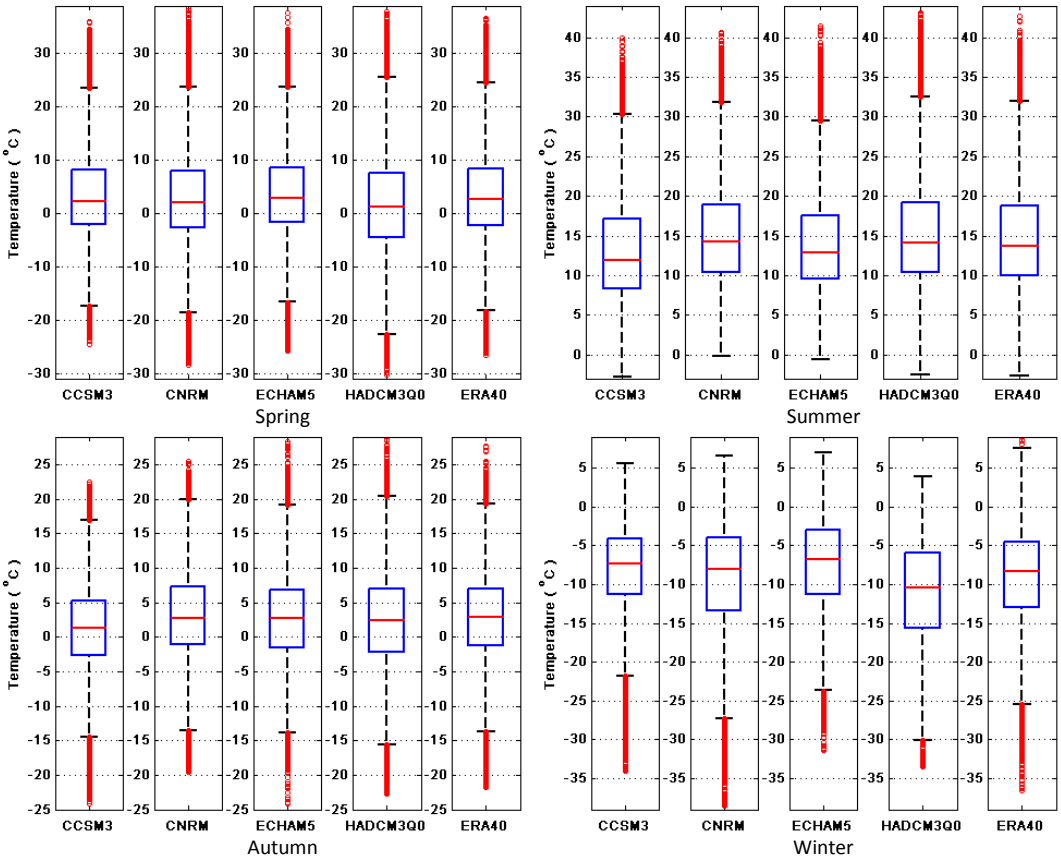

Figure 6.2. Indoor temperature distribution in Stockholm for different GCMs during CTL period.

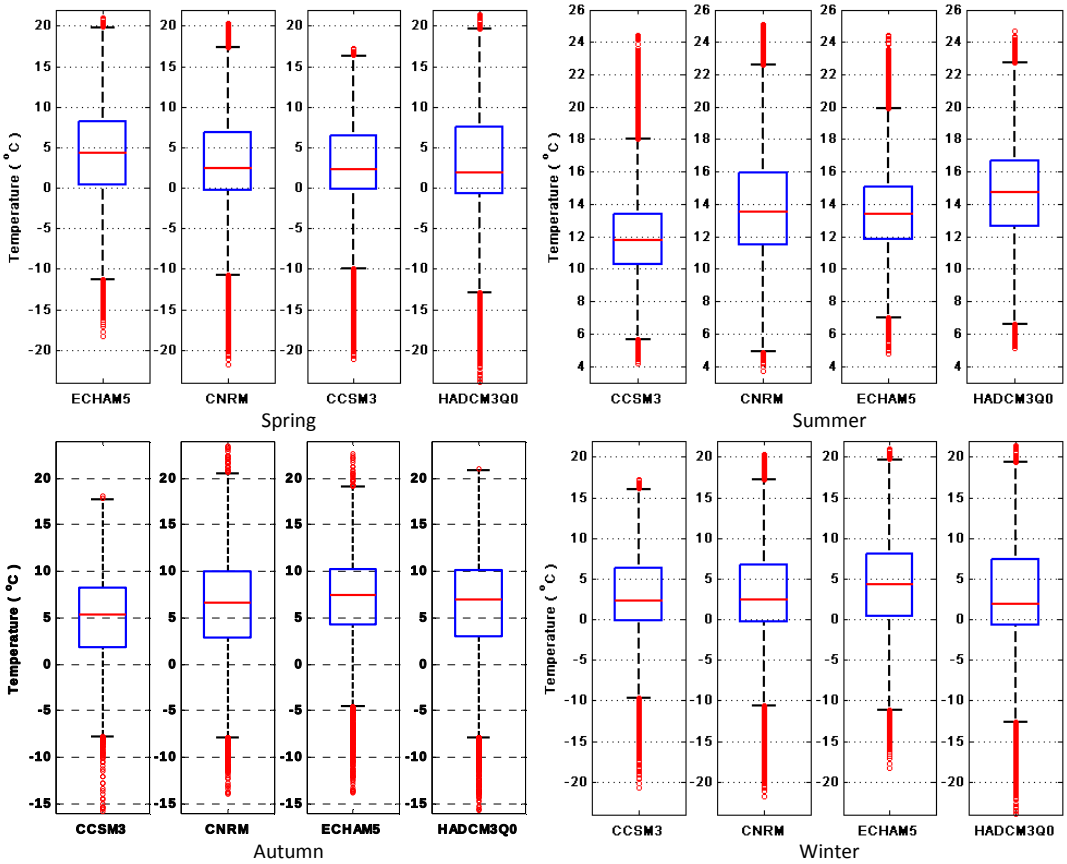

Figure 6.3. Outdoor temperature distribution in Stockholm for different GCMs during SCN period.

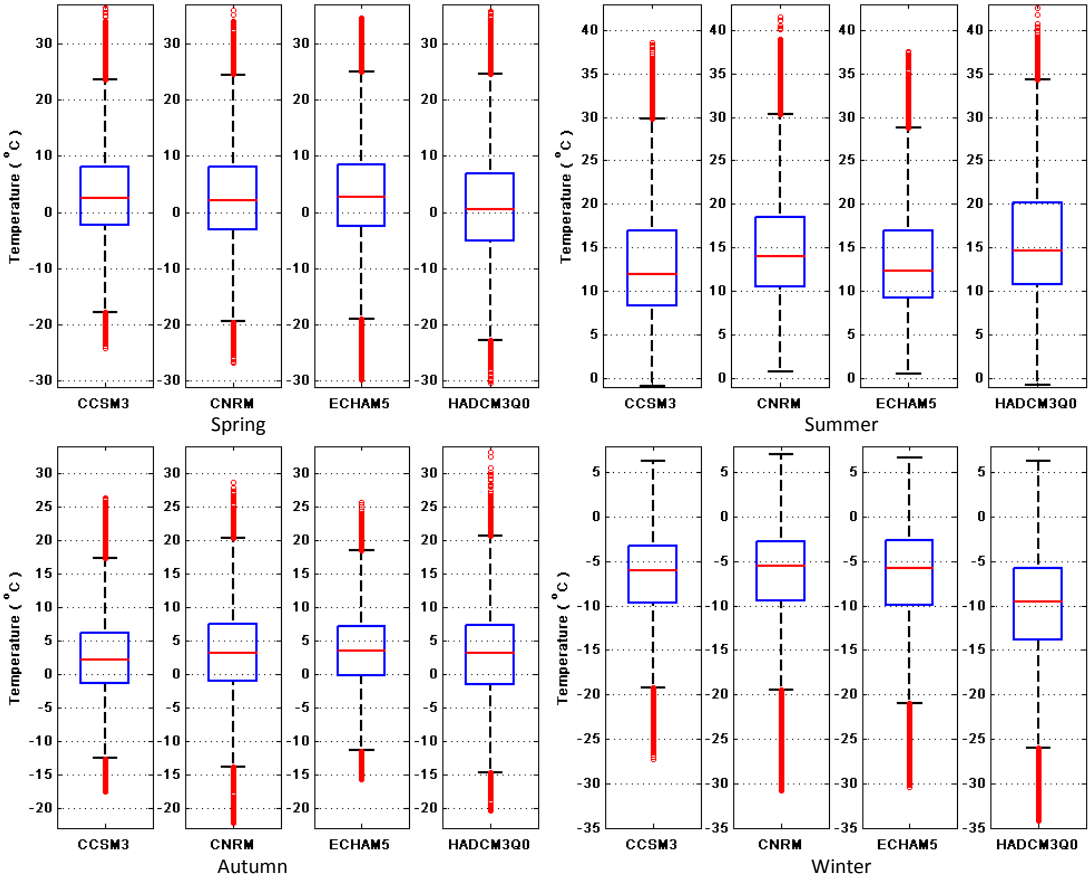

Figure 6.4. Indoor temperature distribution in Stockholm for different GCMs during SCN period.

Looking at figures 6.1 and 6.3 reveals the effects of global warming on the temperature distributions. All the global climate models show a warmer climate in the future. For example looking into summer in figures show the box has been shifted upward in the SCN period and the medians have reached to values around 2°C more than the CTL period. The pattern which the boxplots of the four GCMs make in each season during CTL is somehow repeated during the SCN period. Differences between GCMs are more visible in the coldest and warmest seasons; winter and summer. The extreme values of each model are mostly in these two periods. During both the CTL and SCN periods the HADCM global model has the widest temperature span. The whishkers show the lowest temperature in winter and highest in summer for this GCM. The indoor temperature projects the same variations inside. Looking at Figure 6.3 the ECHAM5 predicts warmer winters for the future comparing to the rest. The CCSM3 have the coolest summers during SCN the same as the CTL period.

Figures 6.5 to 6.8 show the quantile (inverse CDF) plot of the relative humidity distribution for different GCMs during two periods inside and outside the attic. Figures 6.5 and 6.7 illustrate that the GCM with the lowest relative humidity distribution during CTL excluding spring, CNRM, predicts the

lowest distribution also in the SCN period. In the same manner HADCM has a high distribution during both periods in most of the seasons.

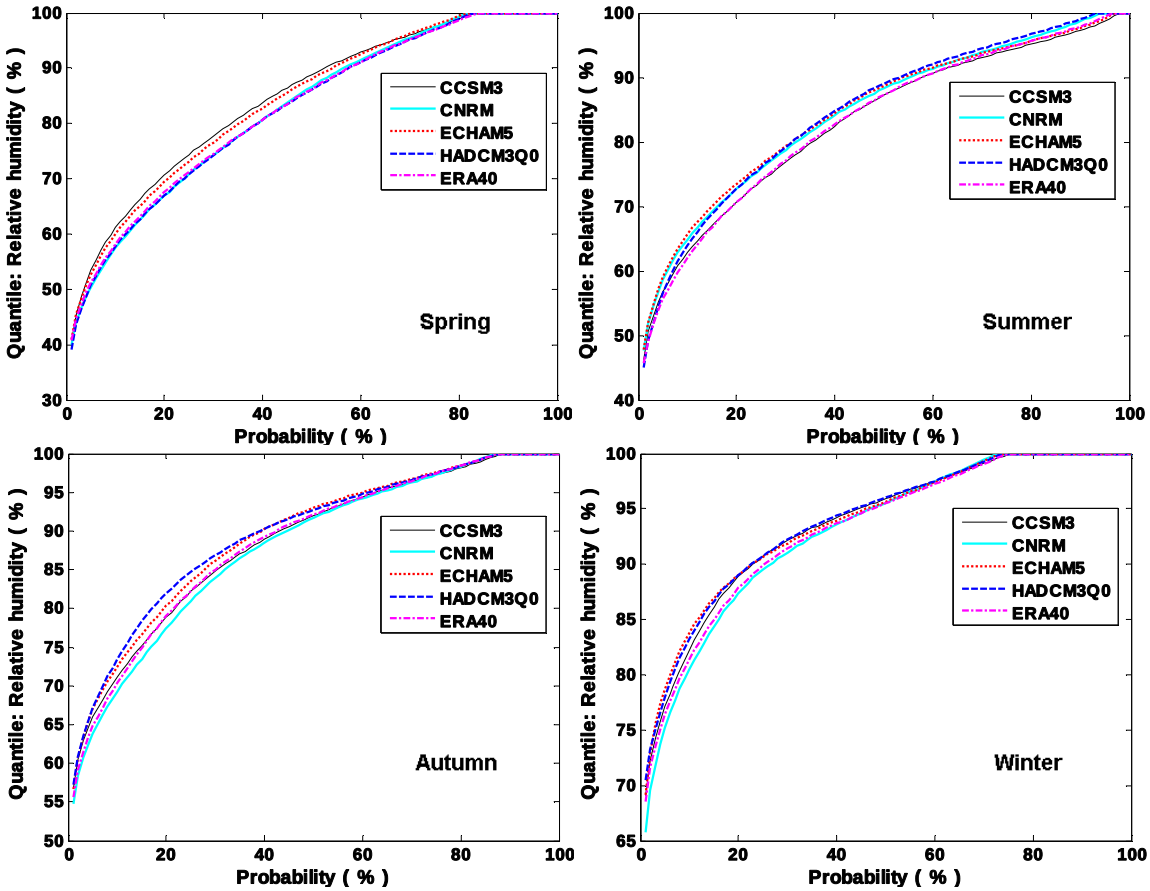

Figure 6.5. Outdoor relative humidity distribution in Stockholm for different GCMs during CTL.

But the situation is not the same inside; for example in figure 6.5 during the CTL period CNRM has the lowest values in autumn but the indoor relative humidity reaches to high values comparing to other GCMs in Figure 6.6. The indoor relative humidity is not a linear function of the outdoor.

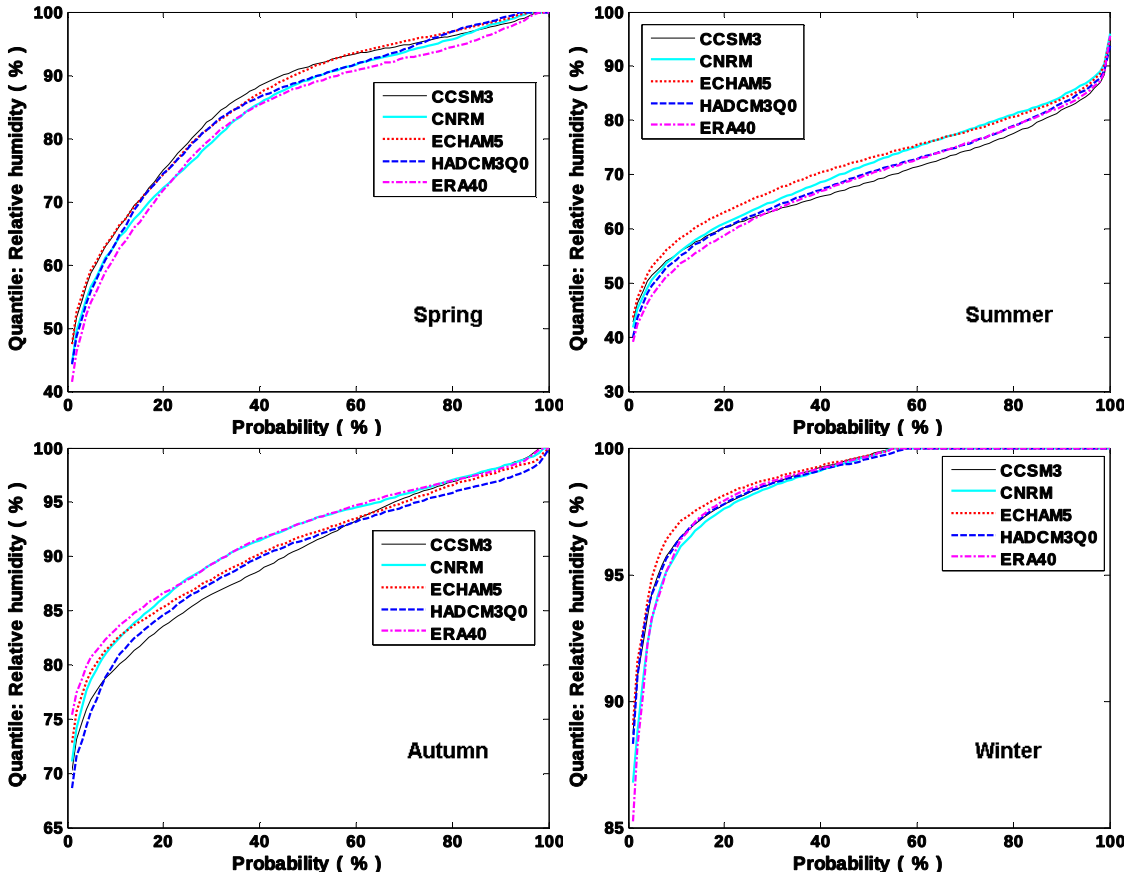

Figure 6.6. Indoor relative humidity distribution in Stockholm for different GCMs during CTL.

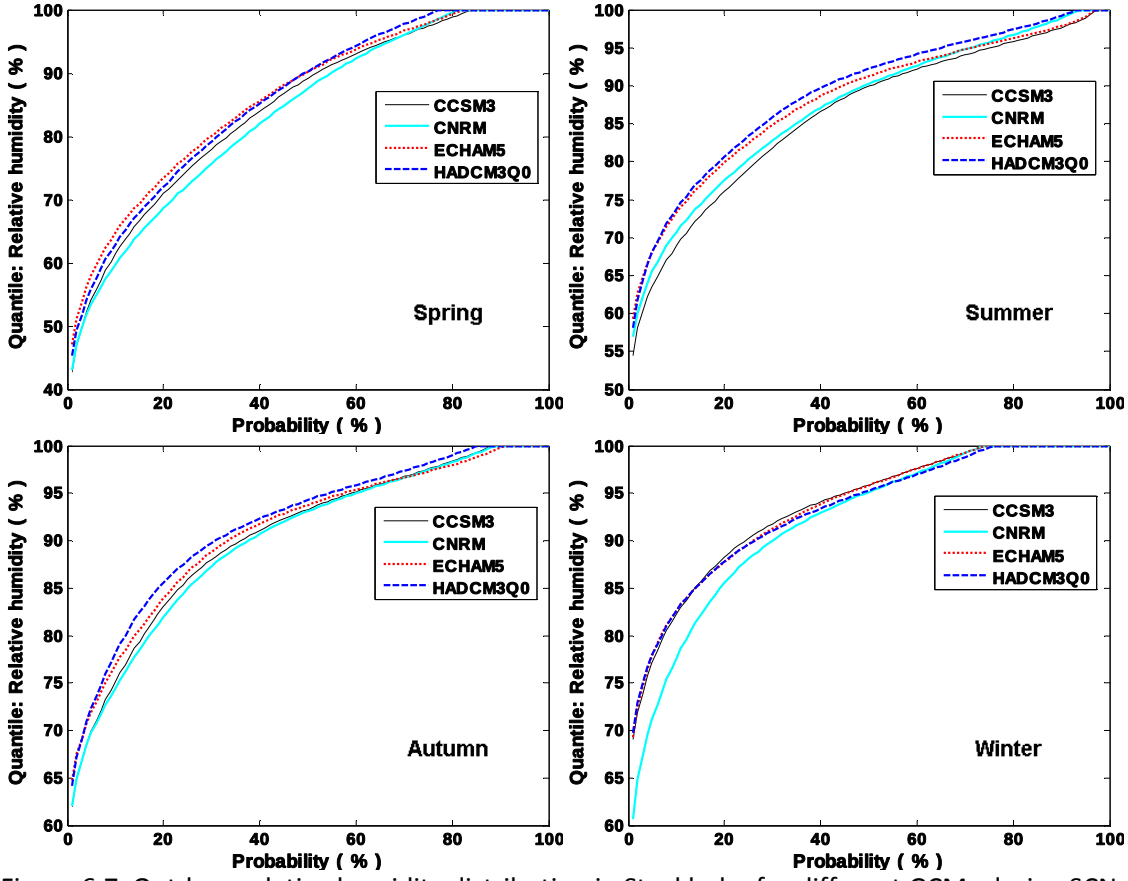

Figure 6.7. Outdoor relative humidity distribution in Stockholm for different GCMs during SCN.

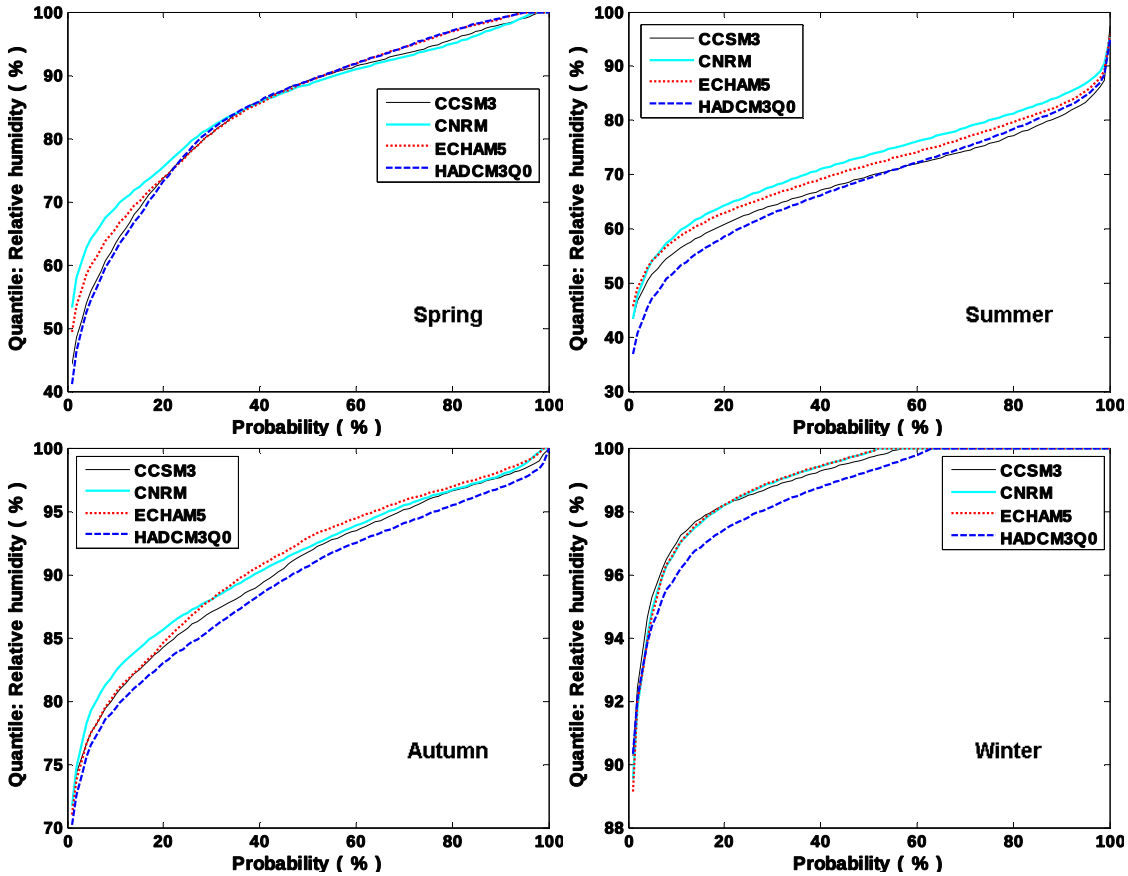

Figure 6.8. Indoor relative humidity distribution in Stockholm for different GCMs during SCN.

During the SCN period despite of having higher outdoor relative humidity in all seasons for HADCM, the indoor relative humidity mostly has the lowest values. It is very visible in figures 6.7 and 6.8. It might be effects of having high solar radiation and temperature with the highest and lowest extreme values. Generally, checking the extreme values of different parameters helps in comparing different GCMs.

During winter the outdoor relative humidity is higher than other seasons. Having lower outdoor temperature results in lower indoor temperature and lower vaporization and moisture transfer to the outdoors which increases the relative humidity inside the attic.

The outdoor relative humidity during summer and winter does not show a big difference between two periods. The RH increment is more visible in autumn and spring. For all the GCMs the relative humidity will increase in the future. Having higher relative humidity and temperature may cause to more mould growth problems.

6.2. Parametric comparison of different GCMs

In this section the indoor and outdoor climate of the attic are analyzed using the decomposition method which has been described in chapter 4. It is not possible to show and discuss all the results in this report, so results for Stockholm during summer for two periods of 1961-1990 (CTL) and 2071-2100 (SCN) are presented here.

Figures 6.9 to 6.17 show different decomposition components of the indoor and outdoor temperature for two periods. The components are 30-year mean ($\overline{T}$), seasonal mean ($\overline{T}+T'_y$), mean cycle ($\overline{T}+\hat{T}_d$) and daily mean ($T_{y,d}$) temperatures. Relations (4.6) to (4.8) show the calculation of each component. In the following figures for the daily mean and seasonal mean temperatures, the temperature values of the 15th year in each period has been used. It means for the CTL and SCN periods the values of the years 1975 and 2085 are applied to the calculations respectively.

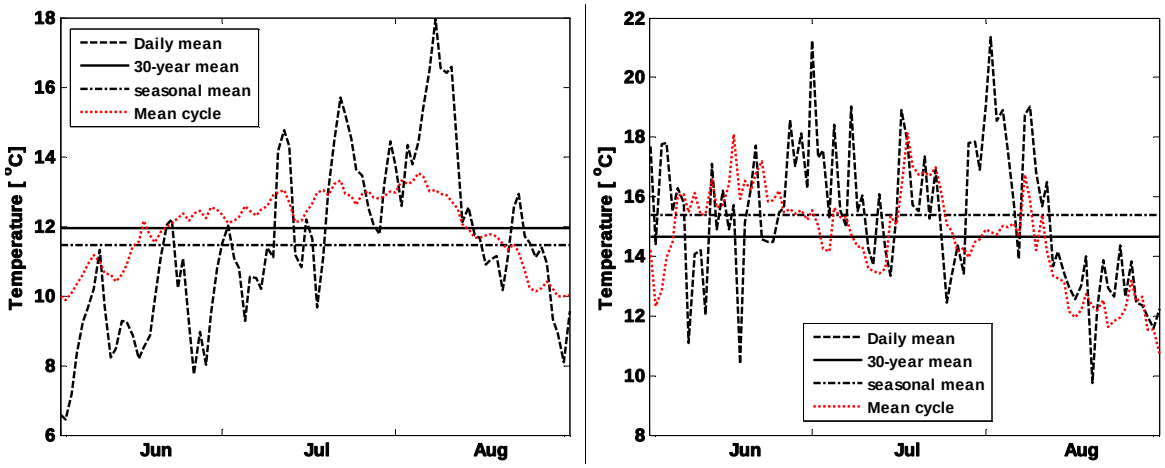

Figure 6.9. Decomposition components of the outdoor temperature in Stockholm during CTL period in summer, ERA40 climate model. left: outdoor climate, right: indoor climate

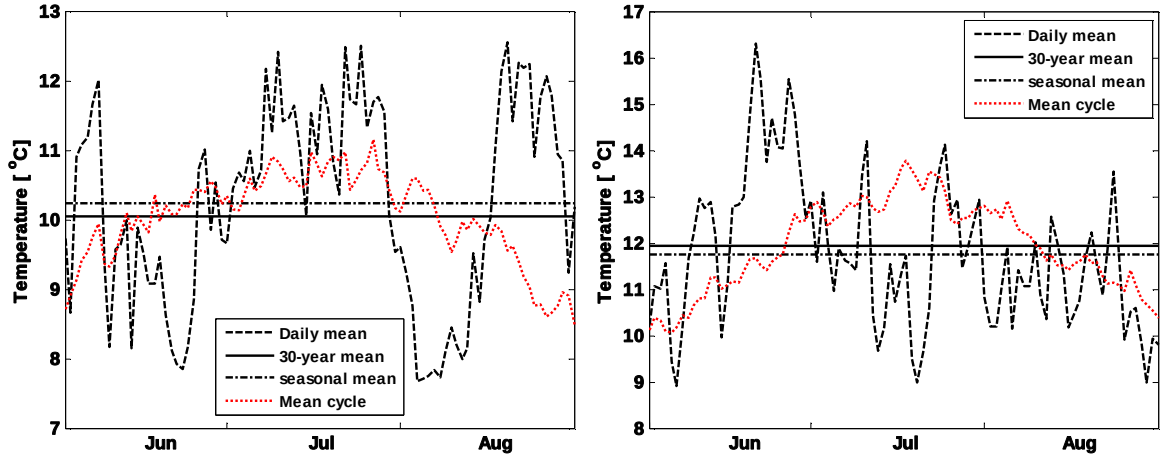

Figure 6.10. Decomposition components of the outdoor temperature in Stockholm during summer, CCSM3 global climate model, left: CTL period, right: SCN period

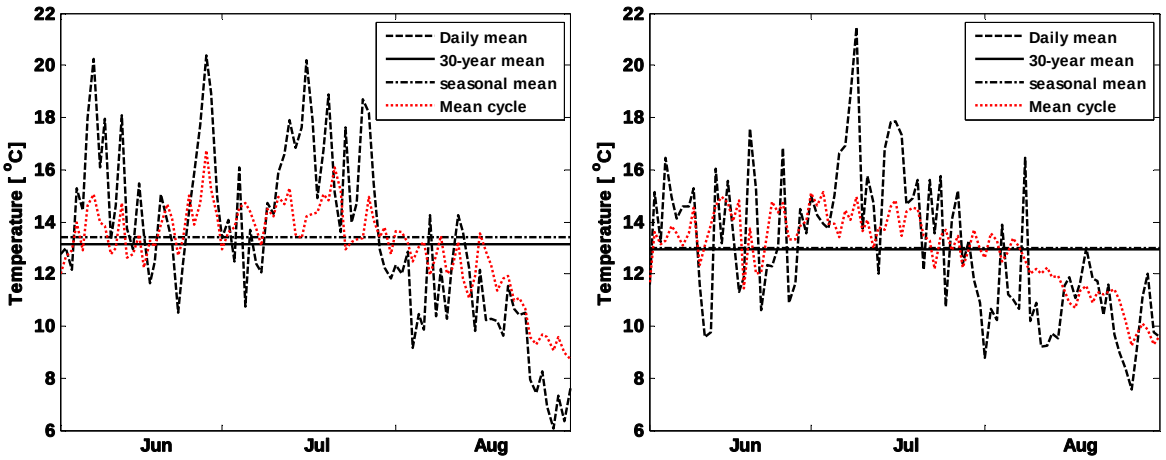

Figure 6.11. Decomposition components of the indoor temperature in Stockholm during summer, CCSM3 global climate model, left: CTL period, right: SCN period

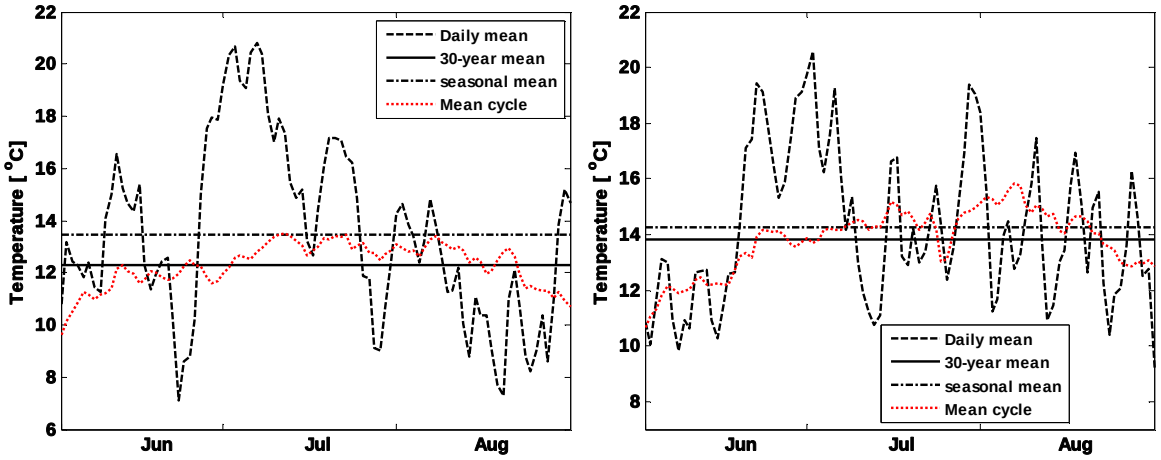

Figure 6.12. Decomposition components of the outdoor temperature in Stockholm during summer, CNRM global climate model, left: CTL period, right: SCN period

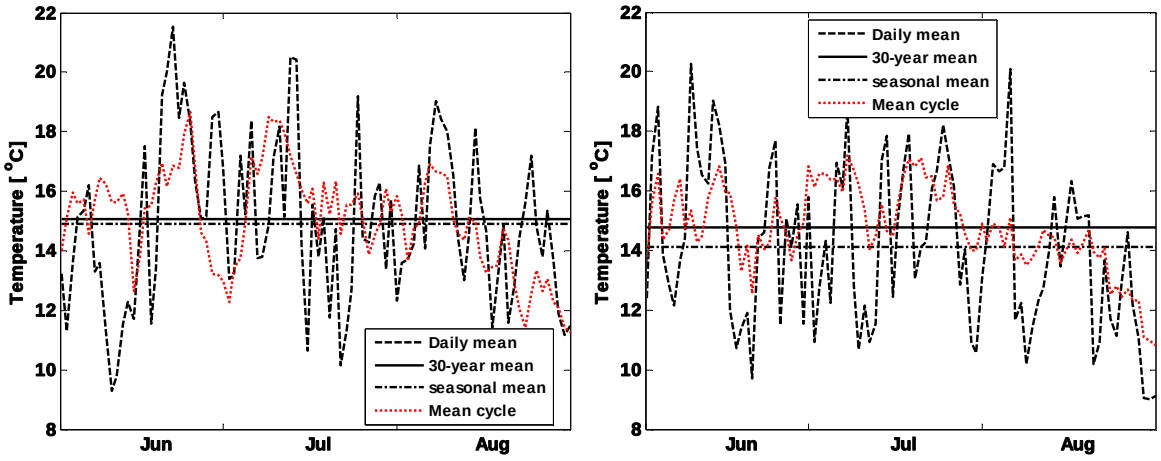

Figure 6.13. Decomposition components of the indoor temperature in Stockholm during summer, CNRM global climate model, left: CTL period, right: SCN period

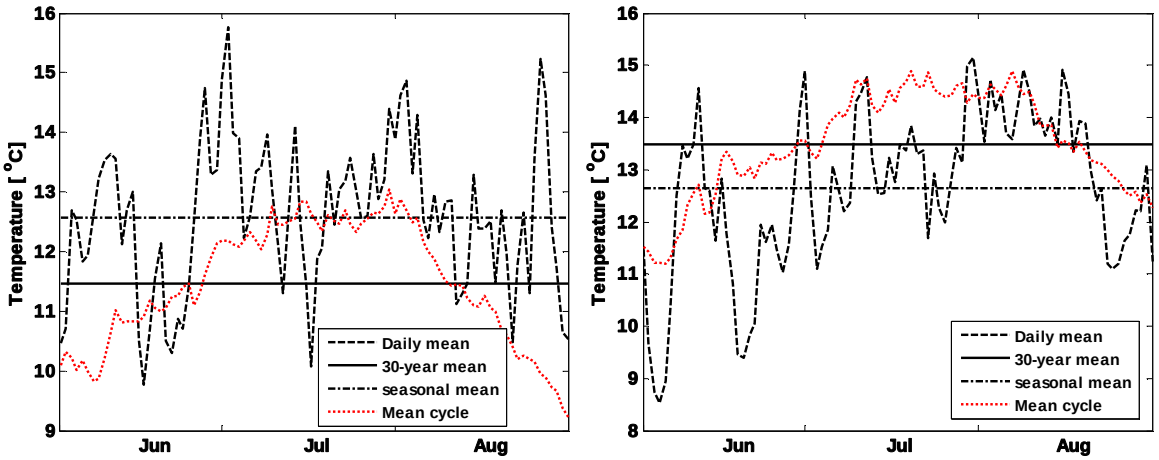

Figure 6.14. Decomposition components of the outdoor temperature in Stockholm during summer, ECHAM5 global climate model, left: CTL period, right: SCN period

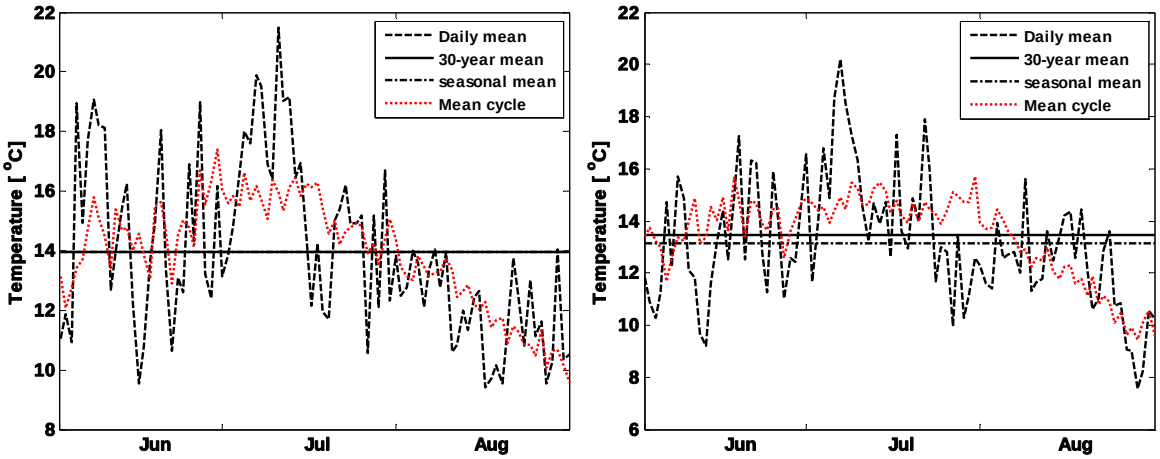

Figure 6.15. Decomposition components of the indoor temperature in Stockholm during summer, ECHAM5 global climate model, left: CTL period, right: SCN period

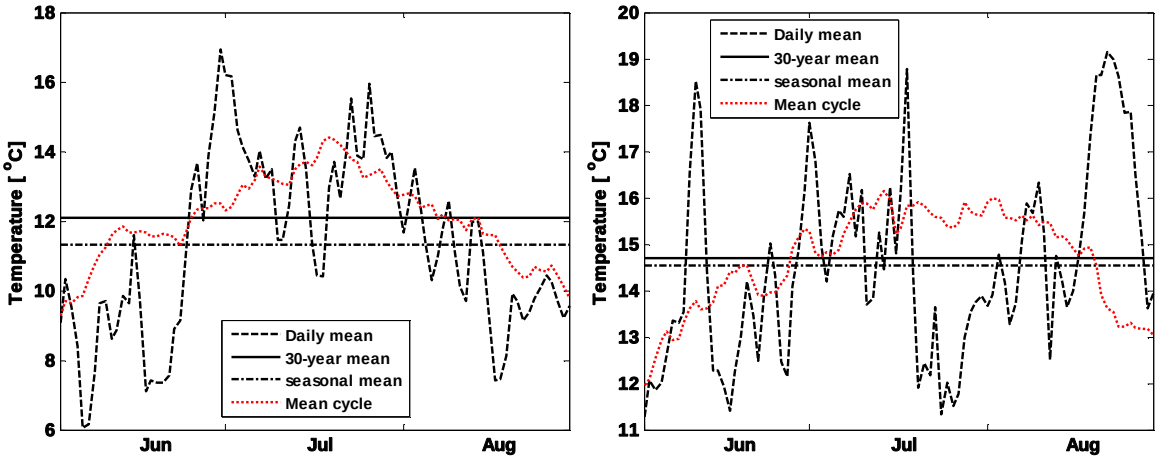

Figure 6.16. Decomposition components of the outdoor temperature in Stockholm during summer, HADCM global climate model, left: CTL period, right: SCN period

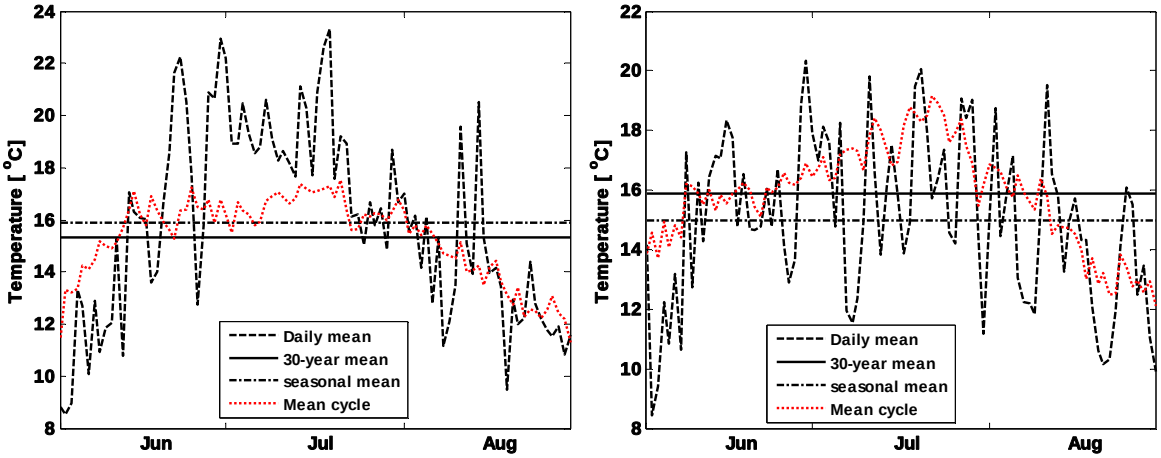

Figure 6.17. Decomposition components of the indoor temperature in Stockholm during summer, HADCM global climate model, left: CTL period, right: SCN period

Comparing the outdoor temperature during CTL period in different GCMs show that the CCSM3 has the lowest 30-year mean and seasonal mean. The values are respectively around 2 and 1 degree less than the ERA40 in Figure 6.9. The other GCMs have the 30-year mean values between 11.5 to 12.3 degrees. Tables 6.1, 6.2 and 6.3 also compare the 30-year mean and seasonal mean of the four GCMs. In CCSM3, CNRM and ECHAM5 the seasonal mean is higher than the 30-year mean. It means in the 15th year of the CTL period the summer mean temperature is higher than the mean temperature of all the summers in the CTL period. Looking at the outdoor temperature during SCN period shows that in all the GCMs the difference between the 30-year mean and seasonal mean decreases. On the other hand both the mean values are higher than the CTL period. It means the temperature increment in the future, during summer in this case, is more influenced by the temperature raise in the whole period, comparing to the CTL period. All the GCMs predict the global warming and the temperature increment of around 2 degrees for these figures. It means having higher temperatures during summer in the future is more trend-induced and the seasonal increment plays the second role (in the cases that have been considered here). During the SCN period there is only one GCM having a higher seasonal mean than the 30-year mean: CNRM in Figure 6.12. In the GCMs with the lower seasonal mean than the 30-year mean, the daily temperature (dashed line) in more instances is under the solid line (30-year mean).

According to tables 6.1 and 6.2 there can be a significant difference between the 30-year mean values of different GCMs. For example the HADCM3 and CCSM3 models show the temperature difference of around 3 degrees both inside and outside during the SCN period. It is a considerable difference which can affect the future designing policies.

Table 6.1. Comparing different mean values of the GCMs for the outdoor climate

CTL period (1961-1990)						SCN period (2071-2100)			
	ERA40	CCSM3	CNRM	ECHAM5	HADCM3	CCSM3	CNRM	ECHAM5	HADCM3
30-year mean (Summer)									
$\overline{T}$	11.96	10	12.3	11.47	12.08	11.9	13.82	13.5	14.7
$\overline{RH}$	0.83	0.83	0.84	0.85	0.85	0.86	0.87	0.88	0.89
$\overline{GR}$	169	165	163	157	161	149	146	137	137
Seasonal mean (Summer)									
$\overline{T}+T_y'$	11.46	10.2	13.45	12.57	11.3	11.76	14.3	12.65	14.5
$\overline{RH}+RH_y'$	0.82	0.84	0.83	0.82	0.85	0.88	0.89	0.87	0.91
$\overline{GR}+GR_y'$	177	155	175	174	158	141	137	142	119

Table 6.2. Comparing different mean values of the GCMs for the indoor climate

CTL period (1961-1990)						SCN period (2071-2100)			
	ERA40	CCSM3	CNRM	ECHAM5	HADCM3	CCSM3	CNRM	ECHAM5	HADCM3
30-year mean (Summer)									
$\overline{T}$	14.7	13.1	15.1	13.96	15.31	12.9	14.8	13.4	15.87
$\overline{RH}$	0.69	0.68	0.71	0.72	0.69	0.69	0.73	0.71	0.68
Seasonal mean (Summer)									
$\overline{T}+T_y'$	15.4	13.4	14.9	13.95	15.9	13.0	14.1	13.1	14.98
$\overline{RH}+RH_y'$	0.68	0.72	0.72	0.73	0.69	0.67	0.75	0.7	0.73

Table 6.3. Percentage differences between CTL and SCN periods

Difference in 2071-2100 (SCN-CTL)/CTL [%]								
Outdoor					Indoor			
	CCSM3	CNRM	ECHAM5	HADCM3	CCSM3	CNRM	ECHAM5	HADCM3
30-year mean (Summer)								
$\overline{T}$	18.88	12.4	17.67	21.6	-1.4	-2	-3.7	3.68
$\overline{RH}$	3.87	3.4	4.2	5	1.1	3	-0.3	-1.73
$\overline{GR}$	-9.46	-10.2	-12.7	-14.9	NA	NA	NA	NA
Seasonal mean (Summer)								
$\overline{T}+T_y'$	14.9	5.1	0.62	28.4	-3.1	-5.2	-5.8	-5.8
$\overline{RH}+RH_y'$	4.3	5.6	6	7.3	-7.6	3	-4.2	6
$\overline{GR}+GR_y'$	-9.4	-21.8	-18	-24.9	NA	NA	NA	NA

Looking at relation (4.8) and the definition of the mean cycle in the beginning of this section helps to understand the concept of the mean cycle. Looking at the mean cycle and 30-year mean period in figures tells more about the GCMs. The mean cycle shows how the temperature varies during summer in the 30-year period. In all the GCMs the mean cycle reaches to its maximum level in mid July during the CTL period. It shifts to late July and early August during the SCN period. The amplitude of the mean cycle fluctuations around the 30-year mean temperature tells how much the point we are looking at, is far from the mean value. Having a mean cycle with smaller fluctuations

around the 30-year mean deals with stronger trend/period induced changes or weaker short time effects of the GCM. For example having a warmer summer with smaller fluctuations of the mean cycle during SCN period, comparing to CTL, means the GCM tends to increase the total mean temperature and there is less chance to have big seasonal variations in a year. In other words the GCM keeps the temperature values closer to the mean value and does not let the temperature to have high fluctuations around the mean value. Comparison of the mean cycle and the daily temperature shows how far the daily temperature is from the mean temperature of that day in the whole 30-year period. This difference is less in the attic and the indoor daily temperature profile follows the mean cycle pattern more than the outdoor.

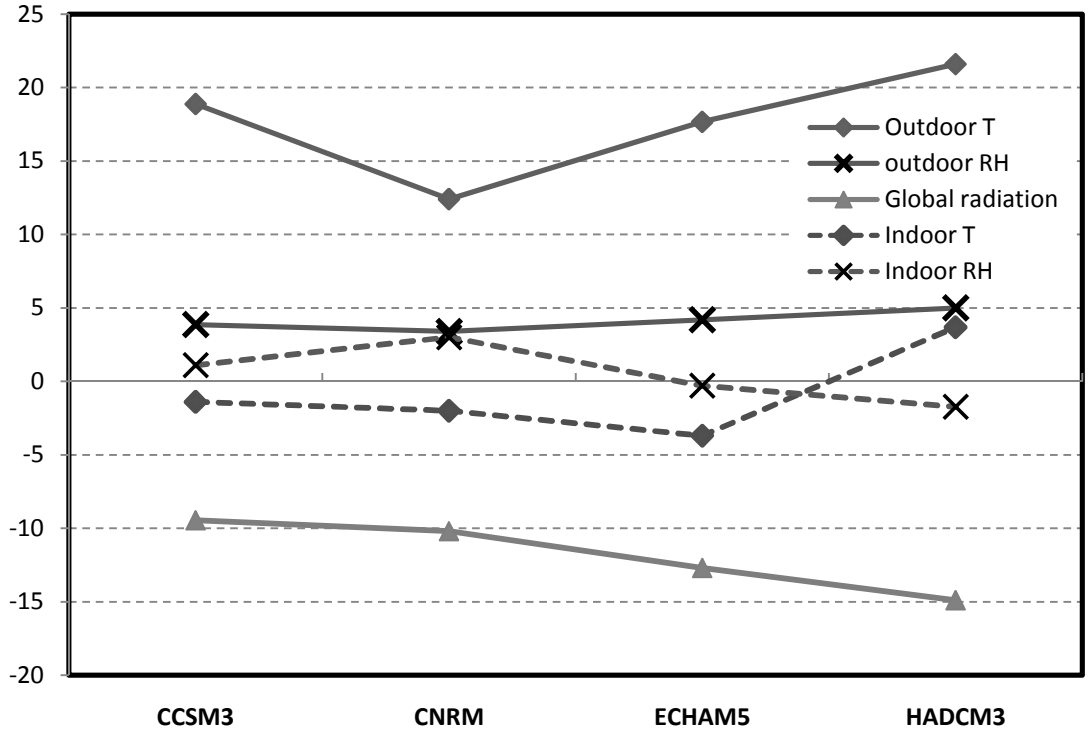

Figure 6.18. Percentage of variations in two periods for the GCMs. Values are from Table 6.3.

Temperature inside the attic changes more rapidly. Having a wavy daily mean temperature profile with sharper edges denotes the big changes of the indoor temperature. The difference between the indoor and outdoor 30-year mean value during the SCN period is less than the CTL period in all the GCMs. For example in the case of ECHAM5 in figures 6.14 and 6.15 the difference between the indoor and outdoor 30-year mean temperatures is around 2.5^{o}C during the CTL period and close to zero degrees in the SCN period (see tables 6.1 and 6.2). Similarly the indoor and outdoor seasonal mean temperature difference is smaller during 2071-2100. Having smaller indoor and outdoor differences may relate to less amount of global radiation during the SCN period. Table 6.3 compares

the outdoor and indoor conditions between two periods. It shows that the SCN outdoor 30-year mean is around 18% more than the CTL period for the ECHAM5, but the indoor temperature is around 4% less. Also in CCSM3 and CNRM despite of having higher 30-year for the outdoor temperature, the 30-year mean temperature inside the attic does not increase during SCN period. In all the GCMs the global radiation decreases during the SCN period. It affects the indoor temperature of the attic. On the other hand in HADCM3, with the highest increment and decrement of the 30-year mean values of temperature and global radiation respectively, the 30-year mean of the indoor temperature increases. It may be explained by the large increment of the seasonal mean in HADCM3. Table 6.3 shows that the seasonal mean temperature in SCN is around 28% more than the CTL period. It is a large increment in comparison with the other GCMs.

According to Table 6.3, relative humidity increases in the future for all the GCMs. But the indoor conditions do not show the same trend. The 30-year mean value increases in CCSM3 and CNRM and decreases in ECHAM5 and HADCM3. Figure 6.18 gives a total view of the changes between two periods. It is not easy to find a pattern for variations of the indoor relative humidity between different GCMs according to variations of the other parameters. We face the nonlinearity of the moisture conditions in the building. This fact makes the prediction of the indoor conditions difficult and time consuming in the case of having different uncertainties in the outdoor conditions.

Figures 6.19 to 6.23 show the variability components of different parameters for the indoor and outdoor climate and compare the CTL and SCN periods. The order of appearance of the variability components is the same for all the GCMs for two periods except the indoor relative humidity in Figure 6.23; the intraseasonal and seasonal variabilities have different orders between GCMs and between indoor and outdoor relative humidity.

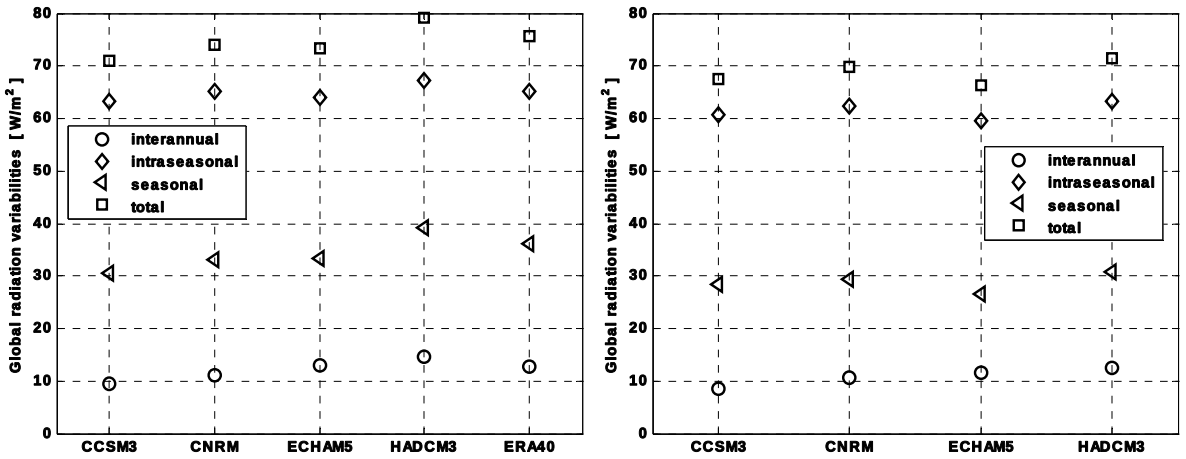

Figure 6.19. Global radiation variability components in Stockholm during summer, left: CTL period, right: SCN period

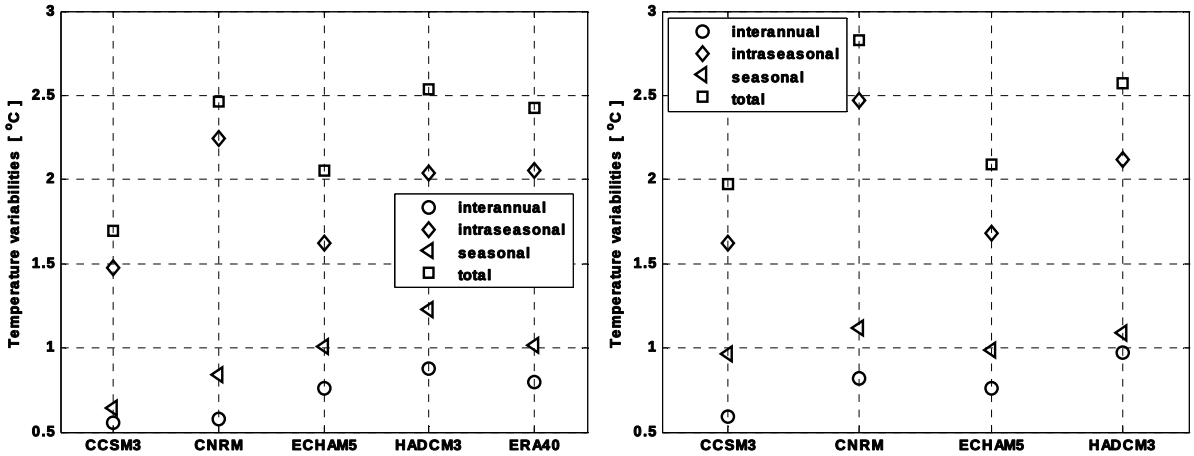

Figure 6.20. Outdoor temperature variability components in Stockholm during summer, left: CTL period, right: SCN period

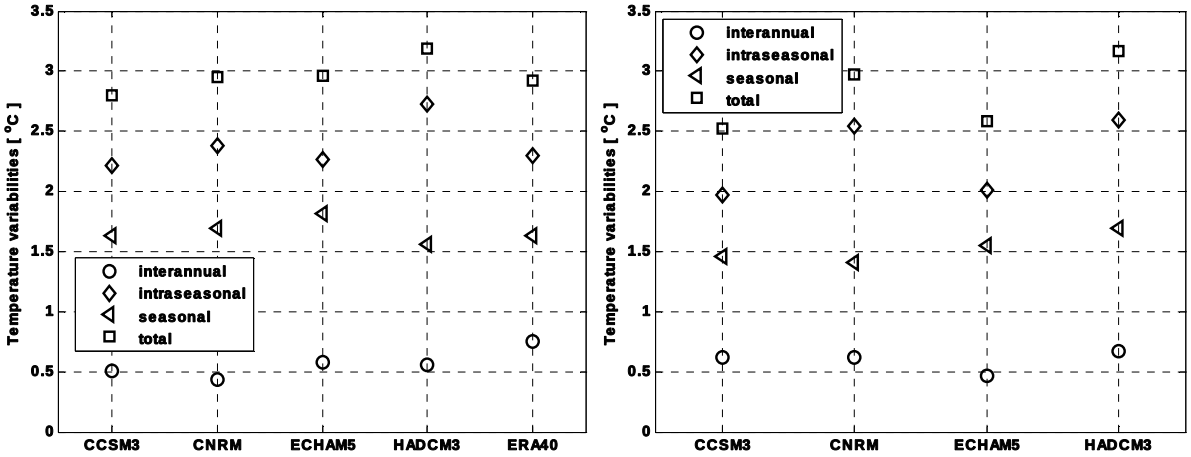

Figure 6.21. Indoor temperature variability components in Stockholm during summer, left: CTL period, right: SCN period

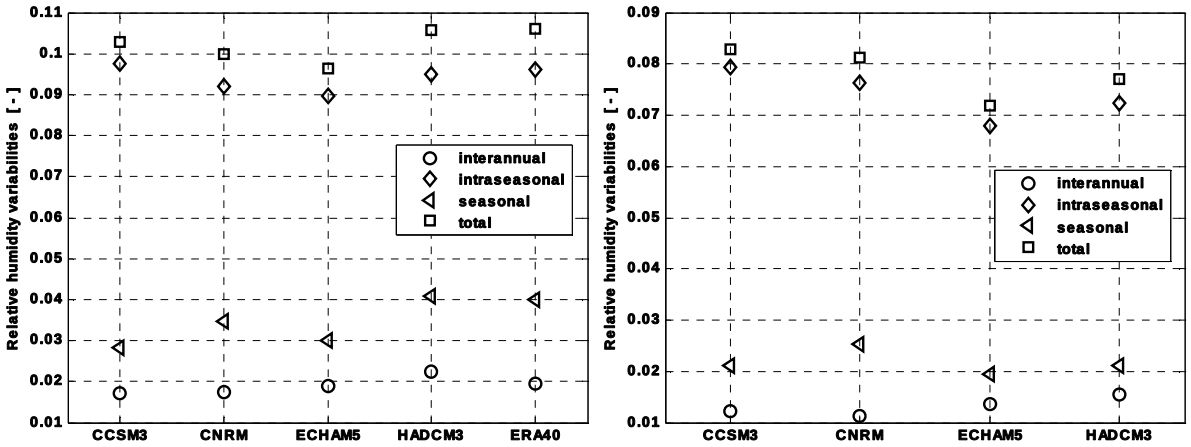

Figure 6.22. Outdoor relative humidity variability components in Stockholm during summer, left: CTL period, right: SCN period

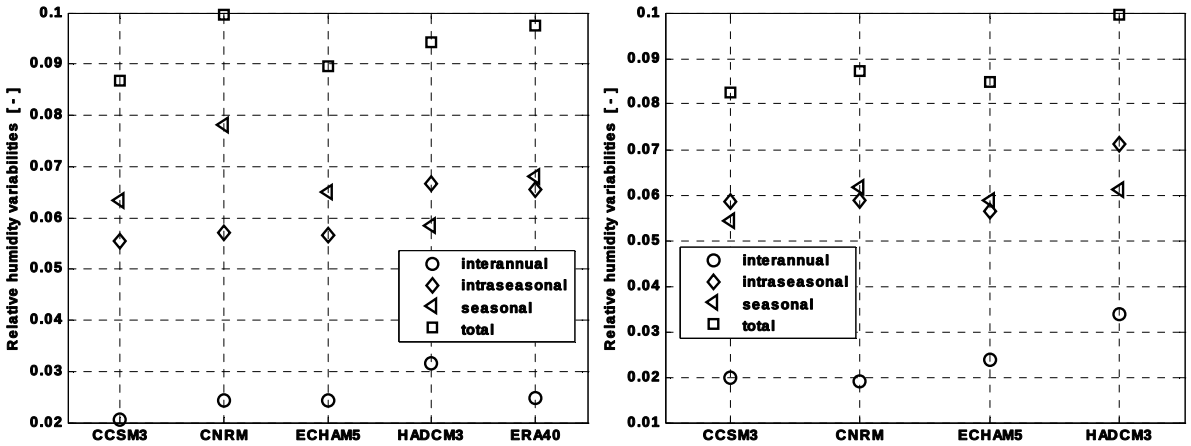

Figure 6.23. Indoor relative humidity variability components in Stockholm during summer, left: CTL period, right: SCN period

The magnitude of the temperature total variability increases in the attic. Looking at figures 6.20 and 6.21 and comparing the indoor and outdoor variabilities of the CTL and SCN periods confirms the increment of the total variability inside the attic. The intraseasonal and seasonal variabilities also increase to values larger than the outside. Figures 6.22 and 6.23 show a considerable decrement and increment of the intraseasonal and seasonal variabilities, respectively, in the attic comparing to the outdoor relative humidity.

The *interannual variability* of a 30-year period gives a general view of the deviation of a daily parameter from its 30-year mean value. Relation (4.8) represents the annual mean value of the deviation of the season in each year from the 30-year mean value of the season. Calculating the variability gives a representative value for the whole period. In other words the interannual variability is kind a gauge for showing the difference of the seasonal mean, i.e. $\overline{T}+T_y'$, and 30-year mean values of a parameter in the whole period which is 30 years in this case. According to figures 6.19 to 6.23 the HADCM3 global climate model has the highest interannual variability indoor and outdoor for all the parameters. In Table 6.4 shows HADCM is the only GCM which the interannual variability of the indoor relative humidity increases during SCN. The interannual variability has the lowest values between the variabilities for all the GCMs. Their difference between GCMs decrease inside the attic.

The *intraseasonal variability* of a parameter is a measure of the amplitude of daily variations around the seasonal cycle. Generally the intraseasonal variability is small over oceans and along coasts, and comparatively large over land regions. The intraseasonal day-to-day variations depend on synoptic variability and cloud cover. The variations are also highly correlated with surface short wave and net radiation (Fischer & Schär 2009). The intraseasonal summer temperature variability for the outdoor

climate increases for all the GCMs. In Table 6.4 the CCSM and CNRM have the maximum increment of around 10% during SCN period comparing to the CTL period. The indoor temperature does not show the same changes as the outdoor climate. For example in the CCSM the indoor intraseasonal variability decreases in the future despite of having higher values for the outside. On the other hand in CNRM both the indoor and outdoor values are increasing in the SCN period. It shows that the variations of indoor conditions, even for the temperature, are not following exactly the outdoor variations. Different variabilities of a parameter are representing the changes of that parameter in different time scales and periods.

Table 6.4. Percentage differences (100*[SCN-CTL]/CTL) of different variability components between the CTL and SCN periods for the outdoor climate

GCM	Variability	Temperature	Relative humidity	Global radiation	
CCSM	Interannual	7.2	-28.5	-11.2	Outdoor
	Intraseasonal	10	-18.7	-4.1	
	Seasonal	51	-25.8	-7	
	Total	15.3	-19.5	-4.8	
	Interannual	21.3	-3.2	NA	Indoor
	Intraseasonal	-11	5.7		
	Seasonal	-10.7	-14.3		
	Total	-9.7	-5		
CNRM	Interannual	42.3	-35.6	-3	Outdoor
	Intraseasonal	9.9	-17.2	-4.4	
	Seasonal	33.3	-25.9	-11.2	
	Total	14.9	-18.8	-5.7	
	Interannual	42	-21	NA	Indoor
	Intraseasonal	7	3.2		
	Seasonal	-15.8	-21		
	Total	0.8	-12.3		
ECHAM5	Interannual	-0.4	-29	-10.7	Outdoor
	Intraseasonal	3.4	-24.3	-5.7	
	Seasonal	-1.8	-35	-20.4	
	Total	1.7	-25.4	-9.5	
	Interannual	-19.3	-2.2	NA	Indoor
	Intraseasonal	-11.1	-0.2		
	Seasonal	-14.3	-9.6		
	Total	-12.6	-5.2		
HADCM	Interannual	11.2	-30.4	-14.9	Outdoor
	Intraseasonal	4	-23.9	-5.9	
	Seasonal	-11.7	-48.3	-21.5	
	Total	1.5	-27.3	-9.8	
	Interannual	20.8	5.7	NA	Indoor
	Intraseasonal	-4.9	5.5		
	Seasonal	8.5	4.7		
	Total	-0.6	5.8		

Looking to the indoor and outdoor variations in different periods using variabilities may give us different images of the variations. The indoor temperature intraseasonal variabilities are magnified inside the attic, the value of each GCM in Figure 6.21 is bigger than the outdoor value in Figure 6.20.

Having lower values of intraseasonal variability for the outdoor relative humidity during SCN in all the GCMs shows that changes in the future are more affected by the seasonal cycle comparing to CTL. It means the changes are more trend-induced. In all the GCMs excluding ECHAM5 the intraseasonal variability of the indoor relative humidity increases and does not show the same behavior as the outdoor conditions between the two periods. The intraseasonal variabilities of the relative humidity have smaller values inside the attic. Also the changes between two periods are much smaller than the outside. Inside the attic variations of the relative humidity from the 30-year mean value is less than the outside during the both periods. Having lower relative humidity inside the attic during summer decreases the variations. Looking at the other indoor variability changes in table 6.4 and comparing with the outdoor values shows the more steady conditions of the indoor relative humidity. On the other hand the intraseasonal variabilities of the indoor temperature are larger than the outdoor. The daily variations of the temperature around the seasonal cycle are magnified in the attic. But the differences between the GCMs decrease inside the attic. For example the difference of the indoor temperature intraseasonal variability between CCSM3 and CNRM is less than the outdoor for both the periods in figures 6.20 and 6.21.

Seasonal variability is the variability which has been induced by the seasonal cycle. Having a more pronounced seasonal cycle implies larger temperature differences in the season which will enhance the seasonal variability ($\hat{\sigma}$) and consequently the total variability (σ_{tot}). Changes in the seasonal cycle may also affect the shape (skewness) of the daily temperature distribution (Fischer & Schär 2009).

The mean seasonal cycle in relation (4.7) calculates the mean value of deviations from the 30-year mean value in the whole period of 30 years for each day. So it gives a periodical view of each day. In this case the period is 30 years and the number of days is 92, equal to the number of summer days. In other words relation (4.7) generates a periodical view of the deviations from the 30-year mean value for the season we are looking at. Relation (4.8), which was used for calculation of the interannual variability, provides the annual view of deviation from the 30-year mean value for the season. The seasonal variability represents the magnitude of the daily variations of the season in the whole period. It gives an estimation for the amplitude of seasonal variations in the period.

In figures 6.20 and 6.21 during the CTL period HADCM3 has the largest seasonal variability outdoors but the smallest indoors. It is the same for the relative humidity. According to Table 6.4 during SCN period in CCSM the outdoor temperature seasonal variability increases to 51% more than the CTL

period. But it decreases for 17% in CNRM. Different GCMs do not show the same pattern of changes for the seasonal variability of temperature. For the relative humidity all the GCMs show the decrement in the future, indoor and outdoor. The only exception is the HADCM3 for the indoor climate. It is interesting to see that the outdoor condition of the HADCM3 shows the biggest decrement of the relative humidity seasonal variability, it is around -48%. The indoor conditions are affected by many other factors.

Having larger seasonal variabilities of temperature in a GCM during the SCN period in summer means the number of summer days with higher temperature values increase (if we assume the daily temperature does not go much below the 30-year mean in summer). In other words the number of hot days in summer will increase. Looking more general, it means in the whole period of SCN the summer temperature profile reach to higher (or lower) temperature levels comparing to CTL. So the periodical summer temperature profile will fluctuate more. In the case having lower seasonal variability, considering the higher 30-year mean temperature in SCN, the summer season follows the trend more than the CTL period. The indoor temperature during SCN follows the trend more than CTL in all the GCMs expect HADCM3.

During summer the intraseasonal variability affects the total variability more than the others. In paper V which the variabilities have been calculated during autumn the seasonal variability takes the upper hand. During summer there is more chance to have high peaks in the temperature profile. It means more irregularity or sharper fluctuations happen in the temperature profile which makes the intraseasonal variability the dominant variability. Selecting the time period in analyzing the data affects the analysis and the consequent conclusions.

The outdoor temperature total variability increases in all the GCMs, but not with the same rate. The maximum is for CCSM3, 16%. ECHAM5 and HADCM3 show a small increment. It is not possible to predict variations of the indoor total variability based on the outdoor. The total variability of the relative humidity during summer decreases for all GCMs, indoor and outdoor, except the indoor relative humidity of HADCM3. The warm summers of the SCN period decreases the variation level of the relative humidity.

In analyzing the future performance of the buildings affected by the future climate it is important to select the proper time scale for the phenomenon which is going to be considered. For example the main reason of the temperature variations and the rate of it might be different in different seasons. Also one phenomenon may be more influenced by seasonal variations but another one by daily variations.

7. Emission scenarios

In this chapter the hygro-thermal responses of the cold attic in different climate scenarios is considered. The difference of the scenarios is in having different CO_2 emission scenarios. The correlation between the climate in attic and the outer climate and also the sensitivity of the simulation results to different emission scenarios have been analyzed using the decomposition method which has been described in section 4.3.

In meteorology several climate scenarios have been simulated for the future climate. One important parameter in climate scenarios is the CO_2 emission scenario. The emission scenarios are predicted based on different assumptions like human activities, plant coverage, etc. Applying different emission scenarios to the same climate model results in different weather conditions. The CO_2 emission scenarios have been described in section 2.5.

The weather data that have been used in these simulations are related to the RCA3 regional climate model and ECHAM5 global climate model. The spatial resolution is 50km. In this chapter climate conditions for these cities are presented: Gothenburg during autumn, Stockholm during winter and Östersund during summer. In each city three different emission scenarios have been considered: A2_1, A1B_1 and B1_1. There is no difference between the CTL period for all the emission scenarios. The decomposition components of the outdoor and indoor temperature and relative humidity and also the global radiation are compared for different scenarios. The variabilities of these parameters have been calculated and compared together in figures. The results of two periods have been studied; 1961-1990 and 2071-2100 which are named CTL and SCN. The climate conditions have been analyzed by decomposing of the parameters and their variabilities. The method is the same as the parametric method which has been used in the previous chapter.

In paper IV with the title of “influence of the uncertainties In future climate scenarios on the hygro-thermal simulation of an attic” the same subject has been analyzed for the city of Lund in south Sweden during spring season.

7.1. Gothenburg during autumn

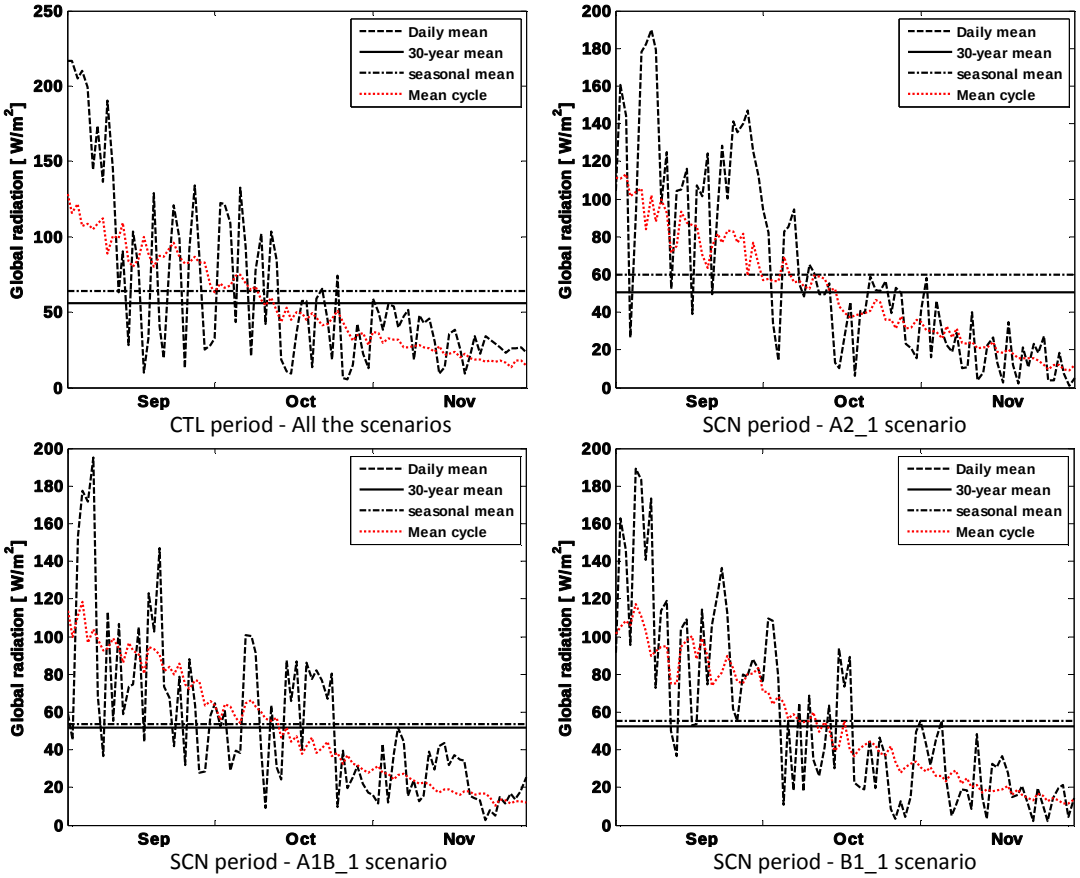

Figure 7.1. Decomposition components of global radiation in Gothenburg during autumn.

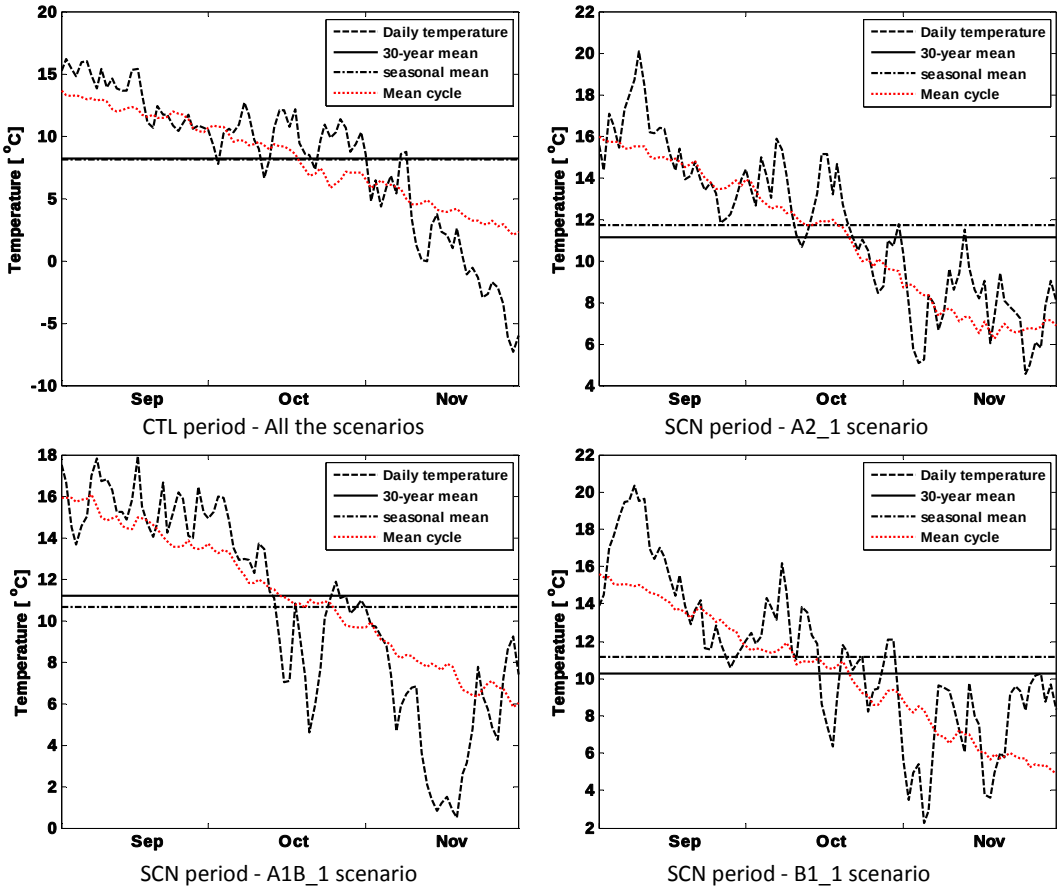

Figure 7.2. Decomposition components of outdoor temperature in Gothenburg during autumn.

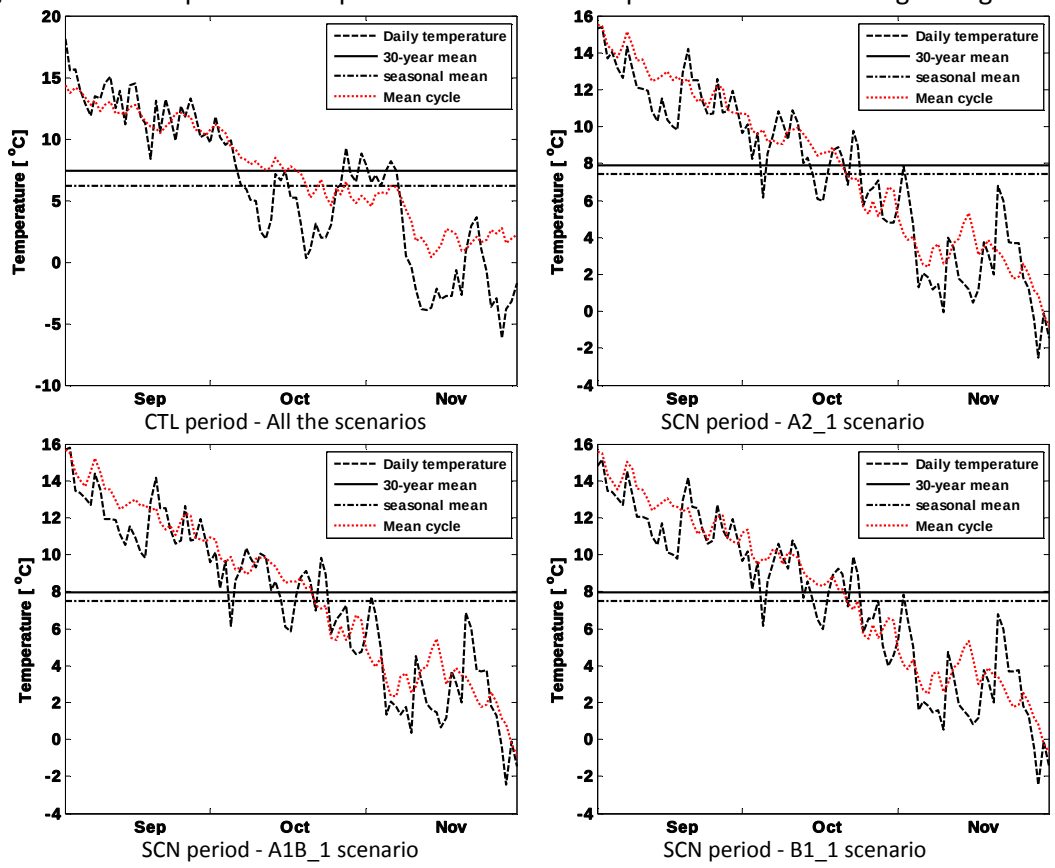

Figure 7.3. Decomposition components of indoor temperature in Gothenburg during autumn.

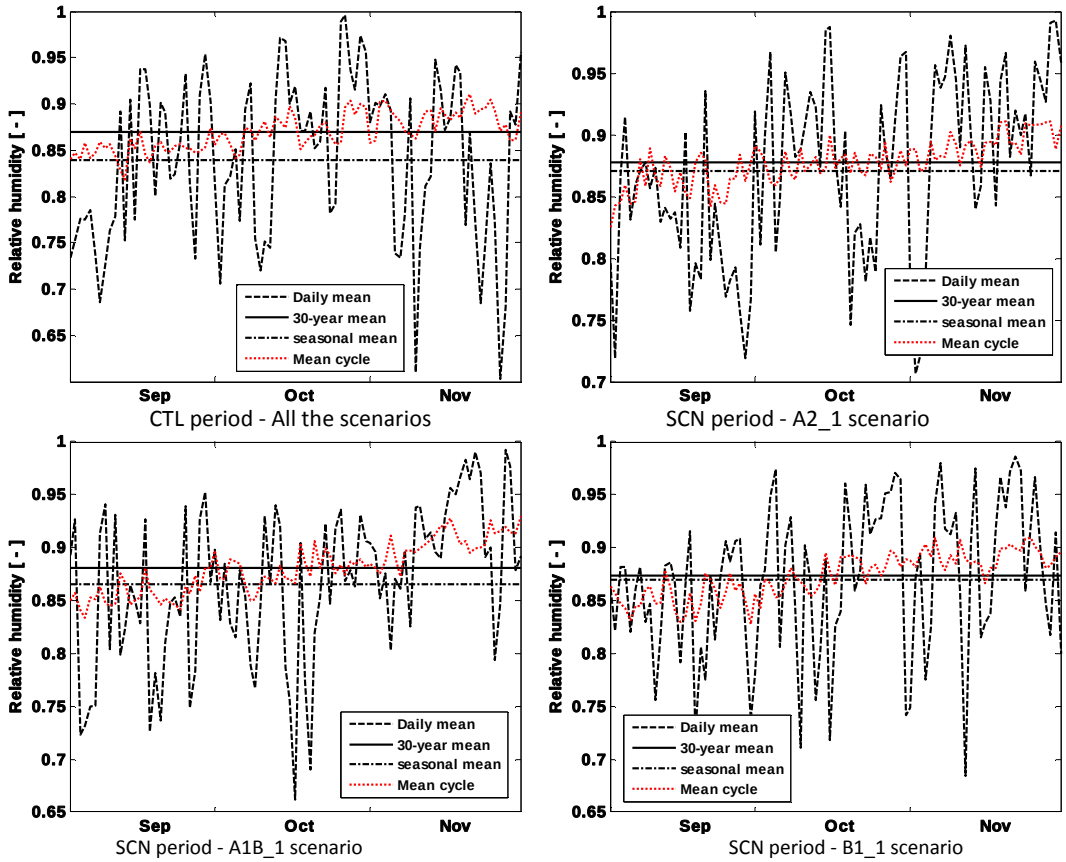

Figure 7.4. Decomposition components of outdoor relative humidity in Gothenburg during autumn.

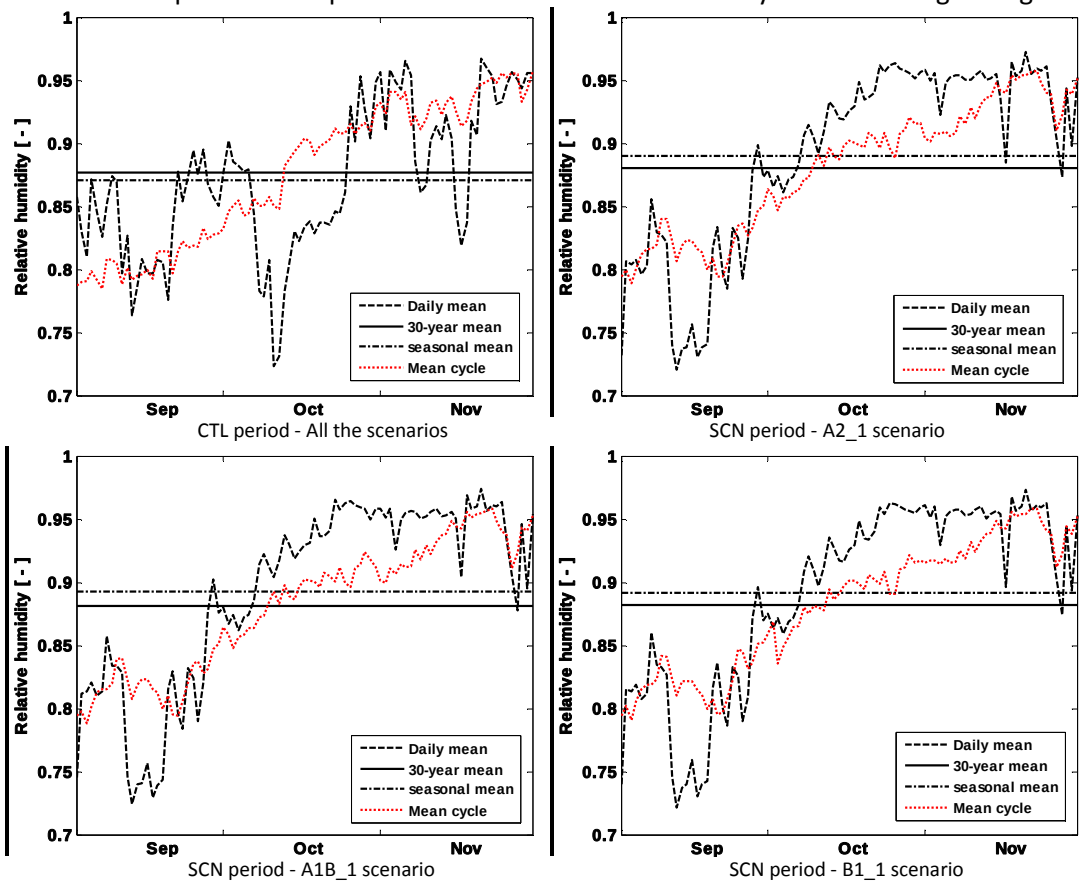

Figure 7.5. Decomposition components of indoor relative humidity in Gothenburg during autumn.

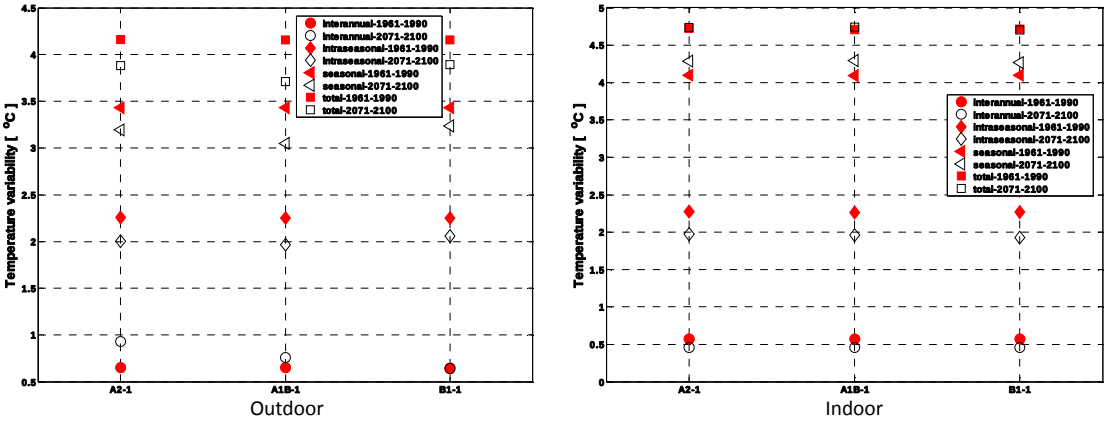

Figure 7.6. Temperature variability components in Gothenburg during autumn.

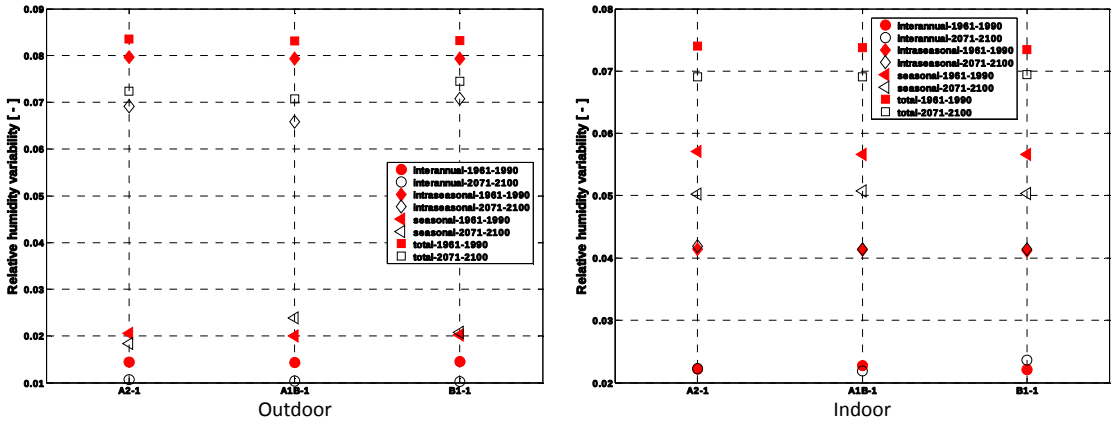

Figure 7.7. Relative humidity variability components in Gothenburg during autumn.

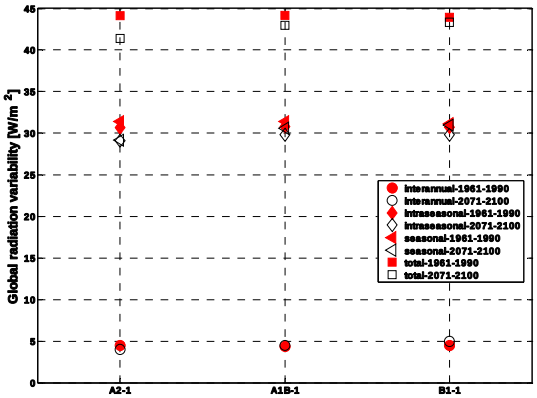

Figure 7.8. Global radiation variability components in Gothenburg during autumn.

7.2. Stockholm during winter

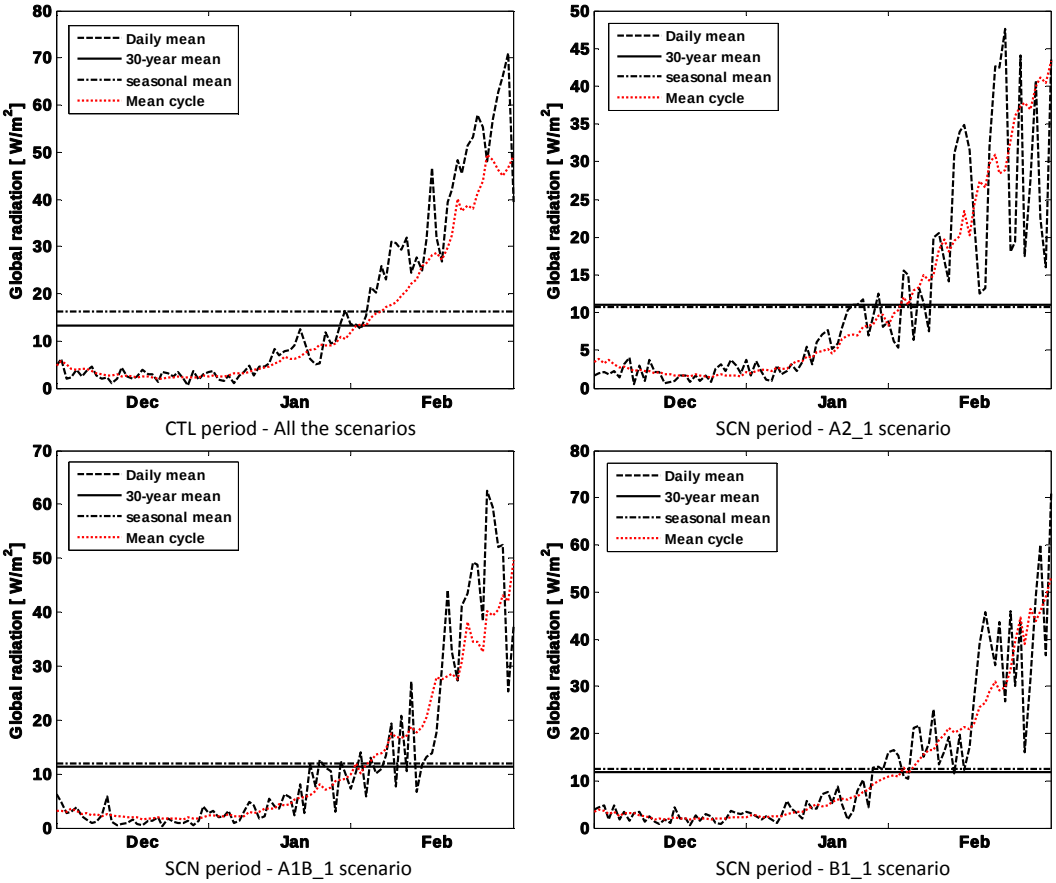

Figure 7.9. Decomposition components of global radiation in Stockholm during summer.

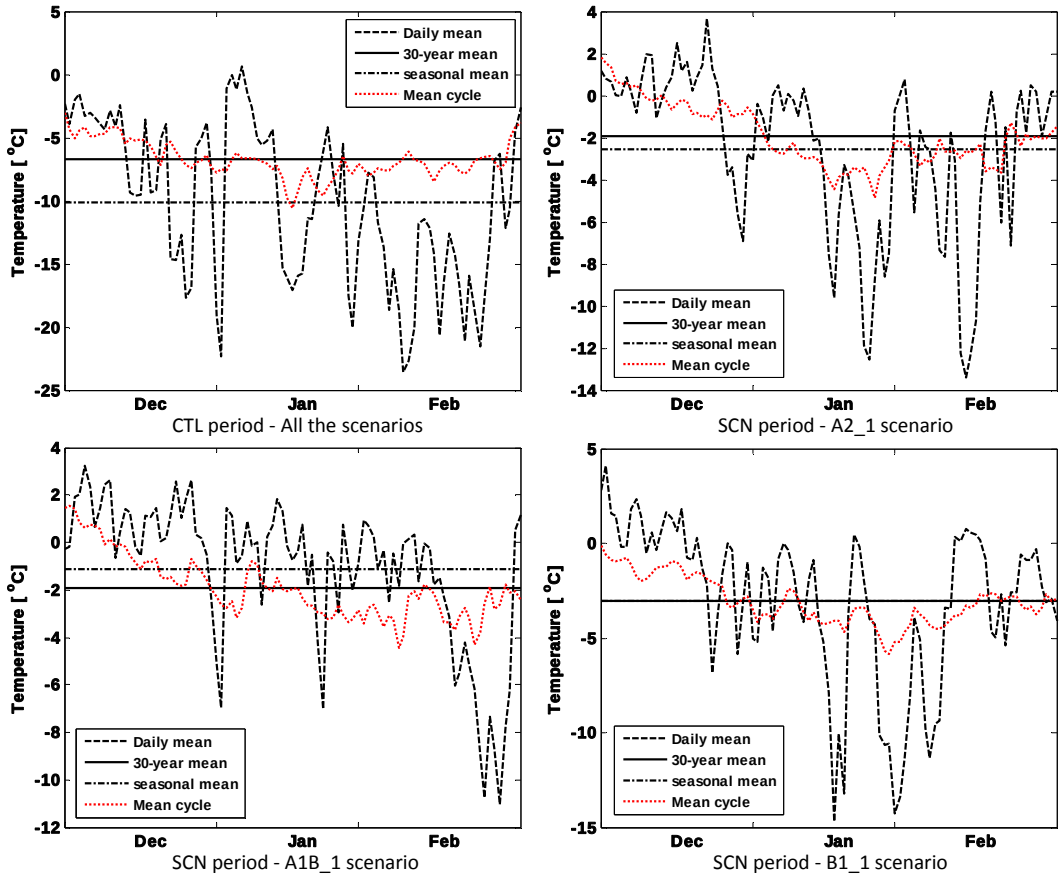

Figure 7.10. Decomposition components of outdoor temperature in Stockholm during winter.

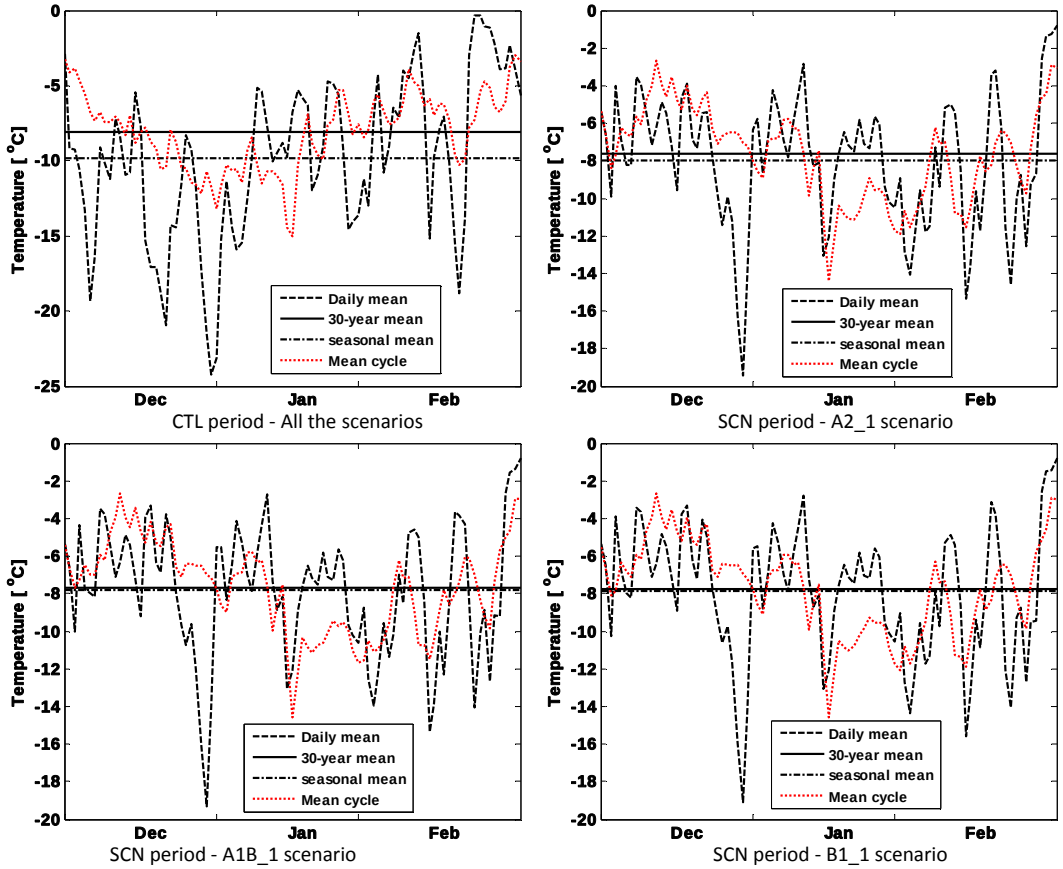

Figure 7.11. Decomposition components of indoor temperature in Stockholm during winter.

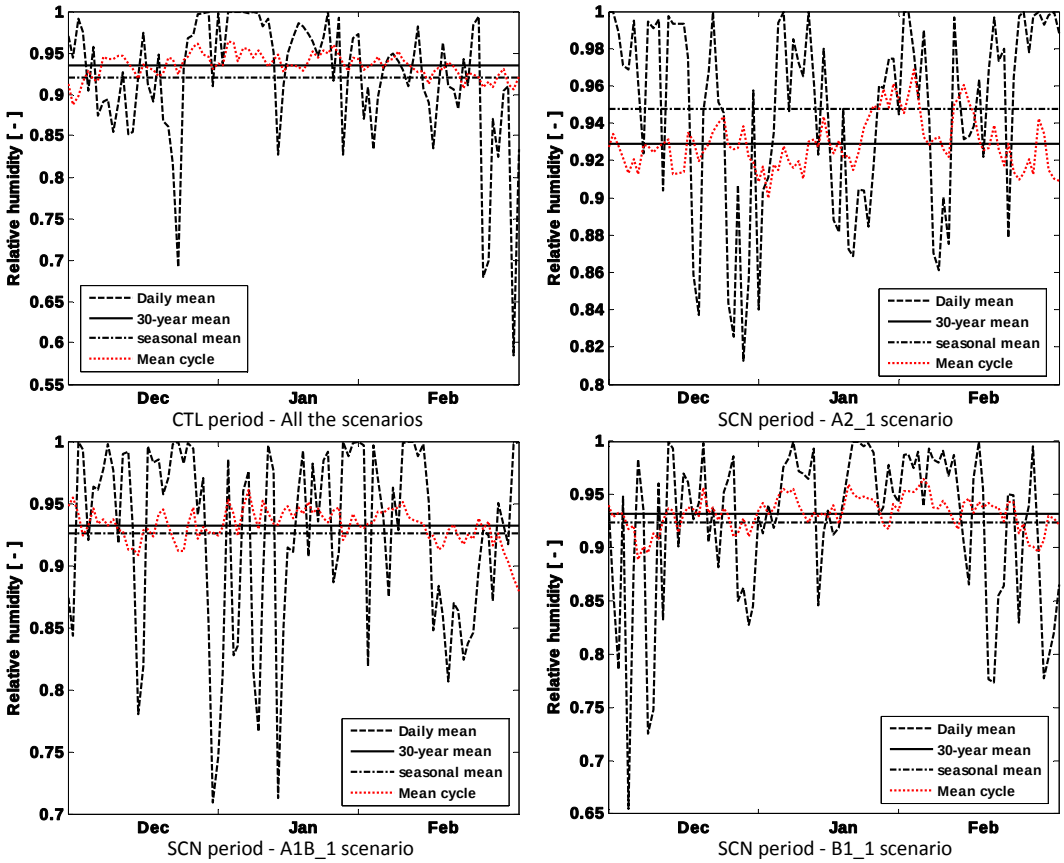

Figure 7.12. Decomposition components of outdoor relative humidity in Stockholm during winter.

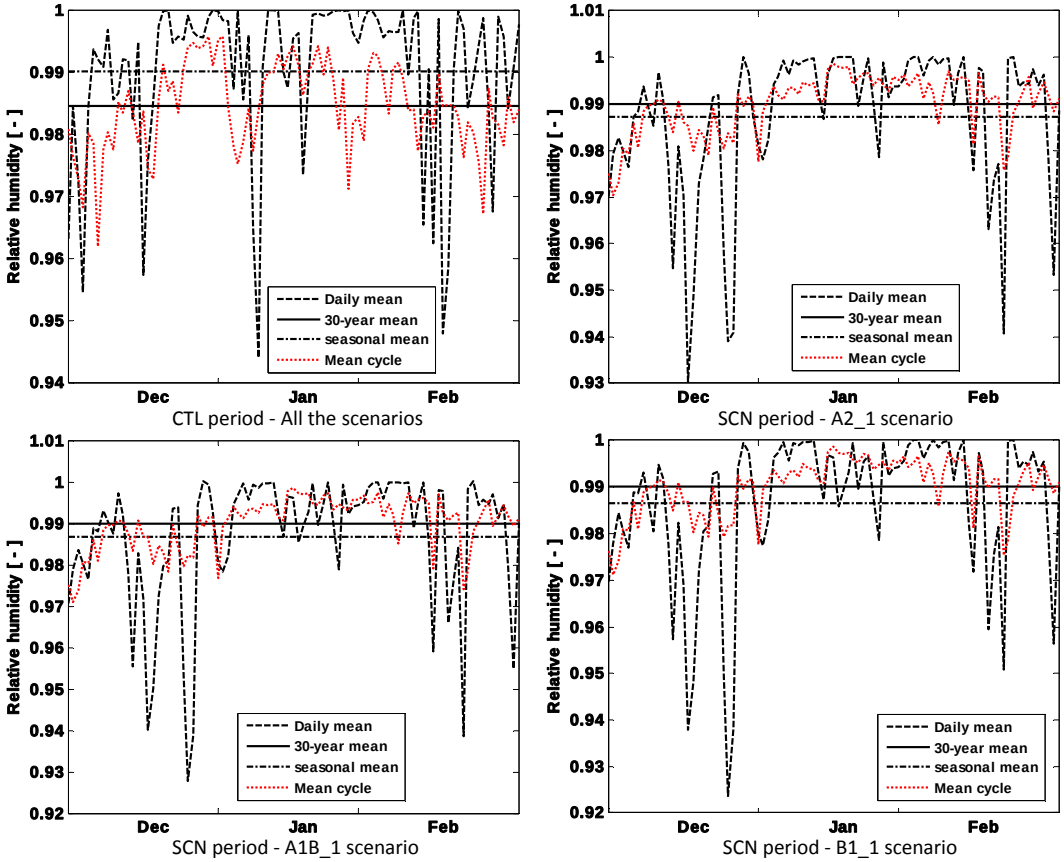

Figure 7.13. Decomposition components of indoor relative humidity in Stockholm during winter.

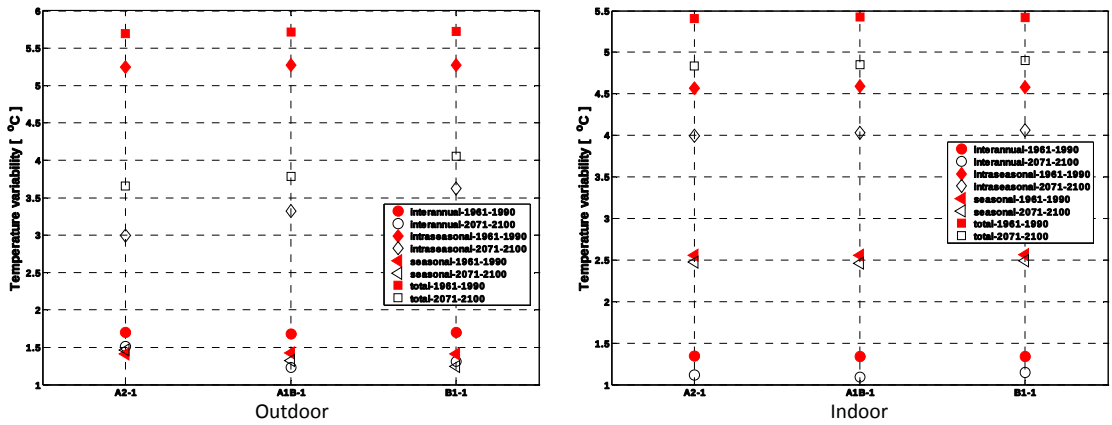

Figure 7.14. Temperature variability components in Stockholm during winter.

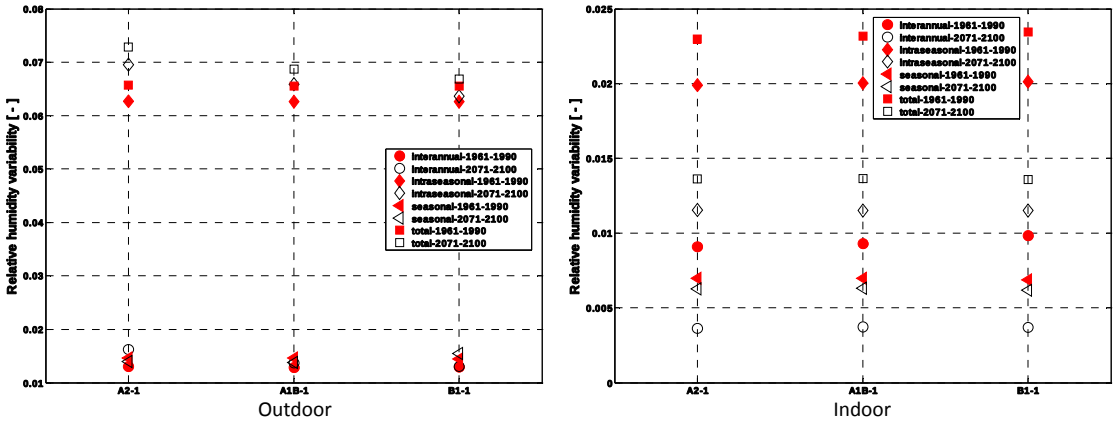

Figure 7.15. Relative humidity variability components in Stockholm during winter.

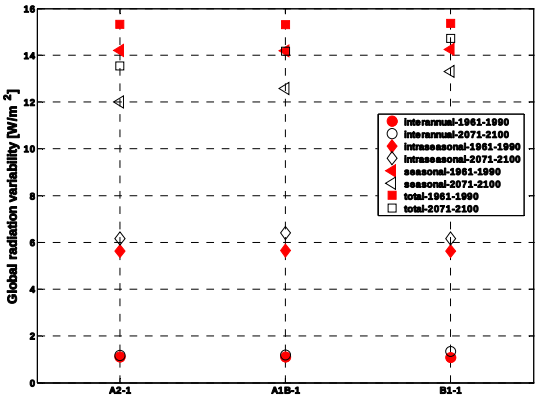

Figure 7.16. Global radiation variability components in Stockholm during winter.

7.3. Östersund during summer

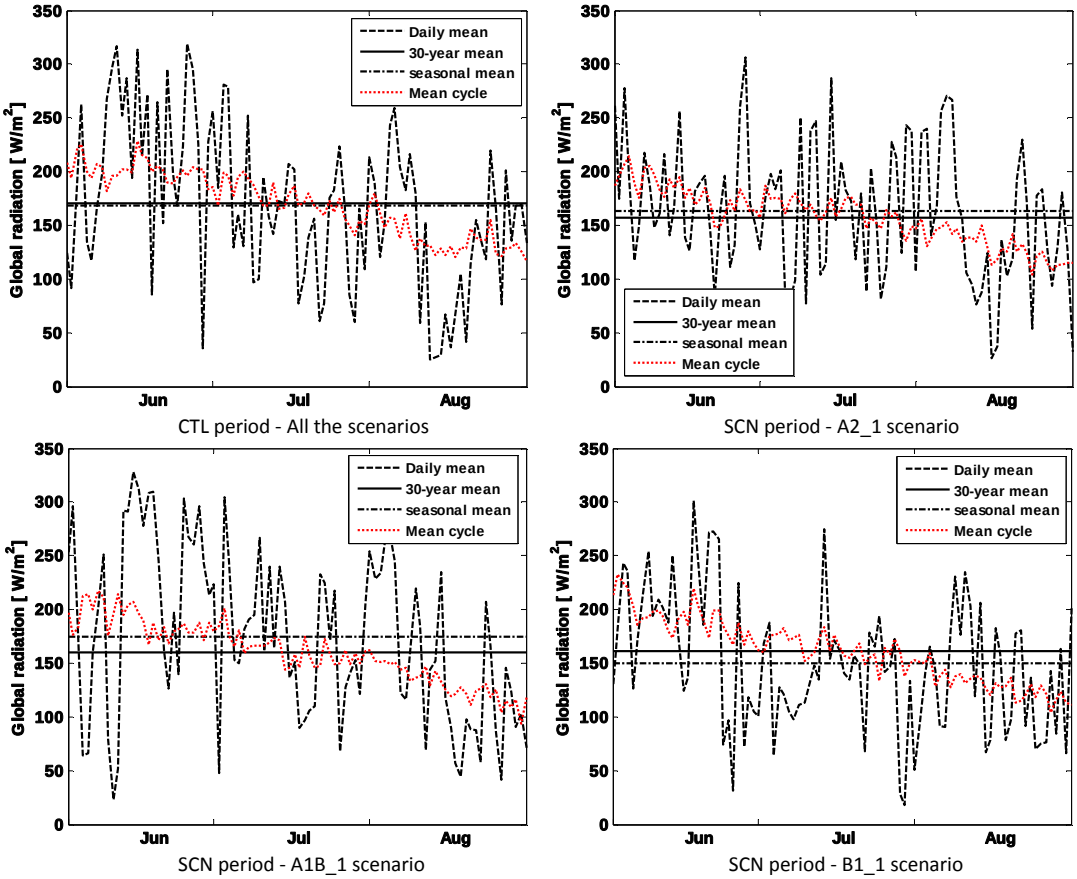

Figure 7.17. Decomposition components of global radiation in Östersund during summer.

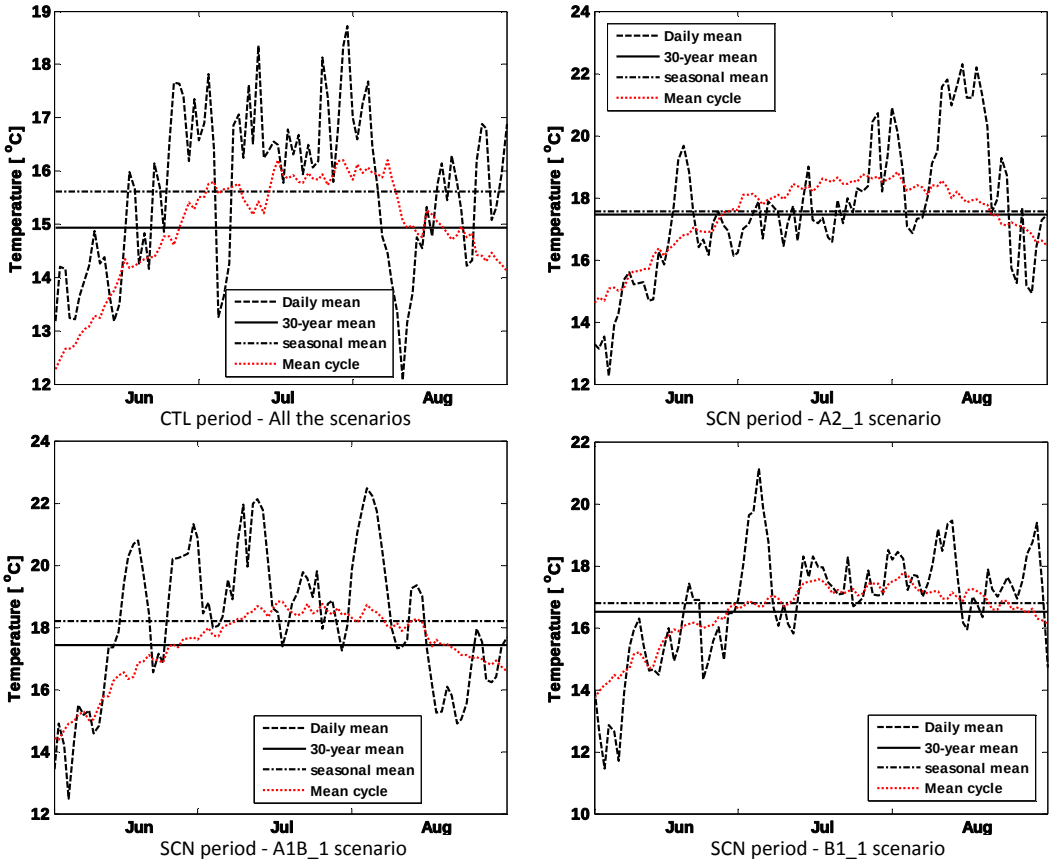

Figure 7.18. Decomposition components of outdoor temperature in Östersund during summer.

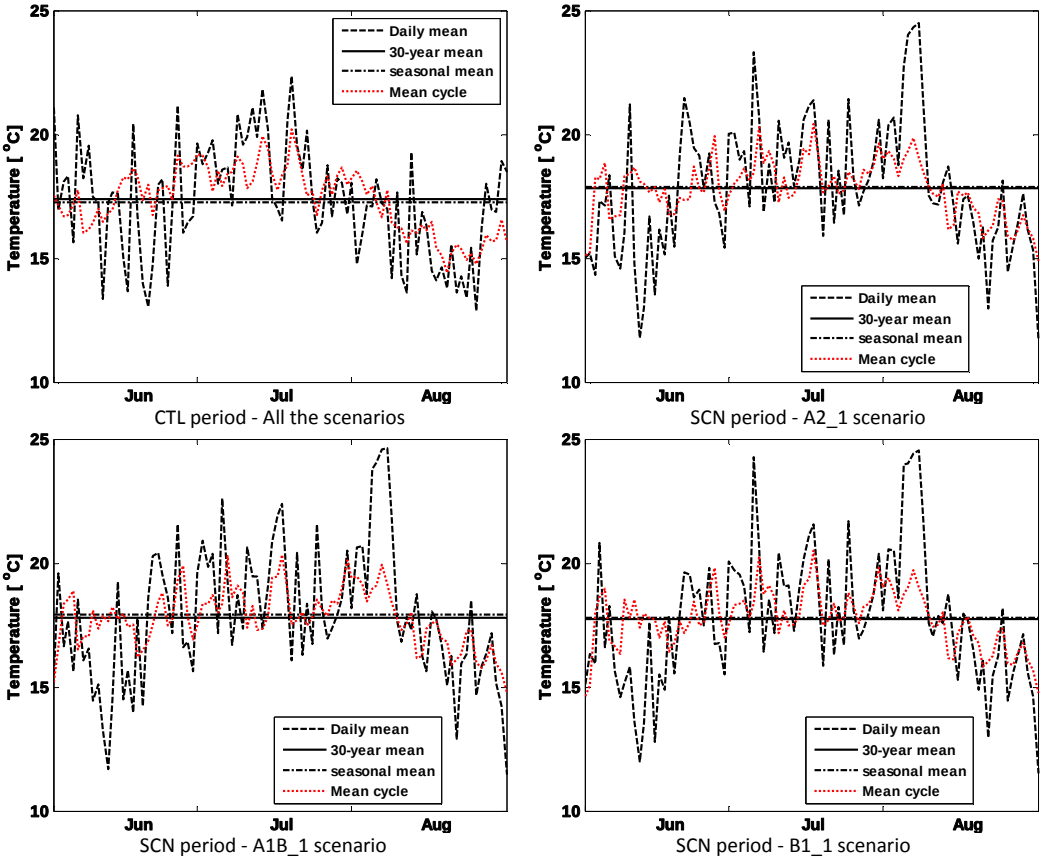

Figure 7.19. Decomposition components of indoor temperature in Östersund during summer.

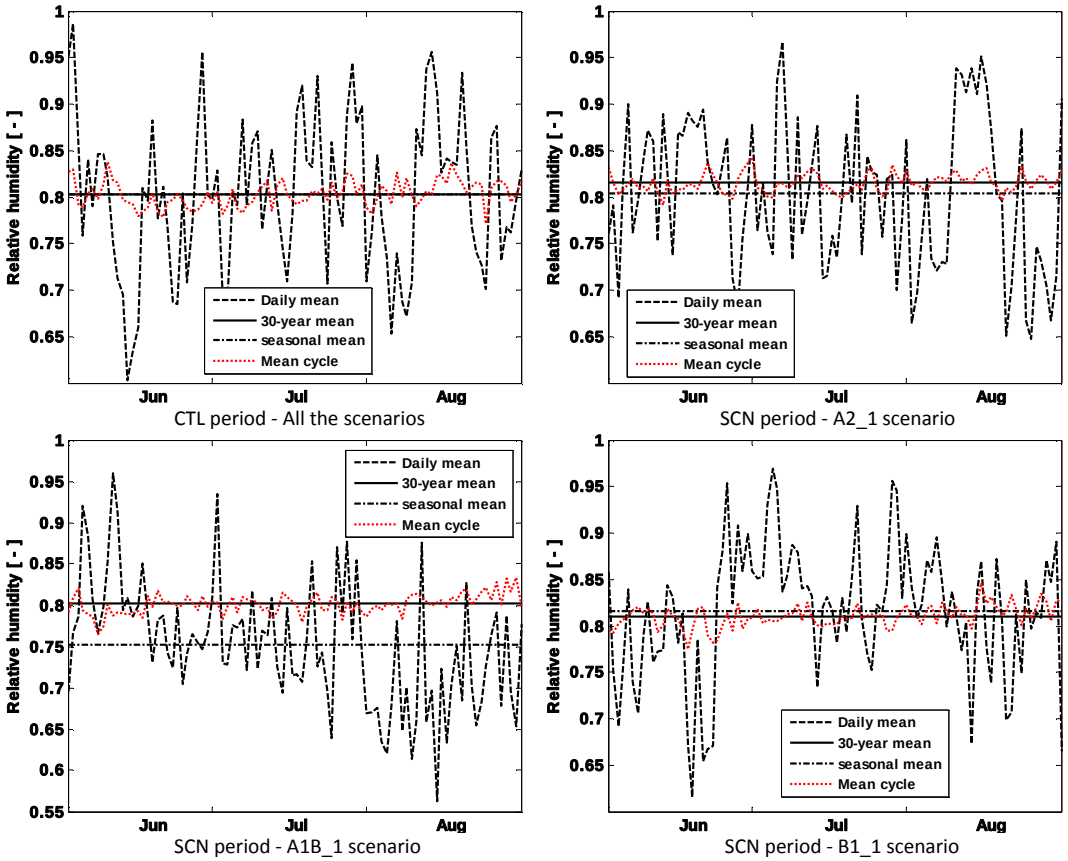

Figure 7.20. Decomposition components of outdoor relative humidity in Östersund during summer.

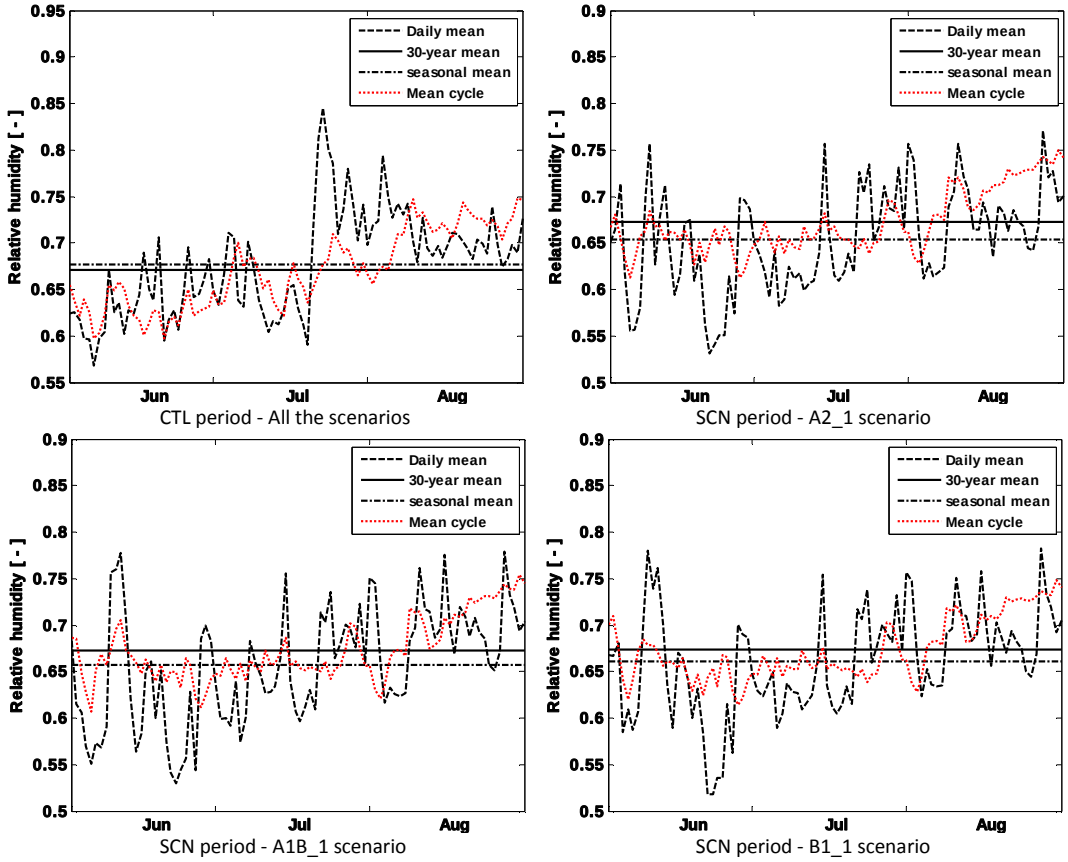

Figure 7.21. Decomposition components of indoor relative humidity in Östersund during summer.

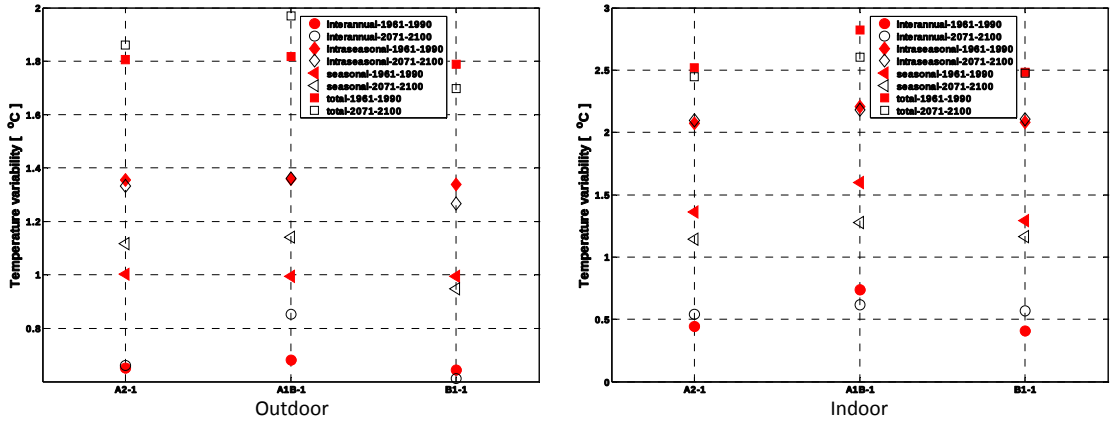

Figure 7.22. Temperature variability components in Östersund during summer.

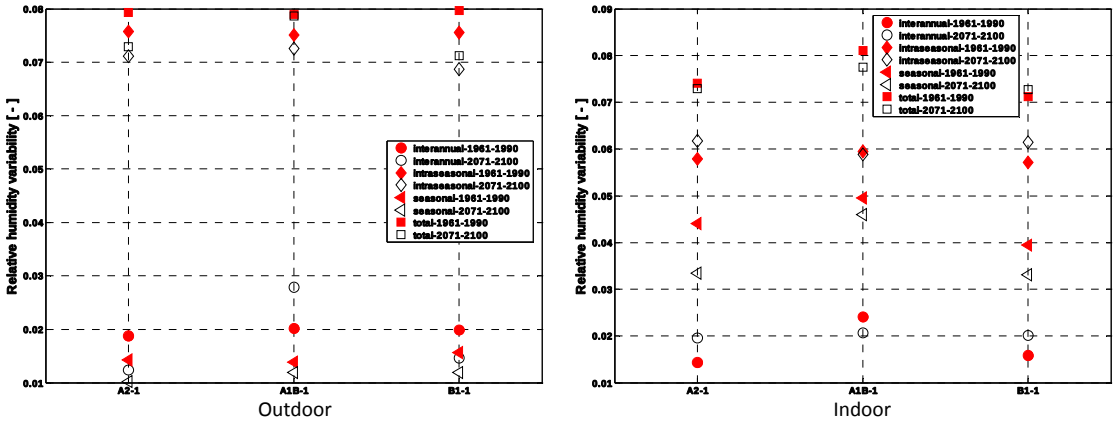

Figure 7.23. Relative humidity variability components in Östersund during summer.

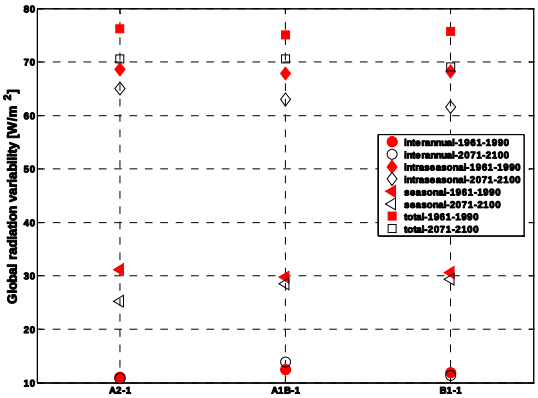

Figure 7.24. Global radiation variability components in Östersund during summer.

7.4. Some general points

For all the cases the temperature is higher in A2-1, then A1B_1 and B1_1 has the lowest temperature. The global radiation has the opposite order. The increment of the emissions decreases the global radiation. The indoor conditions and their variabilities are very similar for different emission scenarios except in Östersund during summer. The variabilities decrease during the SCN period. It shows that the changes are more trend-induced having different emission scenarios.

The effects of different variability components on the increment or decrement of the total variability depends on the season to large extent and also the place. The total variability is more affected by the seasonal variability in Gothenburg during autumn, but in Stockholm during winter the intraseasonal variabilities have larger values. In Gothenburg and Stockholm the interannual variability of the outdoor temperature increases by increment of the emissions. It works in the opposite way for the total variability of the global radiation.

8. Initial Conditions

As it is described in section 2.7 using different initial conditions in climate simulation generates different climate conditions. In this chapter three climate data sets which are the same in the type of RCA, GCM, spatial resolution, emission scenario, etc. are considered. The only difference between the data sets is the initial conditions. The regional climate model is RCA3, the global climate model is ECHAM5 and the emission scenario is A1B. The climate data have the resolution of 50km. Three different initial conditions are specified by numbers; 1, 2 and 3.

Weather conditions of Stockholm during winter are considered in this chapter. Stockholm has shown the coldest winter among the cities with the available climate data. So looking into the winter season of Stockholm provides the chance of comparing different initial conditions considering the lowest extreme values.

In this chapter the simulation results of 140 years (1961-2100) are divided into seven 20-year periods: 1961-1980, 1981-2000, …, 2081-2100. These seven data sets are compared together using nonparametric and parametric methods.

8.1. Nonparametric comparison

The outdoor and indoor climate conditions for different initial conditions are compared together. As it has been described in chapter 3 there is no track of time in the nonparametric methods. By diving the period into 20-year sequences and looking into the winter season, the time resolution increases for the nonparametric comparison.

Figures 8.1-8.7 show the boxplots of the temperature distribution in Stockholm during winter for different time periods. All the data sets with different initial conditions show the gradual increment of temperature by passing the periods. There is no certain rule between data sets with different initial conditions. For example during one period the outliers of ECHAM5-A1B-1 have the lowest values, but another data set has the lowest temperature in another period. One data set may have the biggest size of the box in one period for and smallest in another.

The indoor temperature does not necessarily show the same relation as the outdoor temperature between different data sets. Even warmer outdoor climate does not result in warmer indoor climate (see Figure 8.5). The indoor temperature does not show the gradual increment. In the last period, 2081-2100, the median of the outdoor temperature is around 4 degrees more than the median of 1961-1980. But the difference for the indoor temperature is at most one degree. According to

figures 8.1 to 8.7 it is not possible to connect the indoor and outdoor temperatures on regular basis. For example if we do not know the name of the indoor temperature data sets, it is not possible to distinguish them according to patterns of the outdoor temperature distribution.

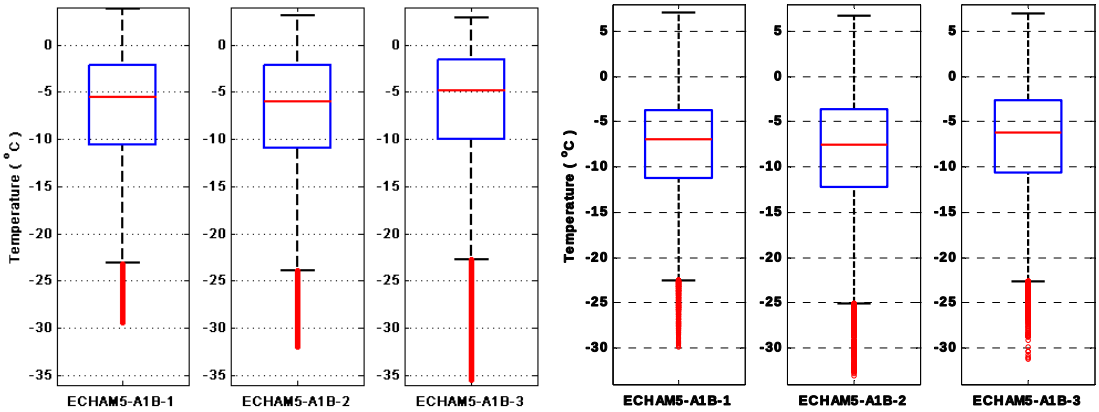

Figure 8.1. Temperature distribution of Stockholm in winter during 1961-1980 for three initial conditions. Left: outdoor, right: indoor.

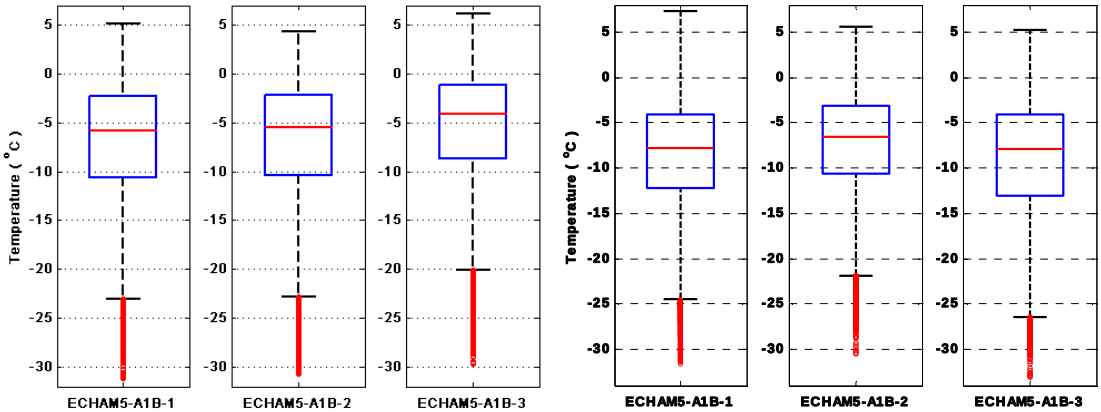

Figure 8.2. Temperature distribution of Stockholm in winter during 1981-20 for three initial conditions. Left: outdoor, right: indoor.

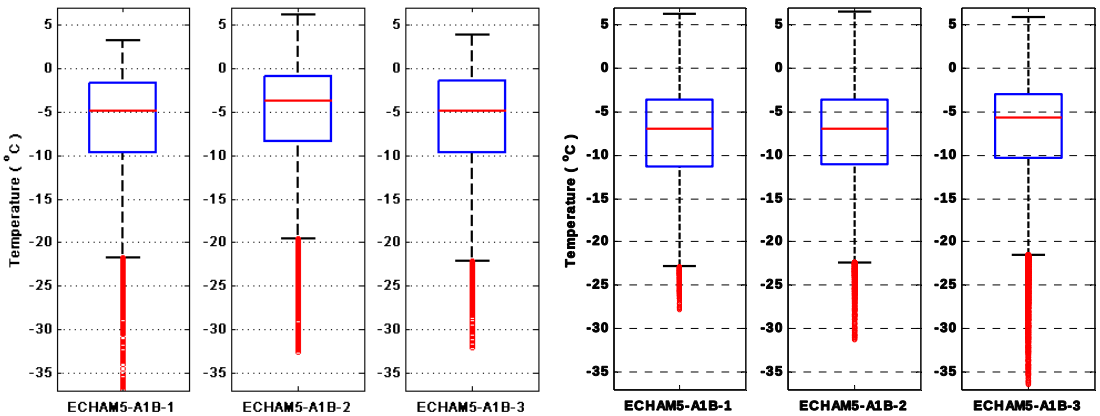

Figure 8.3. Temperature distribution of Stockholm in winter during 21-2020 for three initial conditions. Left: outdoor, right: indoor.

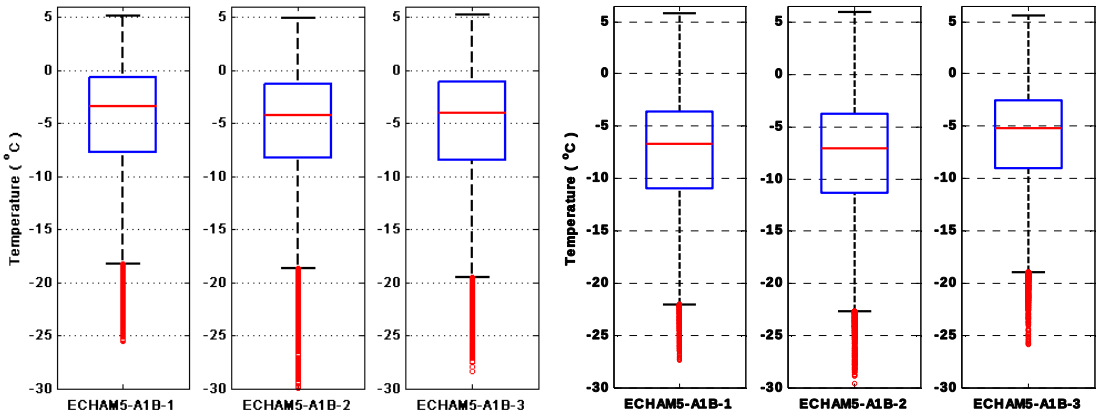

Figure 8.4. Temperature distribution of Stockholm in winter during 2021-2040 for three initial conditions. Left: outdoor, right: indoor.

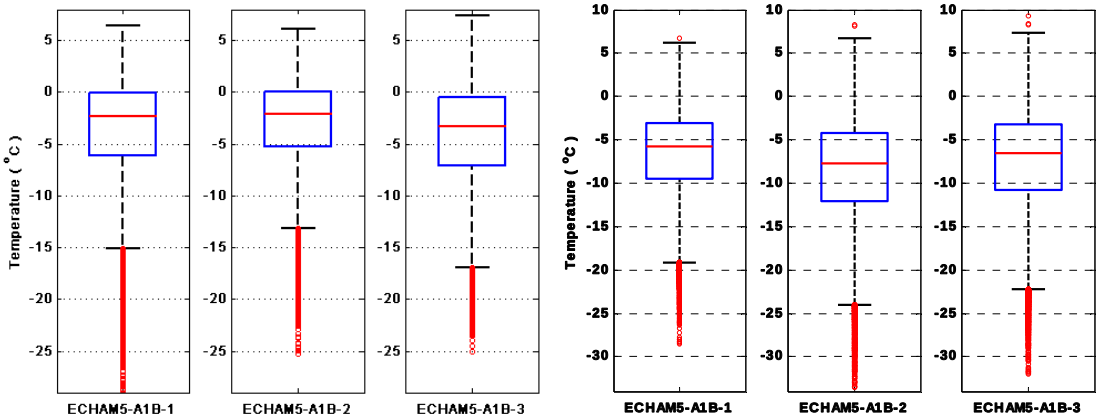

Figure 8.5. Temperature distribution of Stockholm in winter during 2041-2060 for three initial conditions. Left: outdoor, right: indoor.

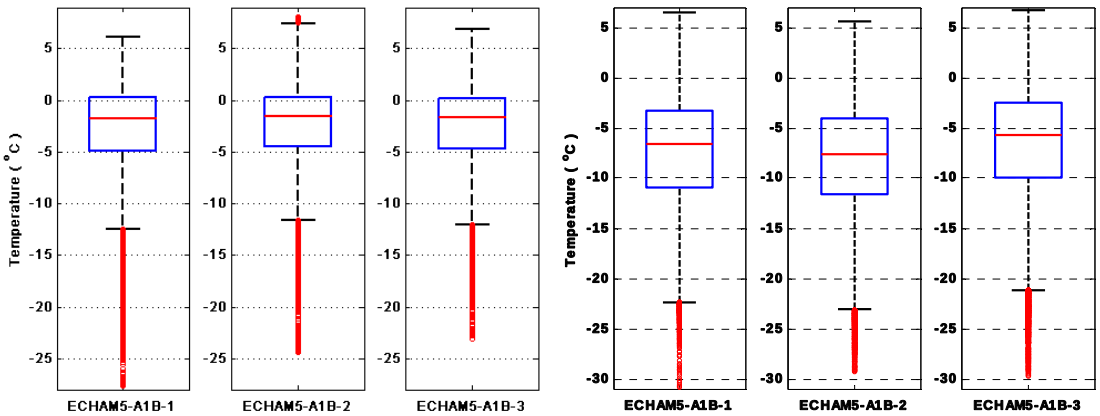

Figure 8.6. Temperature distribution of Stockholm in winter during 2061-2080 for three initial conditions. Left: outdoor, right: indoor.

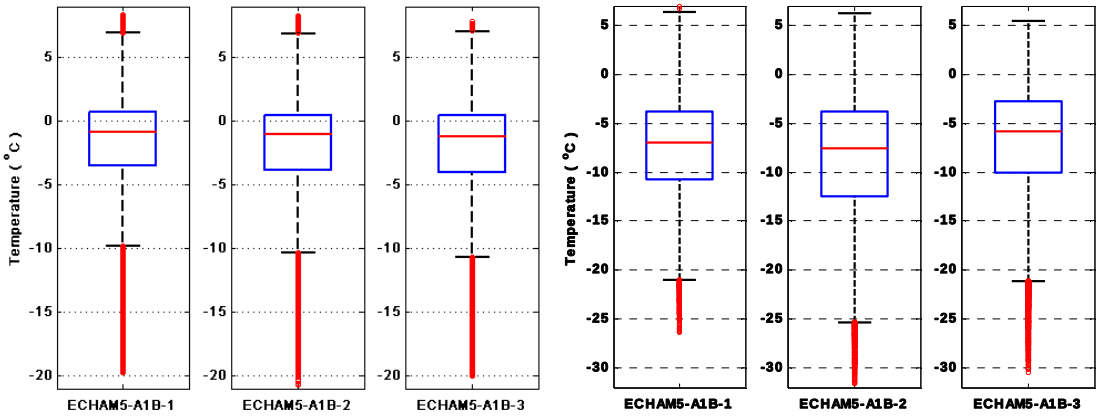

Figure 8.7. Temperature distribution of Stockholm in winter during 2081-21 for three initial conditions. Left: outdoor, right: indoor.

Figures 8.8-8.14 show the quantile plots (inverse CDF) of the relative humidity distribution in Stockholm during winter for the seven periods. The differences between data sets with different initial conditions are more visible for the indoor relative humidity. In figures 8.8 to 8.14 there is no certain connection between the outdoor and indoor relative humidity distributions; the same as the temperature distribution. The outdoor relative humidity quantiles are very close to each other for different initial conditions. There is specific order between data sets in the periods.

In most the periods the data set with the initial condition of 3 has a considerable difference with the other data sets; except the last two periods where the first initial condition has quite different distribution.

In Figure 8.13 the second and third data sets show a sudden decrement of the indoor relative humidity. Otherwise there is a tendency to increase the indoor relative humidity from the first period (1961-1980) to the last one (2081-2100).

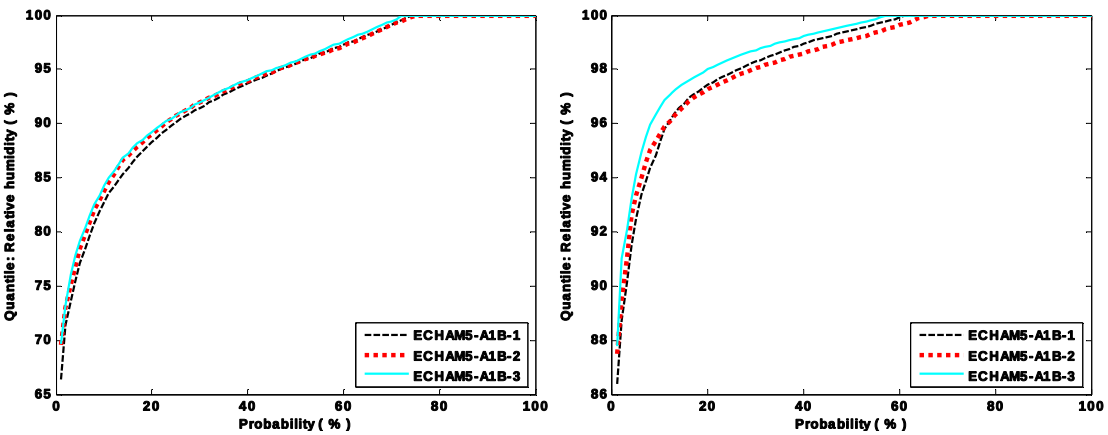

Figure 8.8. Relative humidity distribution of Stockholm in winter during 1961-1980 for three initial conditions. Left: outdoor, right: indoor.

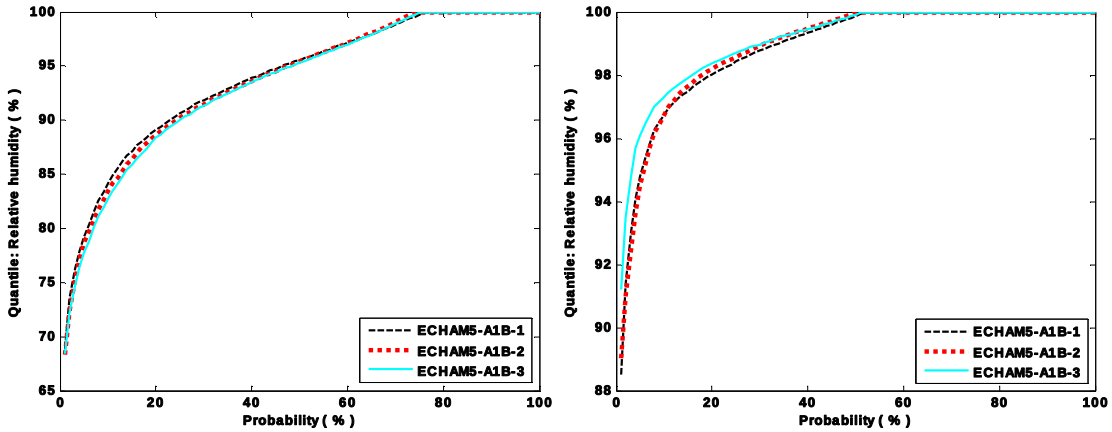

Figure 8.9. Relative humidity distribution of Stockholm in winter during 1981-20 for three initial conditions. Left: outdoor, right: indoor.

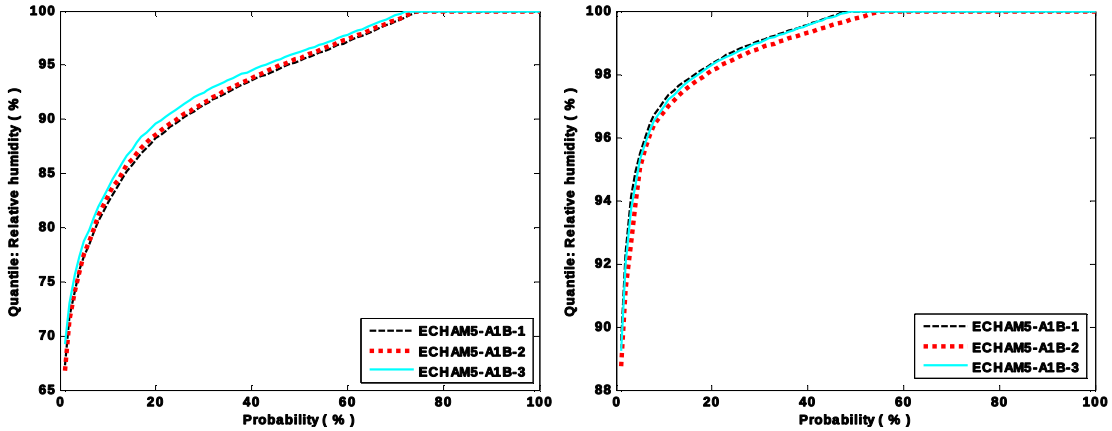

Figure 8.10. Relative humidity distribution of Stockholm in winter during 21-2020 for three initial conditions. Left: outdoor, right: indoor.

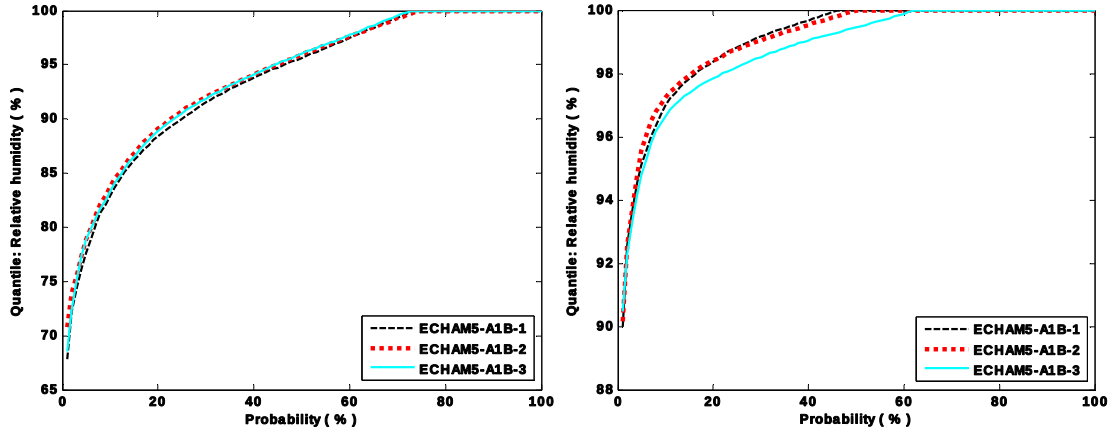

Figure 8.11. Relative humidity distribution of Stockholm in winter during 2021-2040 for three initial conditions. Left: outdoor, right: indoor.

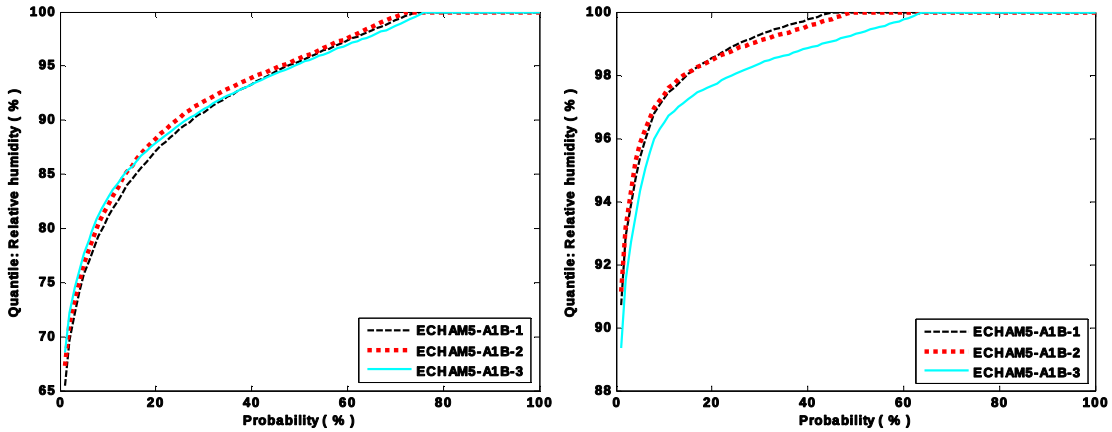

Figure 8.12. Relative humidity distribution of Stockholm in winter during 2041-2060 for three initial conditions. Left: outdoor, right: indoor.

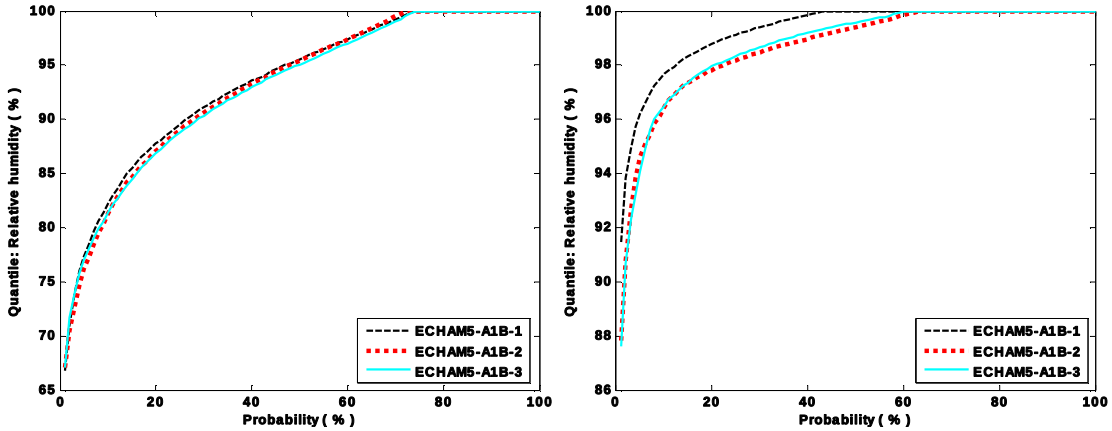

Figure 8.13. Relative humidity distribution of Stockholm in winter during 2061-2080 for three initial conditions. Left: outdoor, right: indoor.

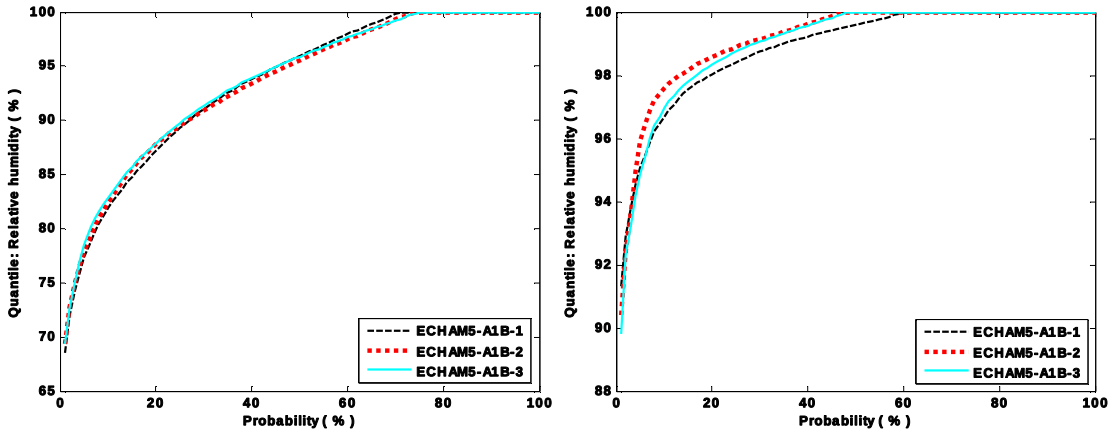

Figure 8.14. Relative humidity distribution of Stockholm in winter during 2081-21 for three initial conditions. Left: outdoor, right: indoor.

8.2. Parametric comparison

In this section the outdoor and indoor climate are compared for different initial conditions considering the time. First the 20-year and seasonal mean values are compared together. The seasonal mean values have been calculated for the 10^{th} year of each period. Tables 8.1 to 8.5 contain the mean values of global radiation, outdoor and indoor temperature and relative humidity.

In table 8.1 the 20-year mean value of the global radiation decreases for all the initial conditions passing the periods. The rate of decrement is not the same. For example between 2021-2040 and 2041-2060 the 20-year mean decreases around 1.4 W/m^2 for the second data set but 0.4 W/m^2 for the first one.

Having different initial conditions may affect the weather data considerably. Table 8.2 show that the 20-year mean temperature increases for 5.2^oC in the data with the first initial condition. The increment is around 4.1^oC for the third initial condition. There is around 1^oC difference between the temperature increments of the two data sets. The temperature difference between different data sets in the same periods is usually less than one degree.

The 20-year mean of the indoor temperature in Table 8.3 does not show the increment by passing the periods the same as the outdoor temperature. The second and third initial conditions show the biggest difference between the 20-year mean values during 2061-2080 and 2081-2100. It is interesting to see that they have very close values of outdoor mean temperature for the same periods in tables 8.2. The indoor temperature variations are not predictable based on the outdoor variations using this scale of time. Having different initial may cause the considerable 20-year mean temperature difference of around 1.5^oC in the attic (like the 2061-2080 period).

The 20-year mean values of relative humidity are very close for different periods and initial conditions during winter.

Table 8.1. Seasonal and 20-year mean global radiations of different periods for three initial conditions [W/m^2]

Mean value [W/m^2]	Initial condition	1961-1980	1980-2000	2001-2020	2021-2040	2041-2060	2061-2080	2081-2100
20-year	**1**	13.31	13.73	13.1	12.9	12.5	12.06	11.1
	2	13.71	13.75	12.9	13.17	11.77	11.47	10.99
	3	13.14	13.21	13.3	13.03	12.05	11.54	11
Seasonal	**1**	14.05	14.07	12.45	11.24	14.35	12.3	10.34
	2	14.77	12.03	13.67	13.5	9.76	11.36	11.15
	3	13.73	13.54	13	11.64	14.71	12.28	8.34

Table 8.2. Seasonal and 20-year mean of the outdoor temperature in different periods for three initial conditions

Mean value [°C]	Initial condition	1961-1980	1980-2000	2001-2020	2021-2040	2041-2060	2061-2080	2081-2100
20-year	1	-6.92	-7	-6.31	-4.82	-3.59	-2.86	-1.73
	2	-7.22	-6.85	-5.37	-5.34	-3.14	-2.42	-2.07
	3	-6.52	-5.56	-6.20	-5.29	-4.22	-2.72	-2.07
Seasonal	1	-6.84	-6.53	-8.6	-2.36	-4.99	-2.7	-0.25
	2	-7.15	-3.16	-5.09	-5.53	-0.88	-0.61	-4.21
	3	-7.87	-4.92	-6.40	-2.73	-6.66	-3.12	-0.34

Table 8.3. Seasonal and 20-year mean of the indoor temperature in different periods for three initial conditions

Mean value [°C]	Initial condition	1961-1980	1980-2000	2001-2020	2021-2040	2041-2060	2061-2080	2081-2100
20-year	1	-7.85	-8.56	-7.77	-7.69	-6.71	-7.56	-7.54
	2	-8.44	-7.26	-7.72	-7.99	-8.56	-8.23	-8.6
	3	-7.12	-8.95	-7.26	-6.19	-7.46	-6.78	-6.94
Seasonal	1	-8.87	-8.06	-7.94	-7.64	-6.82	-9.07	-7.68
	2	-8.72	-8.26	-7.08	-9.77	-6.68	-11.23	-5.44
	3	-7.83	-8.52	-4.57	-5.33	-7.57	-7.5	-6.2

Table 8.4. Seasonal and 20-year mean of the outdoor relative humidity in different periods for three initial conditions

Mean value [-]	Initial condition	1961-1980	1980-2000	2001-2020	2021-2040	2041-2060	2061-2080	2081-2100
20-year	1	0.93	0.94	0.93	0.93	0.93	0.93	0.93
	2	0.94	0.93	0.93	0.94	0.93	0.93	0.93
	3	0.94	0.93	0.94	0.94	0.93	0.93	0.93
Seasonal	1	0.93	0.93	0.93	0.95	0.90	0.95	0.94
	2	0.93	0.92	0.94	0.96	0.93	0.96	0.94
	3	0.96	0.93	0.94	0.95	0.92	0.94	0.94

Table 8.5. Seasonal and 20-year mean of the indoor relative humidity in different periods for three initial conditions

Mean value [-]	Initial condition	1961-1980	1980-2000	2001-2020	2021-2040	2041-2060	2061-2080	2081-2100
20-year	1	0.983	0.988	0.99	0.99	0.99	0.992	0.988
	2	0.983	0.989	0.988	0.99	0.99	0.986	0.991
	3	0.987	0.991	0.99	0.987	0.986	0.987	0.99
Seasonal	1	0.99	0.99	0.993	0.992	0.987	0.995	0.984
	2	0.981	0.994	0.987	0.99	0.991	0.994	0.99
	3	0.988	0.988	0.987	0.986	0.991	0.986	0.991

Figures 8.15 to 8.17 show the mean cycle temperature ($\overline{T} + \hat{T}_d$) for indoor and outdoor climate of the three initial conditions. The gradual increment of the outdoor temperature by passing the time is recognizable. The effect of having different initial conditions on the indoor temperature is more visible in these figures. For example the indoor mean cycle temperature of 1981-2000 for the second initial condition in Figure 8.16 is mostly more than -10°C, but for the other initial conditions it has smaller values in many days. On the contrary of 1981-2000, Figure 8.16 has colder winter during 2081-2100 comparing to other initial conditions. The mean cycle represents the periodical mean of each day. It gives information about each day in the whole period. It has the time resolution of one day. So having different initial conditions affects the indoor temperature on daily basis. In the case of simulating the phenomenon which is very dependent on daily variations of the indoor temperature it may be necessary to consider different initial conditions. Figures 8.18 to 8.20 compare the mean cycle of the first and last periods, 1961-1980 and 2080-2100, for different initial conditions. The comparison has been made also by fitting a cubic function to the mean cycle profile. Figures 8.18 and 8.20 show that the difference between the climate data with three initial conditions increases inside the attic. For the future climate the trends of the outdoor temperature are closer than the indoor temperature. An obvious case is the difference of the second initial condition from the tow others, specially indoors. The indoor conditions magnify the differences.

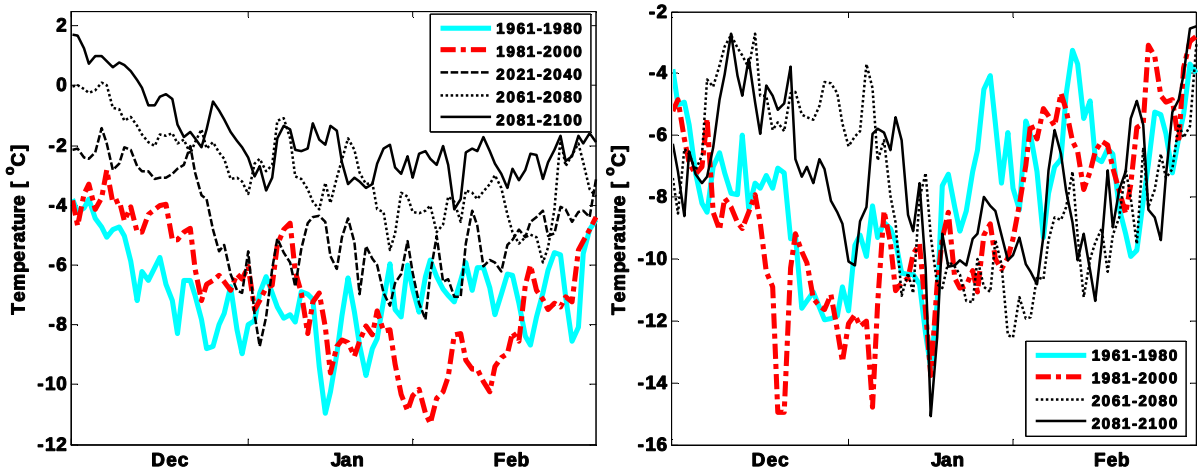

Figure 8.15. Mean cycle of winter temperature in Stockholm for A1B-1. Left: outdoor, right: indoor

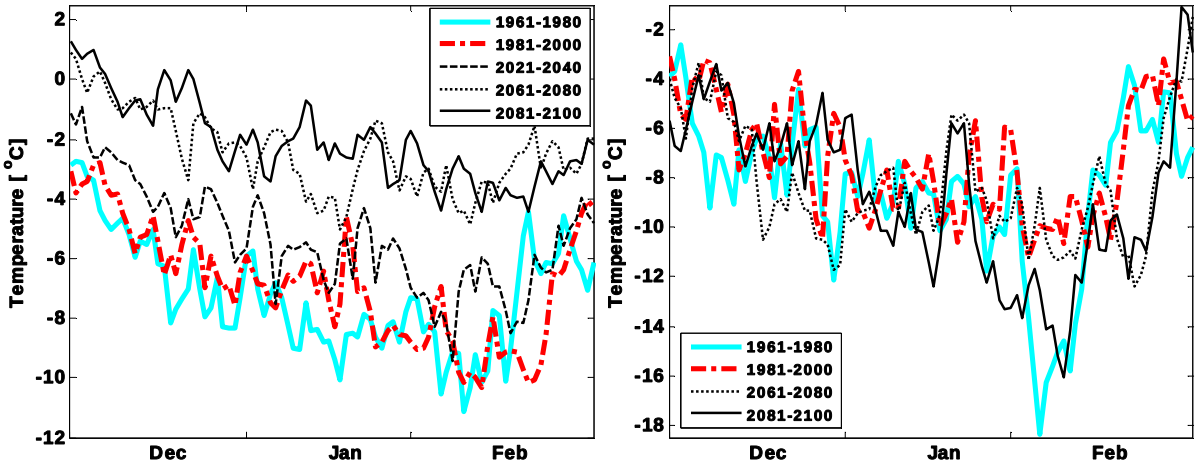

Figure 8.16. Mean cycle of winter temperature in Stockholm for A1B-2. Left: outdoor, right: indoor

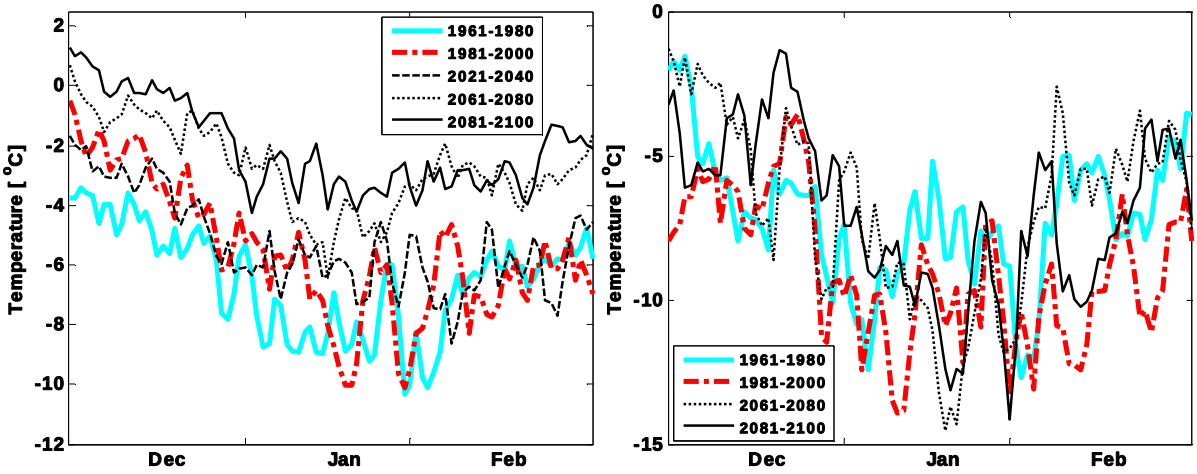

Figure 8.17. Mean cycle of winter temperature in Stockholm for A1B-3. Left: outdoor, right: indoor

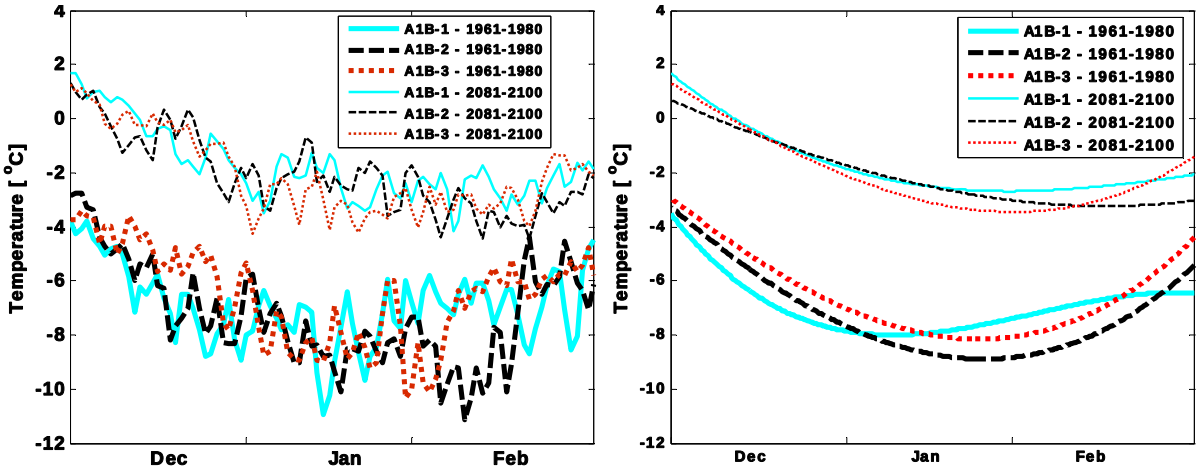

Figure 8.18. Outdoor temperature in two periods for three different initial conditions. Left: mean cycle, right: cubic fit to the mean cycle

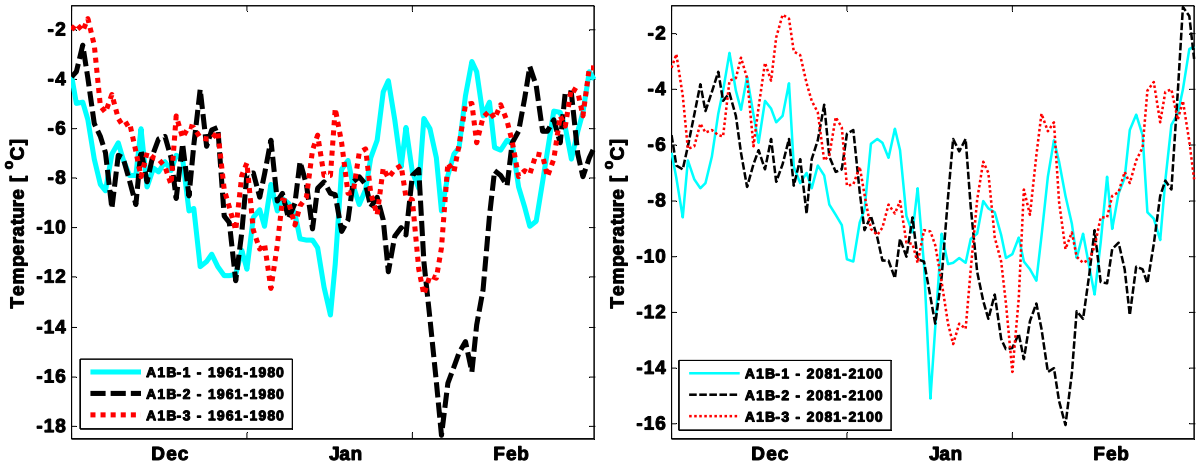

Figure 8.19. Mean cycle of indoor temperature in two periods for three different initial conditions

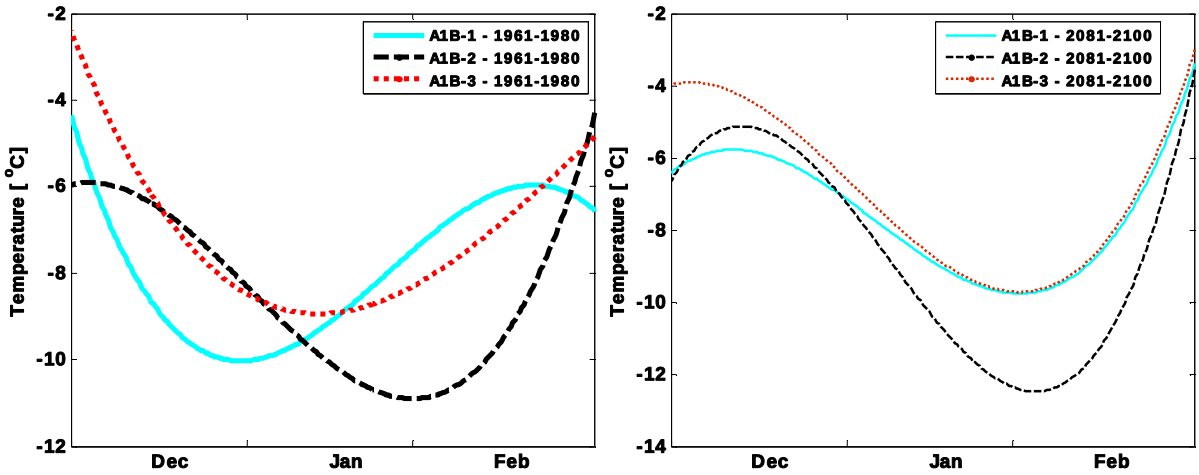

Figure 8.20. Cubic fit to the mean cycle of indoor temperature in two periods for three different initial conditions

The concept of different variabilities has been described in the previous chapters. Tables 8.6 to 8.10 show variability components of global radiation, outdoor and indoor temperature and relative humidity.

For the global radiation the seasonal variability plays the major role in increasing the total variability. In all the other tables the intraseasonal variability affects the total variability more than other variabilities. The global radiation total and seasonal variabilities decrease for all the initial conditions. The values for the last period are very close to each other for all the three cases. Different variability parameters are very similar but the rate of decrement is not the same.

The total variability of the outdoor and indoor temperature is more influenced by the intraseasonal variability. In tables 8.7 and 8.8 the intraseasonal variability has larger values for all the initial conditions. For the outdoor temperature both the intraseasonal and total variabilities decrease at the end of the whole period. The rates are not the same, but the values are close to each other. It

shows that the variations of the outdoor temperature are not very influenced by the initial conditions. There are some other reasons that may affect the variations more than having different initial conditions. For example having different global models cause larger differences in the variations. The differences between temperature variabilities are more inside the attic. Looking at Figure 8.20 and comparing the mean cycle of the second initial condition with the others confirms that the second initial condition generates a quite different seasonal temperature profile inside the attic. The variations of the temperature total variability are not the same for the three data sets inside the attic. But in all of them the total variability does not changes that much and keeps in the same level during different periods.

The indoor and outdoor relative humidity variabilities are very similar in tables 8.9 and 8.10. It is possible to neglect the effects of different initial conditions on changes of relative humidity variability.

Table 8.6. Variabilities of the global radiation for three initial conditions [W/m^2]

Initial condition	Variability	1961-1980	1980-2000	2001-2020	2021-2040	2041-2060	2061-2080	2081-2100
1	Interannual	1.15	0.99	1.16	1.17	1.34	1.11	1.14
	Intraseasonal	5.89	5.42	5.78	6.11	6.02	6.18	6.32
	Seasonal	14.14	14.7	13.83	13.9	13.68	13.66	12.08
	Total	15.36	15.7	15.03	15.23	15.01	15.03	13.68
2	Interannual	1.15	0.91	1.43	0.71	1.29	1.10	1.09
	Intraseasonal	5.91	5.58	5.78	5.85	6.27	5.91	6.26
	Seasonal	14.85	14.8	14.1	14.24	12.63	12.28	12.12
	Total	16.02	15.84	15.31	15.41	14.17	13.67	13.68
3	Interannual	1.36	0.85	1.36	1.07	1.25	1.11	1
	Intraseasonal	6.22	5.60	6.10	5.69	5.75	6.30	6.27
	Seasonal	13.81	14.44	14.39	14.01	12.77	12.81	11.96
	Total	15.21	15.51	15.68	15.16	14.06	14.32	13.54

Table 8.7. Variabilities of the outdoor temperature for three initial conditions [^{o}C]

Initial condition	Variability	1961-1980	1980-2000	2001-2020	2021-2040	2041-2060	2061-2080	2081-2100
1	Interannual	1.75	1.6	1.7	1.62	1.48	1.43	1.22
	Intraseasonal	5.4	5.03	5.29	4.38	3.92	3.65	3.23
	Seasonal	1.41	2.14	1.49	1.67	1.73	1.45	1.31
	Total	5.85	5.7	5.75	4.95	4.53	4.17	3.7
2	Interannual	1.8	1.81	2.07	1.06	1.07	1.73	1.25
	Intraseasonal	5.48	5.26	4.92	4.4	3.64	3.18	3.19
	Seasonal	1.87	1.95	1.69	1.75	1.36	1.33	1.4
	Total	6.07	5.89	5.60	4.85	4.03	3.86	3.7
3	Interannual	2.21	1.33	1.80	1.82	1.64	1.20	0.93
	Intraseasonal	5.50	4.92	5.17	4.53	4	3.54	3.22
	Seasonal	1.76	2.24	1.58	1.59	1.21	1.45	1.48
	Total	6.18	5.56	5.70	5.14	4.49	4	3.67

Table 8.8. Variabilities of the indoor temperature for three initial conditions [^{o}C]

Initial condition	Variability	1961-1980	1980-2000	2001-2020	2021-2040	2041-2060	2061-2080	2081-2100
1	Interannual	1.30	1.28	1.54	1.68	1.01	1.42	0.9
	Intraseasonal	4.57	4.66	4.27	4.30	4.10	4.13	3.86
	Seasonal	2.30	2.82	2.12	1.90	1.79	2.67	2.34
	Total	5.28	5.59	5.02	4.99	4.59	5.12	4.60
2	Interannual	1.53	1.24	0.88	1.76	1.52	1.60	1.86
	Intraseasonal	4.47	4.15	4.48	4.57	4.59	4.32	4.59
	Seasonal	3.07	2.28	2.09	2.09	2.39	2.47	3.24
	Total	5.63	4.90	5.03	5.32	5.39	5.22	5.92
3	Interannual	1.54	1.25	2.24	1.73	1.14	0.96	0.95
	Intraseasonal	4.49	5.11	4.72	3.80	4.32	4.08	4.24
	Seasonal	2.33	2.47	2.35	1.77	2.89	3.16	2.85
	Total	5.28	5.81	5.73	4.53	5.32	5.25	5.20

Table 8.9. Variabilities of the outdoor relative humidity for three initial conditions [-]

Initial condition	Variability	1961-1980	1980-2000	2001-2020	2021-2040	2041-2060	2061-2080	2081-2100
1	Interannual	0.01	0.01	0.01	0.02	0.02	0.01	0.01
	Intraseasonal	0.06	0.06	0.06	0.06	0.07	0.06	0.07
	Seasonal	0.02	0.02	0.02	0.01	0.02	0.02	0.02
	Total	0.07	0.06	0.07	0.06	0.07	0.07	0.07
2	Interannual	0.01	0.01	0.02	0.01	0.02	0.02	0.01
	Intraseasonal	0.06	0.06	0.06	0.06	0.07	0.07	0.06
	Seasonal	0.02	0.02	0.01	0.01	0.02	0.02	0.02
	Total	0.06	0.06	0.07	0.06	0.07	0.07	0.07
3	Interannual	0.01	0.01	0.01	0.01	0.01	0.01	0.01
	Intraseasonal	0.06	0.06	0.06	0.06	0.06	0.07	0.06
	Seasonal	0.02	0.02	0.02	0.02	0.02	0.02	0.01
	Total	0.06	0.06	0.06	0.06	0.06	0.07	0.07

Table 8.10. Variabilities of the indoor relative humidity for three initial conditions [-]

Initial condition	Variability	1961-1980	1980-2000	2001-2020	2021-2040	2041-2060	2061-2080	2081-2100
1	Interannual	0.01	0	0	0	0	0	0
	Intraseasonal	0.02	0.02	0.02	0.01	0.01	0.01	0.01
	Seasonal	0.01	0.01	0.01	0.01	0.01	0	0.01
	Total	0.03	0.02	0.02	0.02	0.02	0.01	0.01
2	Interannual	0.01	0	0	0	0	0.01	0
	Intraseasonal	0.02	0.02	0.02	0.01	0.01	0.02	0.01
	Seasonal	0.01	0.01	0.01	0.01	0	0.01	0.01
	Total	0.02	0.02	0.02	0.01	0.01	0.02	0.02
3	Interannual	0.01	0	0	0	0	0	0
	Intraseasonal	0.02	0.01	0.01	0.01	0.02	0.02	0.01
	Seasonal	0.01	0.01	0.01	0.01	0.01	0.01	0.01
	Total	0.02	0.01	0.02	0.02	0.02	0.02	0.02

Having different initial conditions do not induce considerable changes in the variations of the parameters during the different time periods that have been considered. Having the same climate

models and emission scenario causes the very similar behavior of the climate simulations which keeps the variation of the parameters along the simulation time in the same level. The difference in the initial conditions is more appeared in the values of the parameters not their variations.

It is interesting to see that the nonparametric comparison of the relative humidity reveals the differences between climate data with different initial conditions more than the parametric methods. Also looking at the temperature mean cycle was a useful method to understand the differences.

9. Conclusions

The analysis of the attic climate using different weather data sets considering the uncertainties of the climate models was presented. Some general conclusions based on the results are presented hereafter. Each chapter contains more detailed conclusions.

9.1. Statistical methods

It is important to analyze the long term data sets with proper statistical methods. The nonparametric statistical method of boxplot and the Ferro hypothesis are robust for comparison of different data sets without having any assumption about probability distribution of the data. They are applicable when the distribution of the data in time is not important. The Ferro hypothesis is very applicable for the comparison of data with different spatial resolutions. It provides a good view of the data distribution by using quantiles and increases the accuracy of the comparison in the comparison to the box plots. The method also distinguishes if the differences are caused by scale or location difference.

The parametric method of decomposition of variabilities is a robust method for analyzing the data. Decomposition of the climate parameters and calculation of their variability components enable to have a multi-time-scale analysis of the data. The method provides statistics about the data and its variations for a long period with different time resolutions. It considers daily, seasonal, annual and periodical variations of the data. Different variabilities of a parameter, which are calculated by this method, represent the changes of that parameter in different time scales and periods. However, selection of the time period in the analysis affects the results and the consequent conclusions. In analyzing the future performance of the buildings it is important to select the proper time scale for the phenomenon which is going to be considered.

9.2. Spatial resolution

The comparison of the spatial resolution has shown that the data sets are very similar for the 25km and 50km resolutions. The biggest difference is in Stockholm mostly during the period of 1961-1990. The differences between two spatial resolutions are mostly related to the extreme value. It is possible to rely on the 50km spatial resolution of the data.

9.3. Global climate models

According to nonparametric comparison of the data sets with different global climate models (GCM) the differences between GCMs are larger during summer and winter, when the extreme values occur. Having different GCMs may affect the values considerable, i.e. may change the 30-year mean temperature around 3 degrees. The difference in relative humidity conditions between different GCMs is not as large as the temperature or global radiation. For all the GCMs the relative humidity will increase in the future and the increment is more visible during autumn and spring. Having higher relative humidity and temperature may cause more mould growth related problems.

Selecting the GCM can affect the future designing policies. The HADCM global model has shown the most extreme values.

All the GCMs show that the changes in the future are trend induced. On the other hand the outdoor temperature total variability increases in all the GCMs, but not with the same rate.

The indoor temperature of the attic is very dependent on the outdoor temperature and global radiation. Most of the global radiation models show that the indoor temperature does not increase with the same rate as the outdoor temperature because of having lower global radiation in the future. The nonlinearity of the hygro-thermal response of the attic does not allow finding a correlation for the variations of the indoor relative humidity between different GCMs according to the variations of the other weather parameters. This fact makes the prediction of the indoor conditions difficult and time consuming in the case of having different uncertainties in the outdoor conditions.

Variations of the indoor conditions, even for the temperature, are not following exactly the outdoor variations. Inside the attic the differences between the GCMs is less than the outside. The outdoor climate conditions distinguish the difference of the global climate models more than indoor. It is then not possible to predict variations of the indoor total variability based on the outdoor.

The GCMs are different in the mean values especially for the temperature. For variabilities, the biggest difference is for the intraseasonal variability between different GCMs. It means the daily anomalies, which are not induced by the seasonal cycle and periodical variations, induce considerable variations in the GCMs.

9.4. Emission scenarios

Studying the climate data sets with different emission scenarios shows that, by increasing the CO_2 emission, the temperature increases and global radiation decreases. The attic climate conditions and

their variabilities are very similar for different emission scenarios. The indoor conditions do not project the difference of emission scenarios as much as the outdoor climate. It is shown that the variabilities decrease during the SCN period. It is also shown that having different emission scenarios induces considerable changes in the trend comparing to changes because of anomalies.

The effects of different variability components on the increment or decrement of the total variability depends on the season to large extent and also to the location.

9.5. Initial conditions

All the data sets with different initial conditions show the gradual increment of temperature by passing the periods. But the attic temperature does not show the like-wise gradual increment. Though the relative humidity inside the attic reflects the differences between different initial conditions, there is no certain connection between the outdoor and indoor relative humidity distributions. The global radiation decreases for all the initial conditions passing the periods.

Having different initial conditions may affect the weather data considerably but not its variations. Having the same climate models and emission scenario causes the very similar behavior of the climate simulations, i.e. it keeps the variation of the parameters along the simulation time in the same level. The difference in the initial conditions is more visible in the absolute values of the parameters and not in their variations. The variations are more controlled by the climate model.

Having different initial conditions affects the indoor temperature on daily basis. In the case of simulating a phenomenon, which is very dependent on daily variations of the indoor temperature, it may be necessary to consider different initial conditions. The differences between temperature variabilities are visible inside the attic.

It is interesting to see that the nonparametric comparison of the relative humidity reveals the differences between climate data with different initial conditions more than the parametric methods. Also looking at the temperature mean cycle was a useful method to understand the differences.

Ideas for the future work

In most of the presented cases the climate conditions have been analyzed by decomposing the climate parameters and their variabilities into their constructive components. An idea came into mind during this work, but it has not been tested yet. The idea is to run the building simulations with the decomposed weather data. So in the case of having four decomposition components, the simulation is run four times. The simulation time will not be the same for the components because of the decomposition of the parameters into components with different time scales. Surely in the nonlinear model, the composition of the simulation results does not give the same result as the ordinary simulation. The variabilities of component give a view of variations of the components in the considered time period. It might be possible to run the simulations not for the whole period, but for the whole range of variations. But it depends on the time response of the model. If this idea proves to work then it may be possible to decrease the number of simulations for different weather data sets. For example it might be possible to avoid hourly simulations of the whole period.

The energy simulation of a prototype Swedish residential building has been done using the same climate data as the attic simulations. The energy consumption for different cases will be analyzed to find out the effects of climate change and climate uncertainties on energy calculations. The described idea may work better in the energy simulations.

Calculations will be made on representative building constructions, construction parts or details, so called test cases, whose design is known as particularly sensitive to climate variations. Results of calculations will give a base for risk analyses, which can give predictions on consequences of deviations in performance of buildings. Finding the probable frequency of normal and extreme natural phenomena will be considered.

References

ASHRAE, 2001. *Fundamentals 2001*, Atlanta, USA: American Society of Heating, Refrigerating and Air Conditioning Engineers.

Ferro, C.A.T., Hannachi, A. & Stephenson, D.B., 2005. Simple nonparametric techniques for exploring changing probability distributions of weather. *Journal of Climate*, 18(21), 4344-4354.

Fischer, E. & Schär, C., 2009. Future changes in daily summer temperature variability: driving processes and role for temperature extremes. *Climate Dynamics*, 33(7), 917-935.

Gordon, C. et al., 2000. The simulation of SST, sea ice extents and ocean heat transports in a version of the Hadley Centre coupled model without flux adjustments. *Climate Dynamics*, 16(2), 147-168.

Hagentoft C-E. 2009. Effects on function and cost of controlled ventilation of cold winds. *Report for the SBUF-project 11871*. Division of Building Technology. Chalmers Univeristy of Technology, Sweden.

Hagentoft, C.E. et al., 2008. Mould growth control in cold attics through adaptive ventilation. NSB2008, Copenhagen, Denmark.

IEA, 1996. IEA SHC Annual Report.

Kjellström, E. et al., 2005. *A 140-year simulation of European climate with the new version of the Rossby Centre regional atmospheric climate model (RCA3)*, SMHI.

Kjellström, E. et al., 2007. Modelling daily temperature extremes: recent climate and future changes over Europe. *Climatic Change*, 81, 249-265.

Kunzel, H.M., 1996. IEA Annex 24 HAMTIE. *Final Report–Task*, 1.

Marti, O. et al., 2006. Key features of the IPSL ocean atmosphere model and its sensitivity to atmospheric resolution. *Climate Dynamics*, 1-26.

Mattsson, B. 2005. A Sensitivity Analysis of Assumptions Regarding the Position of Leakages when Modelling Air Infiltration Through an Attic Floor. 7th Symposium on Building Physics in the Nordic Countries. Reykjavik, Island.

Moran, M.J. & Shapiro, H.N., 2003. *Fundamentals of engineering thermodynamics*, John Wiley & Sons New York.

Nielsen, A., Kjellström, E. & Sasic Kalagasidis, A., 2007. Sustainability of the Swedish built environment towards climate change. Hygro-thermal effects and design criteria for buildings with respect to future climate scenarios. In *10th International Conference on Performance of the Exterior Envelopes of Whole Buildings*. Clearwater Beach, Florida.

Persson, G. et al., 2007. *Climate indices for vulnerability assessments*, SE-601 76 Norrköping, Sweden: Swedish Meteorological and Hydrological Institute.

Salas-Mélia, D. et al., 2006. Description and validation of the CNRM-CM3 global coupled model. *Climate Dynamics*.

Sasic Kalagasidis, A., 2004. *HAM-Tools-An Integrated Simulation Tool for Heat, Air and Moisture Transfer Analyses in Building Physics*.

Sasic Kalagasidis, A. et al., 2009. Hygro-thermal response of a ventilated attic to the future climate load in Sweden. In *Proceedings of the fourth International Building Physics Conference*. Istanbul, Turkey, pp. 519-526.

Taesler, R. & Andersson, C., 1984. A Method for Solar Radiation Computations Using Routine Meteorological Observation. *Energy and Buildings*, 7, 341-352.

Von Storch, H. & Zwiers, F.W., 2001. *Statistical analysis in climate research*, Cambridge Univ Pr.

Wyser, K., Rummukainen, M. & Strandberg, G., 2006. *Nordic regionalisation of a greenhouse-gas stabilisation scenario*, SMHI.